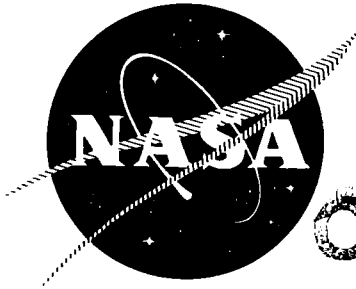


N 69 70 037

~~666 17966~~  
NASA CR-54657

Rocketdyne R-6303



**CASE FILE  
COPY**

**FINAL REPORT**

**INVESTIGATION OF CATALYTIC IGNITION  
OF OXYGEN/HYDROGEN SYSTEMS**

By

R. W. Roberts  
H. L. Burge  
M. Ladacki

prepared for  
**NATIONAL AERONAUTICS AND SPACE ADMINISTRATION**

Contract NAS 3-4185

**ROCKETDYNE RESEARCH DEPARTMENT**  
North American Aviation, Inc.  
6633 Canoga Avenue, Canoga Park, California

NASA CR-54657  
ROCKETDYNE R-6303

FINAL REPORT  
INVESTIGATION OF CATALYTIC IGNITION  
OF OXYGEN/HYDROGEN SYSTEMS

By

R. W. Roberts  
H. L. Burge  
M. Ladacki

prepared for  
NATIONAL AERONAUTICS AND SPACE ADMINISTRATION

December 1965

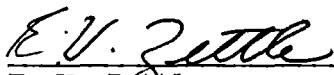
Contract NAS 3-4185

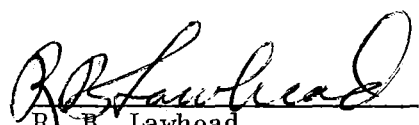
Technical Management  
NASA Lewis Research Center  
Cleveland, Ohio  
Advanced Rocket Technology Branch  
Paul Herr

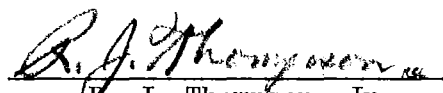
Rocketdyne Research Department  
North American Aviation, Inc.  
6633 Canoga Avenue, Canoga Park, California

INVESTIGATION OF CATALYTIC IGNITION  
OF OXYGEN/HYDROGEN SYSTEMS

Technically Reviewed and Approved By

  
E. V. Zettle  
Group Scientist  
Propulsion Applications Group

  
R. B. Lawhead  
Chief  
Propulsion Processes and  
Applications Section

  
R. J. Thompson, Jr.  
Vice-President and Director  
Research

December 1965



## FOREWORD

This research program was conducted by the Research Department of Rocketdyne, a Division of North American Aviation, Inc., under NASA Contract NAS3-4185, sponsored by the Office of Advanced Research and Technology and managed by the Advanced Rocket Technology Branch of Lewis Research Center. This report covers research accomplished during the period 15 June 1964 through 15 October 1965.

## ABSTRACT

The results and interpretations of an investigation of catalytic ignition of the oxygen/hydrogen system are presented. The experimental phase of the program is divided into three fundamental tasks: (1) Catalyst Selection and Evaluation, (2) Catalyst Life Studies, and (3) Parametric Engine Evaluation. During the first task, selected noble metal and metal oxide catalysts having potential for promoting the liquid phase oxygen/hydrogen reaction were evaluated. On the basis of these evaluations, four noble metal catalysts were compared in liquid phase reactants at an environmental temperature of approximately -400 F. The best of these four was used during a catalytic reactor configuration optimization study, and later during a catalyst life study to evaluate the reignition characteristics of the catalyst. During the final task, the catalytic igniter was used as an ignition source in a large engine (~ 14,000-pound thrust) to evaluate the effects of variations in engine and igniter parameters on liquid oxygen/liquid hydrogen engine ignition and ignition delay characteristics.







## CONTENTS

Foreword . . . . .	iii
Abstract . . . . .	iii
Introduction . . . . .	1
Summary and Remarks . . . . .	5
Chemical Analyses . . . . .	5
Catalyst Selection . . . . .	7
Catalyst Deactivation . . . . .	8
Catalyst Reactivation . . . . .	8
Reactor Configuration Optimization for Liquid Oxygen/ Liquid Hydrogen Ignitions . . . . .	9
Catalyst Life Characteristics . . . . .	10
Parametric Engine Evaluation . . . . .	11
Experimental Catalyst, Propellants and Apparatus . . . . .	13
Catalysts . . . . .	13
Propellants . . . . .	20
Apparatus . . . . .	21
Experimental Procedures . . . . .	33
Catalyst Selection . . . . .	33
Catalyst Life Studies . . . . .	36
Parametric Engine Evaluations . . . . .	38
Results . . . . .	41
Catalyst Selection and Evaluation . . . . .	41
Preliminary Catalyst Evaluations in Reactor Hardware . . . . .	50
Catalyst Life Evaluations . . . . .	53
Catalyst Deactivation . . . . .	58
Catalyst Reactivation . . . . .	60
Reactor Configuration Optimization . . . . .	61



Catalyst Life Evaluations . . . . .	67
Effects of Storage Environment on Activity . . . . .	70
Parametric Engine Evaluations . . . . .	72
Discussion of Results . . . . .	75
Flame Velocities and Flammability . . . . .	75
Catalyst-Limiting Temperatures . . . . .	77
Reactor Response . . . . .	77
Catalytic Reactor Stability . . . . .	78
Catalyst Life . . . . .	79
Catalytic Activity . . . . .	80
Liquid Propellants Reactor Scaling . . . . .	83
Gaseous Propellant Reactor Scaling . . . . .	85
Overall Catalytic Igniter Design . . . . .	87
Large-Engine Ignition Characteristics . . . . .	88
Theoretical Considerations . . . . .	93
Literature Survey . . . . .	93
Flame Velocity Effects . . . . .	95
Catalyst Pellet Limiting Temperatures . . . . .	101
Analytical Prediction of Catalytic Reactor Response	
Characteristics . . . . .	105
Catalytic Reactor Scaling Criteria . . . . .	113
Overall Catalytic Bed Stability . . . . .	120
Catalyst Characteristics . . . . .	133
<u>Appendix A</u>	
Equilibrium Specific Heats for Reacting Mixtures . . . . .	137
Nomenclature . . . . .	143
References . . . . .	149
Contractual Distribution . . . . .	211



## ILLUSTRATIONS

1. Cut-Away of Injector and LOX Dome for the Large Engine Used in the Parametric Engine Evaluation Task Illustrating Modifications to Adapt to the Catalytic Igniter . . . . 174
2. Small-Scale Laboratory Apparatus Used in the Preliminary Catalyst Evaluation Task With  $O_2/H_2$  Reactants . . . . 175
3. Schematic of 1-Inch-Diameter Catalytic Reactor Used in the Catalyst Selection Task Illustrating Location of Catalyst Bed and 4-on-1 Injector . . . . . 176
4. Photograph of 1-Inch-Diameter Combustor Disassembled to Show Major Components (5-Inch Catalyst Bed Configuration) . . . 177
5. Schematic of the Catalytic Reactor Used in the Low-Temperature Catalyst Evaluation Experiments in the Catalyst Life Study Task . . . . . 178
6. Photograph of 1-1/2-Inch-Diameter Reactor Used in the Catalyst Study Task Disassembled to Show Major Component Parts . . . . . 179
7. Assembled View of 1-1/2-Inch Catalytic Reactor Used in the Catalyst Life Study Task . . . . . 180
8. Illustration of the Injector, LOX Dome, and Catalytic Igniter Used in the Parametric Engine Evaluation Task . . . 181
9. Schematic of Large-Engine Chamber Used in the Parametric Engine Evaluation Task Illustrating Size and Relative Dimensions . . . . . 182
10. Photographic Representation of the Injector Used in the Parametric Engine Evaluation Task Illustrating the Injection Pattern and Catalytic Igniter Adapter Port . . . . . 183



11. Side View of the Injector Used in the Parametric Engine Evaluation Task Illustrating the Fuel Manifold and Catalytic Igniter Adapter . . . . .	184
12. Photographic Representation of the Liquid Oxygen Dome Used in the Parametric Engine Evaluation Task Illustrating the Catalytic Igniter Adapter Port and Oxygen Manifold . . . . .	185
13. Schematic of the Catalytic Igniter Used for Large-Engine Ignition in the Parametric Engine Evaluation Task Illustrating Assembly and Component Parts . . . . .	186
14. Photographic Representation of the Catalytic Igniter Used in the Parametric Engine Evaluation Task . . . . .	187
15. Schematic Illustration of the Gaseous Oxygen System Used in the Catalyst Selection Task . . . . .	188
16. Schematic Representation of the Gaseous Hydrogen System Used in the Catalyst Selection Task . . . . .	189
17. Schematic Representation of the Liquid Oxygen System Used in the Catalyst Life Study Task . . . . .	190
18. Schematic Representation of Liquid Hydrogen System Used in the Catalyst Life Study Task . . . . .	191
19. Theoretical Oxygen/Hydrogen Mixture Temperatures as a Function of Hydrogen Inlet Temperature and Mixture Ratio . . . . .	192
20. Comparison of Response Rates for the Engelhard MFSA Catalyst as a Function of the Rate of Approach to Steady-State Operating Temperature for Various Reactant Flowrates . . . . .	193
21. Comparison of Response Rates for the Engelhard MFSA Catalyst as a Function of the Rate of Approach to Steady-State Operating Pressure for Various Reactant Flowrates . . . . .	194
22. Comparison of Response Rates of Engelhard MFP and MFSA and Catalysts and Chemicals, Inc., Cl3-2 Catalysts in Oxidizer-Rich Reactants Under Comparable Conditions of Flowrate as a Function of the Rate of Approach to Steady-State Operating Temperature . . . . .	195



23.	Comparison of Response Rates of Engelhard MFP and MFSA and Catalysts and Chemicals, Inc., Cl3-2 Catalysts in Oxidizer-Rich Reactants Under Comparable Conditions of Flowrate as a Function of the Rate of Approach to Steady-State Operating Pressure . . . . .	196
24.	Temperature Gradation as a Function of Catalyst Bed Length Illustrating the Effects of Excess Catalyst Bed Length on Temperature for a 1.5-Inch-Diameter by 4-Inch-Long Catalyst Bed . . . . .	197
25.	Temperature Gradation as a Function of Catalyst Bed Length for a Near-Optimum Catalyst Bed . . . . .	198
26.	Illustration of the Effects of Reactant Flowrate Cycling on Temperature Within the Catalyst Bed for Two Bed Positions . . . . .	199
27.	Flame Velocity Data Available From Literature (Ref. 20) . . . . .	
28.	Flame Velocity Extrapolated Data to 60 and 210 R for Turbulent and Laminar Flames (Ref. 20) . . . . .	200
29.	Typical Curves Presenting the Rate of Approach to Steady-Stage Chamber Temperature for the Engelhard MFSS Catalyst With the Gaseous $O_2/H_2$ System Illustrating the Effects of Flowrate of Rate of Approach to Equilibrium . . . . .	201
30.	Minimum Catalyst Length Studies Showing Apparent Stability at Different Locations for Varying Total Flowrates for 21 Runs . . . . .	202
31.	Representation of Minimum Catalyst Bed Length Requirements as a Function of Reactant Flowrate Corrected to Comparable Mean Chamber Pressures . . . . .	203
32.	Representation of the Effects of Igniter Flowrate on Ignition Delay for the Nominally 20,000 lbf Thrust LOX/LH <sub>2</sub> Engine Operating at a Mixture Ratio of 5.5. The Igniter Chamber Temperature is Constant at 1500 F . . . . .	204



33.	Illustration of Typical Large-Engine Ignition Transients, Comparing Normal Ignition in Which the Chamber Pressure Uniformly Approaches a Steady-State Value With Erratic Ignition Wherein a Tendency to Quench Was Observed . . . .	205
34.	Flammability Limits of Hydrogen in Oxygen as Determined in Ref. 14 . . . . .	206
35.	Pneumatic Filling Constant to 95-Percent Steady-State Pressure for Various Assumed Sizes of Reactor and Steady- State Temperatures . . . . .	207
36.	Stability Solution for Steady-State Operation in a Packed Catalyst Bed . . . . .	208



## TABLES

1. Tabulation of Catalysts Evaluated With the Oxygen/ Hydrogen System . . . . .	153
2. Spectrographic Analysis of Catalysts . . . . .	155
3. Catalyst Surface Characteristics . . . . .	156
4. Results of Catalytic Activity Evaluations With Oxidizer- Rich Propellants . . . . .	157
5. Results of Catalytic Activity Evaluations With Fuel- Rich Propellants . . . . .	159
6. Summary Results of Catalyst Evaluations in Both Fuel-Rich and Oxidizer-Rich Service Extracted From Tables 3 and 4 . .	160
7. Results of Thermal Shock Treatment on Physical Structure and Relative Activity . . . . .	161
8. Summary of Results With Gaseous Reactants . . . . .	162
9. Summary of Results of Catalyst Life Studies . . . . .	163
10. Effects of Various Treatments on Catalytic Activity for the Engelhard MFSA Catalyst . . . . .	169
11. Effects of Storage Environment on Activity for the Engelhard MFSA Catalyst . . . . .	170
12. Summary of Results of Parametric Engine Evaluations . . .	171
13. Experimental Constants for Catalytic Reaction Rate Analyses With Fuel-Rich and Oxidizer-Rich Reactants . . . . .	172
14. Summary of Results of Catalytic Reactor Design Criteria Investigations . . . . .	173





## INTRODUCTION

Considerable effort has been expended during recent years to develop a propulsion system for utilizing the oxygen/hydrogen propellant combination in upper stage rocket engines. One of the problems resulting from the requirements of an upper stage is associated with multiple restart capability. Because the oxygen/hydrogen combination is inherently non-hypergolic, some form of ignition system is required. The requirements for large numbers of starts eliminates consideration of hypergolic slugs (e.g., TEA-TEB). A second possibility, that of the use of additives in either or both propellants to induce hypergolicity is not now the state-of-the-art. Spark igniters, although used for such applications, are complicated and require extensive development for high reliability at high altitude conditions. As a result of these problem areas, strong consideration is being given to the use of the catalytic igniter as an ignition device for use in oxygen/hydrogen engines.

The feasibility of using catalysts to promote the oxygen/hydrogen reaction in igniter configurations has been demonstrated during several research programs (Ref. 1 to 6). Feasibility with both gaseous and liquid propellants at environmental temperatures as low as those of liquid hydrogen has been demonstrated; however, certain areas of investigation remained to be studied before final development of a catalytic ignition system for an upper-stage engine could be initiated. For example, only a cursory evaluation of the durability characteristics of the catalysts in oxygen/hydrogen service had been undertaken. Similarly, very little consideration had been given to the evaluation of specific parameter variations in large engine applications, such as



ignition delay time, start-up characteristics, or minimum ignition enthalpy requirements. In addition, the range of potential catalysts for promoting the reaction of oxygen with hydrogen had been surveyed only partially, and the need existed to explore more fully the range of available catalysts.

Accordingly, a 12-month research program was conducted to obtain a large portion of the information listed above. The program was divided into three tasks:

Task I, Catalyst Selection and Evaluation

Task II, Catalyst Life Studies

Task III, Parametric Rocket Engine Ignition Study

The first task included a continuation of the search for superior reduction-type catalysts initiated under contract NAS3-2565, and an evaluation of promising oxidation-type catalysts. The second task was an experimental program to evaluate catalyst life characteristics, in terms of ignition cycles with selected catalysts. The design of the reactor hardware for this task was based on theoretical analysis that is also presented in this report. The third task was conducted using a nominally 20,000-pound thrust rocket engine as the test vehicle. A small catalytic reactor was used as an ignition source for the oxygen/hydrogen engine and ignition delay, ignition energy requirements, and start-up characteristics were evaluated over a range of engine operating conditions.

The research program was initially planned to use inlet hydrogen temperatures down to -400 F; however, during the course of Task II,



difficulty was experienced in obtaining stable ignitions over the range of operating conditions of interest, and the program was modified to include only gaseous propellants in the catalytic ignition phase of the third task. Furthermore, because of the problems of obtaining stable ignitions with liquid reactants during Task II, Task III was reduced in scope to allow for more concerted effort in exploring the specific problems inherent to the catalytic ignition of liquid phase oxygen/hydrogen reactants at environmental temperatures near -400 F.





## SUMMARY AND REMARKS

The objectives of this program were primarily the following.

1. The evaluation of commercially available metal oxide and previously unavailable noble metal catalysts for promoting the oxygen/hydrogen reaction
2. Evaluation of the durability characteristics of the "best" noble metal catalyst in application with liquid phase oxygen/hydrogen reactants
3. The generation of specific design criteria for catalytic liquid oxygen/liquid hydrogen reactors
4. The evaluation of specific parameter variations, such as ignition delay time, start-up characteristics, and minimum ignition enthalpy requirements, for large engine systems utilizing catalytic reactors as ignition energy sources.

The results of this investigation have revealed a number of facts concerning catalysts and catalytic ignition of oxygen/hydrogen engines. For the sake of clarity and continuity of thought, a summary of the results and remarks concerning these results of both experimental and analytical efforts is presented chronologically, consistent with the sequence in which the efforts progressed.

## CATALYST SELECTION

A large number of commercially available catalysts have been investigated during previous efforts (Ref. 1 to 6 ) and in this program for possible



application in a fuel-rich environment. In addition, the possibility of the use of oxidizer-type catalysts for use in oxidizer-rich service was evaluated. Of the catalysts evaluated in fuel-rich reactants, the Engelhard MFSA and 4X-MFSA formulations are the most attractive. Certain of the other catalysts have higher ambient temperature activities, but none matches the excellent relative activity retention characteristics of the MFSA and 4X-MFSA in low-temperature (-320 F and lower) application. In oxidizer-rich reactants only the MFSA catalyst was determined to have high activity at -320 F. This catalyst showed an unusually low sensitivity to changes in environmental temperature in both fuel-rich and oxidizer-rich applications. The Engelhard MFP catalyst had an activity level at ambient temperature sufficient to promote the oxygen/hydrogen reaction, both fuel-rich and oxidizer-rich, but was inadequate at low temperatures (-250 F and lower). This latter catalyst appeared initially to be quite promising because of the high ambient temperature activity and the manner of catalyst formulation. The MFP catalyst consists of iron-oxide impregnated on silicon carbide, both very-high-temperature-resistant metals.

On the basis of the results, it is apparent that the Engelhard MFSA catalyst represents the best commercially available formulation for dual-purpose (fuel-rich or oxidizer-rich) applications, and further that the MFSA and 4X-MFSA catalysts offer the greatest potential for reaction promotion in low environmental temperature application. While none of the metal oxide catalysts was satisfactory at low environmental temperature, the Girdler Chemical Company's T-3 catalyst is worthy of comment because of its excellent activity retention characteristics at low temperatures. Should the activity of this catalyst be raised to a higher level (doubled or tripled), the formulation would have excellent application in oxidizer-rich reactants.



In addition to the purely experimental evaluations, an analytical evaluation of the results of the relative activity measurements has resulted in a relationship for expressing relative activity as a function of temperature for the various catalysts. This relationship is useful in predicting reaction rates at various positions within a catalyst bed once the initial reaction has been initiated. Analytical investigations are continuing for determining the precise meaning of certain of the analytical results.

#### CATALYST EVALUATION

The results of an experimental evaluation of the Engelhard MFP and Catalysts and Chemicals, Inc. Cl3-2 in comparison with the Engelhard MFSA catalyst in reactor hardware with both fuel-rich and oxidizer-rich reactants have shown the Cl3-2 catalyst to be incapable of promoting the fuel-rich oxygen/hydrogen reaction. The MFP catalyst adequately promotes the fuel-rich reaction, but only at environmental temperatures higher than -190 F. The MFSA catalyst, in contrast, promotes the fuel-rich oxygen/hydrogen reaction at environmental temperatures as low as -400 F. In oxidizer-rich reactants, the Cl3-2 and MFP catalysts promote the oxygen/hydrogen reaction at ambient temperature, but require a catalyst mass/reactant flowrate nearly twice that required for the MFSA catalyst. These studies were curtailed because of the lack of suitable candidates for selection on the basis of laboratory relative activity measurements, and because of the inability of the briefly evaluated catalysts to promote satisfactorily the oxygen/hydrogen reaction.



## CATALYST DEACTIVATION

In evaluating catalyst life characteristics in liquid phase reactants at cryogenic environmental temperatures, it became apparent that the Engelhard MFSA catalyst is subject to deactivation during storage. This catalyst lost nearly 90 percent of the original activity over 6-month storage period. An evaluation of the specific effects of typical and accelerated storage conditions indicated that exposure to (1) normal atmospheric conditions, (2) 100-percent relative humidity conditions at ambient temperature, (3) heated (150 F) oxygen-enriched environment, and (4) complete water immersion for short term durations had no severe permanent detrimental effects on catalyst activity. The only appreciable permanent effect was a moderate reduction in catalyst activity probably caused by moisture effects during exposure to the 100-percent relative humidity condition at ambient temperature and pressure. In general, these results are only indicative of what may be expected in long-term storage, since the tests were conducted only over a 1-month period, largely under accelerated storage conditions.

## CATALYST REACTIVATION

In view of the deactivation experienced by the Engelhard MFSA catalyst, and because of the long delivery time required for receipt of new catalyst quantities, a brief effort was made to evaluate the relative reactivation characteristics of various catalyst treatments. In general, it was determined that the catalyst deactivation was not permanent, or irreversible, and that catalyst reactivation could be accomplished, and in fact catalyst activity was enhanced, by exposure of the catalyst to a hot, dry hydrogen or nitrogen environment. This refuted an original





thesis that the catalyst deactivation was caused by irreversible water promoted noble metal crystal growth. The apparent deactivation mechanism was then concluded to be a preferential surface adsorption of some unknown agent which resulted in occlusion of the active catalyst sites rather than one involving modification of these active sites. Catalyst reactivation in the presence of hot, dry hydrogen or nitrogen is therefore considered to result from preferential desorption of the occluding agent and adsorption of the hydrogen or nitrogen, thereby rendering the catalytic surface available for continued reaction promotion.

#### REACTOR CONFIGURATION OPTIMIZATION FOR LIQUID OXYGEN/LIQUID HYDROGEN IGNITIONS

An extensive experimental and analytical evaluation of optimum reactor configuration was conducted with the partially deactivated Engelhard MFSA catalyst in liquid phase reactants. In general, it was determined that for a 1.5-inch-diameter reactor operating at nominally 50 pounds of thrust and a chamber pressure of 100 psi in a -400 F environment, the minimum catalyst bed length is approximately 3 inches, and the optimum reactant mixing zone length is 0.75 inch. Reactant channelling along the reactor walls was an apparent problem which was resolved by installing antichannelling rings extending 1/8 inch (one catalyst pellet diameter) into the reactor and spaced at 1-inch intervals. The antichannelling rings served to redirect reactants from the wall into the catalyst bed, and thereby improve reactant/catalyst contact efficiency and, hence, reaction efficiency. These results are considered to be quite important, because they point out that the liquid hydrogen/liquid oxygen reaction can be promoted with a low relative activity catalyst (10 to 20 percent)



provided the reactor is mechanically and kinetically matched to the liquid hydrogen/liquid oxygen flowrates and injection. Mechanical considerations show the need for moderately good propellant mixing and prevention of channelling. The kinetics are concerned with mass and heat transfer to the liquid oxygen drops, because in equilibrium, at the mixture ratio of interest the liquid hydrogen will freeze up to seven times its weight, thus negating any chance of ignition. By taking advantage of the oxygen droplet's heat capacity, it is possible to warm a liquid hydrogen-chilled bed to the point where ignition can occur. The drops must, however, be reasonably distributed and mixed with the hydrogen to prevent undesirable high local temperatures.

#### CATALYST LIFE CHARACTERISTICS

The catalyst life characteristics were never fully defined because of a number of difficulties encountered in conducting the experimental life study runs. Fuel boiling instability in the bed resulted in loss of both local and gross mixture ratio control with resultant catalyst bed burning. A total of 11 successful runs was conducted with a single catalyst bed and in cryogenic reactants at an environmental temperature near -400 F. Following the eleventh run, however, a loss of mixture ratio control resulted in an explosion which destroyed the catalyst bed. Catalyst performance during the eleventh run appeared to be equal to that during the first run, however, and it is presumed that no catalyst damage had been sustained as a result of the previous runs. During earlier series of runs, catalyst damage was experienced, but this was obviously, from an inspection of the catalyst bed, caused by loss of local mixture ratio control with resultant streaky burning in the catalyst bed. On the basis of the successful runs, it is tentatively



concluded that during the course of controlled runs, no appreciable catalyst damage is sustained at reaction temperatures of nominally 1500 to 1600 F. Previously obtained data for gaseous operation in both steady-state and pulsed-mode operation certainly indicate that the alumina-based noble metal catalysts can be operated reliably over a wide number of cycles from a life standpoint.

#### PARAMETRIC ENGINE EVALUATION

This phase of the program was conducted in jointly provided NASA and Rocketdyne hardware rated at approximately 20,000-pound thrust incorporating a nominally 50-pound thrust catalytic igniter as shown schematically in Fig. 1. The experimental runs, conducted with liquid propellants in the engine and gaseous propellants in the igniter, were generally divided into two categories of effort, the first concerned with an evaluation of the effects of engine parameter variations on ignition delay with a constant ignition source, and the second with an evaluation of the effects of variations in igniter energy level on ignition delay time. Both of these experimental activities were further divided into subtasks typical of large-engine operation and of gas generator operation. The results of the experimental program demonstrate the feasibility of both large-engine and gas generator ignition using catalytic igniters. It is further demonstrated that, within the scope of this study, engine/igniter energy ratios at least as high as 1000, and perhaps higher, can be safely used in large-engine and gas generator systems. Even under the most severe conditions (i.e., high engine propellant mass flowrate and low mixture ratio, and low igniter propellant flowrate) ignition occurred. It had been anticipated that



ignition might be erratic at these conditions because of the fact that at liquid propellant temperatures the low engine propellant mixture ratio is representative of only a marginally flammable oxidizer/fuel blend. This, however, was not the case, and ignition occurred without incident.



## EXPERIMENTAL CATALYSTS, PROPELLANTS, AND APPARATUS

This program was conducted with both noble metal and metal oxide catalysts, selected on the bases of past experience (Ref. 1 to 3), theoretical considerations, and vendor recommendations; and subjected to comparative evaluations first in laboratory apparatus and later in engine hardware. The catalysts and hardware used during the evaluations are as described in the following section of this report.

## CATALYSTS

The catalysts used during this program were of a variety of types, ranging from noble metal to metal oxides, and were impregnated on substrates ranging from alumina to silicon carbide. The manner of preparation of the catalysts are considered proprietary by the vendors, and are not discussed herein. A list of the catalysts evaluated is presented in Table 1. In addition, the elemental spectrographic analyses and the surface characteristics of the various catalysts are given in Table 2 and 3.

Noble Metal Catalysts

Engelhard Industries, Inc. DS Catalyst. The DS catalyst consists of a high-surface-area alumina pellet, nominally 1/8-inch in diameter, impregnated with palladium equal to about 0.3 weight percent.



Engelhard Industries, Inc. DSS Catalyst. The catalyst was recommended by the vendor as a possible substitute for the DS formulation because the DSS pellet has better resistance to thermal shock without an appreciable decrease in catalytic activity. Like the DS, the DSS catalyst consists of a palladium-impregnated alumina pellet, and is nominally a 1/8-inch-diameter sphere.

Engelhard Industries, Inc. MFSS Catalyst. The MFSS catalyst, while similar in physical appearance to the previous samples, has a somewhat different formulation. The MFSS was found by chemical analysis to be a platinum-rhodium-on-alumina material rather than a palladium-on-alumina-type catalyst. Of interest here is that, according to the vendor, the purpose of the platinum is to enable impregnation of the alumina substrate with rhodium, because the rhodium otherwise tends to slough off rather than adhere to the alumina. Prior impregnation of substrate with platinum serves to provide a base on which the rhodium will adhere.

Engelhard Industries, Inc. MFSA Catalyst. The MFSA catalyst is a later version of the MFSS configuration, and is very similar in physical appearance to the previously described Engelhard catalysts. The primary differences are associated with surface characteristics and chemical composition as shown in Tables 2 and 3. The difference in surface area results from the fact that the MFSA catalyst metals is impregnated on an improved substrate, and is manufactured by a slightly different procedure. The principal difference in composition between the MFSA and the MFSS catalyst is the presence of lead in the catalyst. This material was presumably added to improve the uniformity of noble metal impregnation.



Engelhard Industries, Inc. 4X-MFSA Catalyst. This catalyst is reported by the vendor to be identical to the MFSA catalyst, with one exception. The 4X-MFSA contains nominally four times the noble metal content of the MFSA material.

Davison Chemical Company SMR 55-1097-1 Catalyst. The Davison catalyst consisted of an irregularly-shaped crushed silica gel substrate impregnated with nominally 6-weight percent platinum.

Houdry Process Corporation A-100S Catalyst. This material is a platinum-on-alumina formulation and physically appears as a 1/8-inch diameter by random length (~3/8-inch maximum) extruded cylinder. This sample is of relatively low surface area as seen in Table 3, and is typical of catalysts used in moderate hydrogenation service in the petroleum industry.

Houdry Process Corporation B-100S Catalyst. This catalyst is identical to the A-100S material in all respects including manner of preparation, with the exception that the B-100S catalyst consists of palladium on alumina instead of platinum on alumina, as is the case with the A-100S catalyst.

Houdry Process Corporation A-200SR Catalyst. The A-200SR formulation is similar to the A-100S catalyst in all respects except two. This catalyst has a moderate surface area (nominally 200 square meters per gram) and is prepared to be resistant to catalyst poisoning by sulfur. The physical dimensions are 3/16-inch diameter by random length, not exceeding 3/8-inch.



Shell Development Company 405 Catalyst. The Shell 405 catalyst consists of a high noble-metal content on alumina substrate material, and was specifically developed under contract with the NASA Office of Advanced Research and Technology as a hydrazine decomposition catalyst. This catalyst is provided as a 1/8- by 1/8-inch circular cylinder.

Sundstrand Aviation Catalyst. This catalyst was originally developed by Sundstrand during the course of their efforts in behalf of the Dynasoar program, and consists of a high (>2 percent) weight percent palladium-on-alumina formulation. The substrate is reported to be an extremely hard material, with excellent resistance to thermal shock and attrition caused by crushing, and is provided in the form of a nominally 5/16-inch-diameter sphere.

#### Metal Oxide Catalysts

Catalysts and Chemicals, Inc. C12-3 Catalyst. The C12-3 is an iron oxide- and chromium oxide-on-alumina formulation provided in the form of 1/4- by 1/4-inch cylinders.

Catalysts and Chemicals, Inc. C13-1 Catalyst. This catalyst is a nickel oxide-on-alumina material prepared in the form of 1/4- by 1/4-inch cylinders.

Catalysts and Chemicals, Inc. C20-6 Catalyst. The C20-6 catalyst is an extruded 1/8-inch-diameter by nominally 3/16-inch-long cylindrical material consisting of approximately 3-weight percent cobalt oxide and 10-weight percent molybdenum trioxide on an alumina substrate.





This composition is typical of catalysts used for desulfurizing and denitrogenating hydrocarbons prior to use in reforming processes for manufacture of high-octane gasoline and aromatic hydrocarbons.

Davison Chemical Company Oxidizer 903 Catalyst. This catalyst is a proprietary composition provided in the form of 1/8-inch cylinders nominally 1/8-inch long.

Davidson Chemical Company SMR 55-8182 Catalyst. This material is a proprietary formulation similar in appearance to the Oxidizer 903 catalyst.

Engelhard Industries, Inc. MFP Catalyst. The MFP catalyst is unique among catalysts because of the substrate. This catalyst has iron oxide as the active constituent impregnated on a silicon carbide substrate. None of the other catalysts available used silicon carbide, selected by Engelhard as a potentially high-temperature catalyst base. The MFP catalyst is provided as a 3/16- by 3/16-inch right circular cylinder.

Girdler Chemical Company G-13 Catalyst. The Girdler G-13 catalyst is a nickel oxide-on-alumina material provided in the form of 1/8-by 1/8-inch cylinders.

Girdler Chemical Company G-22 Catalyst. This catalyst consists of pelleted copper chromite prepared in the form of 1/8-by 1/8-inch



cylinders. No substrate material is employed. Barium is impregnated on the copper chromite for the purpose of enhancing catalytic activity.

Girdler Chemical Company G-49B Catalyst. The G-49B catalyst consists of nickel impregnated on kieselguhr, a diatomaceous earth. This catalyst is provided in the form of 1/8- by 1/8-inch cylinders having the surface characteristics presented in Table 3.

Girdler Chemical Company G-62 Catalyst. This catalyst consists of cobalt oxide impregnated on a "special base", proprietary with the vendor. The G-62 catalyst is available in the form of 1/8- by 1/8-inch right circular cylinders.

Girdler Chemical Company G-67 Catalyst. The G-67 catalyst is identical to the G-62 material, but consists of cobalt oxide impregnated on kieselguhr.

Girdler Chemical Company G-67RS Catalyst. The G-67RS catalyst is identical to the G-67 catalyst in all respects, including the nature of active constituent and substrate, except one. The G-67RS catalyst is reduced to cobalt rather than cobalt oxide after preparation, and stabilized to minimize oxidation. The manner of stabilization is proprietary with the vendor.

Girdler Chemical Company T-3 Catalyst. The T-3 catalyst is an experimental catalyst consisting of copper oxide impregnated on kieselguhr.



In physical size and appearance, the T-3 catalyst is similar to most of the other Girdler catalysts. This material is provided as a black-colored 1/8- by 1/8-inch right circular cylinder.

Girdler Chemical Company T-893 Catalyst. The Girdler T-893 catalyst is an experimental "zirconia-promoted nickel-on-refractory oxide" material. This catalyst is provided in the form of 1/4- by 1/4-inch cylinders.

Girdler Chemical Company T-1205 Catalyst. The Girdler T-1205 catalyst is also an experimental composition, and is virtually identical in size, shape, and appearance to the T-3 catalyst. From a chemical composition standpoint, the T-1205 catalyst consists of nickel oxide impregnated on kieselguhr. A promoting agent proprietary in type and composition with the vendor is used to enhance catalytic activity.

Harshaw Chemical Company Zirconia-Chromia Catalyst. As the name implies, this catalyst consists of a mixture of zirconia and chromia pelleted in the form of 1/4- by 1/4-inch tablets. No substrate is used in preparing this catalyst.

Houdry Process Corporation A-25Z Catalyst. The A-25Z catalyst is manufactured by impregnating chromium oxide ( $\text{Cr}_2\text{O}_3$ ) on alumina. The chemical composition of this catalyst is presented in Table 2. Surface characteristics are shown in Table 3. This material is provided in the form of 1/8-inch-diameter by nominally 3/16-inch-long extrusions.



## PROPELLANTS

During this program, both gaseous and liquid propellants were used. The gaseous propellants used during this study were supplied from commercial bottle gases with each gas being passed through a "molecular sieve" drier (calcium-aluminum-silicate) for removal of moisture prior to use. Liquid propellants corresponded to military specifications for liquid-hydrogen and liquid oxygen, respectively.

### Gaseous Hydrogen

The hydrogen was obtained as an ambient-temperature gas from high-pressure storage bottles. These gases contained oxygen, nitrogen, and water in the parts-per-million range as impurities. As supplied, the hydrogen contained less than 15-ppm water, with an overall impurity level of less than 60 ppm.

### Gaseous Oxygen

The oxygen was obtained from 2.13-cu ft K-bottles. The particular gas used was found by analysis to contain appreciable quantities of carbon dioxide (~2500 ppm) and water (~200 ppm), both of which are known to deactivate noble-metal catalysts. Therefore, the oxygen, as in the case of the hydrogen, was passed through a molecular sieve drier for removal of these impurities. The high removal efficiency of the molecular sieve drier is indicated by the fact that the carbon dioxide content of the gas leaving the drier was less than 50 ppm, while the water content was less than 0.5 ppm.



### Liquid Hydrogen

Liquid hydrogen was obtained as a saturated liquid from primary liquid hydrogen storage and complied with military specification MIL-P-25508D for propellant purity.

### Liquid Oxygen

Liquid oxygen was obtained as a saturated liquid from primary liquid oxygen storage, with the propellant purity complying with military specification MIL-P-27201.

## APPARATUS

The apparatus used during this program consisted of a catalytic activity measurement device used in catalyst screening, a 1-1/2-inch-diameter reactor used in evaluating catalyst life characteristics, and modified government-furnished hardware used in the large engine catalytic ignition studies. Each of the respective hardware items and, where applicable, the associated propellant systems are described in the following paragraphs.

### Preliminary Catalyst Evaluation Apparatus

The apparatus used during the preliminary catalyst screening operation was as shown schematically in Fig. 2. This apparatus consists of a flow-metering (and proportioning) system for providing reactant gases to the catalyst bed in a controlled manner, a catalyst bed for effecting



reaction, and a water absorbent material for selectively removing the reaction product (water) from the effluent gas stream. Provision is also made for environmental cooling (to -320 F) of the catalyst and reactants prior to use. The catalyst bed is mounted in a detachable U-tube fitted with a thermocouple for measuring environmental as well as reaction temperature. The adsorbent material ("Drierite") is similarly mounted in a detachable U-tube to facilitate weighing before and after the run. A back-pressure regulator is provided for maintaining constant pressure in the reaction chamber.

#### Crush Strength Test Device

The apparatus used in evaluating crust strength of the various catalysts was similar to devices used in the catalyst industry and consisted of a hydraulic jack of the dead-weight tester type arranged to exert pressure on a catalyst pellet placed between the tester plate and a rigid plate. Force measurements to the nearest 0.1 pound were made by a calibrated pressure gage and a known-diameter tester-plate piston.

#### One-Inch-Diameter Hardware

Reactor. The reactor used during the gaseous phase of the program consisted of a 1-inch-diameter (ID) stainless-steel tube reactor jacketed to provide for prechilling both the reactor and catalyst with liquid nitrogen prior to use. The reactor internal geometry was adapted to provide flexibility in the location and length of the catalyst bed. The downstream end of the reactor was threaded to provide for insertion of an exhaust nozzle, and to provide flexibility in the selection of nozzle diameters. A schematic of the reactor and a photograph of the dissembled reaction assembly are presented in Fig. 3 and 4, respectively.



Catalyst pellets are randomly packed in a 4-inch-long sleeve, and held in place by perforated end plates or screens. Two types of catalyst pellet retainers were used during this study: 70-percent open-area stainless-steel screens, and 31-percent open-area perforated plates. Most of the tests were conducted with the screen upstream and perforated plate down-stream of the catalyst bed.

The downstream end of the combustor was threaded as indicated in Fig. 3 to accommodate a stainless-steel insert. The insert was drilled and machined to a convergent contour and served as the exit nozzle. Various inserts with different diameters were used to control the combustion pressure and velocity distribution through the combustor. A 0.221-inch-diameter nozzle was used almost exclusively throughout this program, however, primarily because this seemed to give good combustion characteristics.

Injection-Mixer. The use of the catalyst-igniter configuration requires that the propellants be homogeneously mixed prior to introduction of the propellants into the catalyst bed. A basic 4-on-1 impinging-stream injector/mixer was used exclusively during the gas phase studies of this program. The injector/mixer had been proved during a previous program (Ref. 2) and because injector optimization was not an objective of this study, no further consideration was given to the injection system. The injector/mixer was made of stainless steel and consisted of five elements of four hydrogen jets impinging on a central oxygen stream at an impingement angle of 30 degrees. Impingement distance from the injection face was  $1/4$  inch. The basic design called for a balanced momentum impingement at a mixture ratio of 1.0. The 4-on-1 impinging-stream injector-mixer is as shown in Fig. 3.



### Catalyst Life Study Hardware

The hardware used during this portion of the experimental program was designed for use with liquid phase reactants at environmental temperatures approaching -400 F. The system (injector, reactor, and nozzle) was designed to operate at nominal thrust levels of 100 pounds at a chamber pressure of 150 psia.

Reactor. The reactor was designed to accommodate a 4-inch-long catalyst bed, 1.5 inches in diameter. Thermocouple bosses were provided for 15 temperature measurements through the length of the catalyst bed. These thermocouples were spaced at 1/4-inch intervals to provide a well-defined temperature profile as a function of catalyst bed length. Additional bosses were provided for chamber temperature and pressure measurements. A threaded nozzle insert adapter allowed for variations in throat diameter. Internal sleeves which fit into the reaction chamber were provided to facilitate insertion and removal of the catalyst bed from the reactor, to enable spacing of the catalyst bed within the reaction chamber, and to minimize heat leak from the reactor. A schematic of the reactor, including injector and catalyst chamber, is shown in Fig. 5. Photographs of the disassembled and assembled reactor are presented in Fig. 6 and 7, respectively. The mass of the reactor was minimized by removal of excess metal surrounding the thermocouple bosses. Mass reduction was considered to be important to facilitate the attainment of liquid hydrogen environmental temperature prior to initiation of a run.

Injector/Mixer. Two injector/mixers were used with this reactor. The first, shown in Fig. 6 and 7, was a conventional 4-on-1 impinging





stream design with four hydrogen jets impinging at a 30-degree impingement angle on a central oxygen jet. Impingement distance from the mixer face was  $1/4$  inch. This injector was all-welded, incorporated no seals or gaskets, and provided a pressure tap in the oxidizer dome to enable measurements of oxygen injection pressure and of the relative time lag between oxygen arrival at the mixer and ignition.

The second design used with the above reactor was similar to the first in all respects except one. The mixer design was based on a 2-on-1 impinging stream pattern, with two oxygen jets impinging at a 30-degree impingement angle on a central hydrogen jet. As the 4-on-1 mixer, this design utilized five elements. Impingement distance was designed as before, with impingement occurring  $1/4$  inch from the mixer face.

#### Large Engine and Igniter Hardware

The large engine and igniter hardware assembly, illustrated schematically in Fig. 1 and pictured in Fig. 8, represented a composite of engine injector, oxidizer dome, and catalytic igniter chamber, as described in the following paragraphs.

Engine Thrust Chamber. The large engine thrust chamber used during this program was government furnished, and was designed for a thrust level of nominally 20,000 pounds at a chamber pressure of 300 psia. The chamber was made of "Rockide"-coated carbon steel, and was designed for use as uncooled hardware. The chamber had the approximate dimensions shown in Fig. 9, including a 7.82-inch-diameter throat, and a contraction ratio of nearly 2.0.



Fuel Manifold. The fuel manifold was manufactured from a circular section of 3-inch stainless-steel tubing welded to a distributor ring. Fuel ports to the fuel manifold were spaced 180 degrees apart, and were fed through a single yoke. Provisions were made in the fuel manifold to enable measurements of fuel injection temperature and pressure.

Engine Injector. The large injector (Fig. 10) incorporated 225 triplet elements, each element consisting of two oxidizer jets impinging on a single fuel jet. The injector design required axial injection of oxidizer, with the oxygen flowing through drilled orifices which passed from the injector back plate through the fuel dome to the injector face plate. To incorporate the catalytic igniter into the injector, the center of the injector was adapted to accept the catalytic igniter, as indicated in Fig. 10 through 11.

Oxidizer Dome. The oxidizer dome was fabricated to adapt to the modified injector, and was as indicated schematically in Fig. 1 and pictured in Fig. 8 and 11. Provisions were made for prechilling the oxidizer dome with liquid nitrogen prior to use, as shown in Fig. 1.

Catalytic Igniter Chamber. The catalytic igniter chamber was designed as shown in Fig. 13 and 14. This chamber incorporated provisions for catalyst bed lengths up to 5 inches long and a diameter of approximately 1.4 inches. The igniter chamber was inserted into the sleeve assembly in the injector as shown in Fig. 1. An annulus 0.020 inch wide between the injector sleeve and the outer diameter of the igniter chamber allowed for isolation of the hot igniter wall from the cold oxidizer and fuel domes. Gaseous hydrogen was passed through the annulus to cool the igniter outer wall.



In addition to the provision for up to a 5-inch-long catalyst bed, the igniter chamber was designed for flexibility in location of the catalyst bed between the injector and the nozzle, and for variation of igniter nozzle area. The latter provision enabled variation of chamber pressure under conditions of nearly constant thrust level.

Igniter Injector-Mixer. A 4-on-1 impinging stream mixer of the type shown in Fig. 6 and 7 and previously discussed was used with the catalytic igniter. The single difference was the variation in orifice sizes to allow for gaseous reactant flow.

#### Test Facilities

Gaseous Oxygen System. The oxygen systems both for catalyst evaluation in reactor hardware and for large engine ignition consisted simply of three manifolded K-bottles which supplied gaseous oxygen to the reactor through an instrumented flow loop. The gaseous oxygen flowed first through a metering orifice for flowrate measurement, then through a sonic orifice, and then to the injector. The sonic orifice serves to isolate the GOX supply system from pressure perturbations when ignition occurs and reaction chamber pressure increases, thus maintaining a constant GOX flowrate. Marotta valves were used to initiate flow. The system was provided with valving to allow for initiation of oxygen flow through a vent system prior to the actual ignition test. As the test was initiated, the oxygen stream was diverted into the reactor, and the system did not suffer the time lags associated with line filling, nor was the metering orifice system over-ranged at the beginning of a run. Figure 15 is a schematic of the oxygen supply system. The oxygen was provided as an ambient-temperature gas.



Gaseous Hydrogen System. The hydrogen supply system is shown schematically in Fig. 16. Hydrogen was supplied to the test stand from high-pressure storage bottles. The flow loop used in the evaluation of catalysts in reactor hardware was the same as that described for oxygen, with one exception: hydrogen was prechilled to selected temperatures before entering the reactor. The chilling was done by means of heat exchange with liquid nitrogen in a double-wall heat exchanger. Hydrogen flowed from the double-orifice arrangement through the inner tube of the heat exchanger. Liquid nitrogen flowed through the annulus from a double-wall dewar container pressurized as necessary with gaseous nitrogen to deliver the desired flowrate. The chilled hydrogen flowed overboard to the atmosphere during the transient phase. When the exit temperature of the hydrogen reached a steady-state value, flow was diverted to the reactor, and the test initiated. The hydrogen supply system for use with the large engine catalytic igniter differed from the above only in the requirement for a heat exchanger. Ambient gaseous hydrogen was used in the large engine catalytic igniter.

Liquid Oxygen System. A single liquid oxygen system schematic is presented in Fig. 17 to describe both the liquid oxygen system for the catalyst life study reactor and the large engine, because the two systems differed only in size, the larger system having a total capacity (125 gallons) nearly triple that of the smaller (43 gallons). The liquid oxygen systems consisted of a liquid nitrogen-jacketed dewar which provided liquid oxygen to the catalytic reactor (or large engine) through a system of valves, flowmeters, and pressure-and temperature-measuring instruments as shown in Fig. 17. Gaseous boil-off was dumped overboard through a vent valve during the hardware chilldown



cycle. Once the hardware was at essentially liquid oxygen temperature, the liquid oxygen main valve was activated and the liquid flowed through the injector to the catalyst bed.

Liquid Hydrogen Systems. The liquid hydrogen systems used with the catalyst life study reactor and with the large engine differed, in addition to facility size, primarily in the physical description of the tanks and in the manner of flow measurement. The liquid hydrogen system used with the catalyst life study engine is shown in Fig. 18. The liquid hydrogen dewar container is a triple-walled vessel containing liquid hydrogen in the inner sphere (25 gallons). The surrounding annulus is evacuated to reduce heat leaks to the inner vessel, and the outer vessel is filled with liquid nitrogen. The outer shell is further covered with 9 inches of insulation to reduce liquid nitrogen boiloff. The liquid hydrogen dewar container is provided with a nominally 25-foot-high vent stack equipped with safety disks, check valves, and pressure-relief valves as indicated.

The small liquid hydrogen flow loop is entirely vacuum jacketed, with the exception of turbine flowmeters and valves, to reduce boiling in the transfer lines and thereby permit accurate flowrate measurements and delivery of liquid hydrogen to the injector. Liquid hydrogen temperatures are measured with platinum resistance thermometers.

The large liquid hydrogen system (200 gallons) consists of a dual-walled vessel with an evacuated annulus surrounding the liquid hydrogen tank to serve as a heat barrier and thereby minimize liquid hydrogen losses from the inner vessel caused by boil-off. The liquid hydrogen system for the large engine differs from that described previously in that a venturi meter is used to measure liquid hydrogen flow.



## Instrumentation

Pressure Measurements. Pressure measurements were obtained by use of Taber, Statham, and Wianko-type pickups. Where necessary, the pickups were close-coupled to reduce pneumatic lag in the transmission of the pressure impulse.

Temperature measurement. Temperature measurements, except for liquid hydrogen temperature, were made through the use of bare-wire thermocouples, either iron-constantan or chromel-alumel. The iron-constantan thermocouple was used for all temperature measurements except the combustion chamber temperature. The latter temperature often exceeds the operating range of iron-constantan; and for that reason, chromel-alumel was used.

Liquid hydrogen temperatures were measured by use of a platinum resistance thermometer specifically designed and calibrated for use with liquid hydrogen.

The catalyst bed thermocouples were inserted to the centerline of the bed. Combustion chamber and catalyst bed temperatures were measured with 36-gage chromel-alumel bare wire thermocouples and recorded on dynalogs and an oscillograph. In addition to the dynalog and oscillograph records, many of the parameters were tape recorded through a Beckman 210 data acquisition system for reproduction on cathode ray tube (CRT) printouts.



Flowrate Measurements. Flowrates of gaseous propellants were measured by a dual technique. A calibrated metering orifice immediately downstream of the propellant reservoir indicated a differential pressure which was converted into a flow measurement. Concurrently, a sonic orifice downstream of the metering orifice served to enable calculation of the flowrate by the nozzle equation for sonic flow. Orifice coefficient and expansion factors were obtained from available literature (Ref. 7 and 8). Each system presented a reliable check on the other in that the two systems agreed within the range of limitations appropriate to each technique.

Liquid propellant flowrate measurements were made by means of Fisher-Porter turbine flowmeters for all flows except liquid hydrogen to the large engine, in which case a venturi flowmeter was used. All volumetric flows were corrected for changes in density caused by temperature and pressure.







## EXPERIMENTAL PROCEDURES

### CATALYST SELECTION

The catalyst selection phase of this program was divided into two major areas: chemical activity measurement, as indicated by degree of conversion of oxygen and hydrogen to water; and physical characterization, as determined by various physical tests. A third area of effort, that of catalyst screening in reactor hardware, represented a brief portion of this task.

#### Chemical Activity

For the purpose of this study, a dynamic or flow method of analysis was selected as the means of measuring catalytic activity. The apparatus is shown schematically in Fig. 2. The specific method of analysis consisted of passing a mixture of oxygen and hydrogen at a pre-established mixture ratio and flowrate through a reactor containing a constant weight of catalyst (5 grams) and fitted with a thermocouple to indicate the presence of reaction. The reacted mixture then passed through a water absorber (indicator Drierite) for removal of water of reaction. The dry gases were then vented. The change in weight of the water absorber during the run reflected the amount of water formed by reaction. Sample bulbs were provided both upstream and downstream of the reactor for sampling both inlet and exit gases. Sample gas analyses, conducted mass spectrographically, provided control checks on the absorber weight-gain method of activity measurement. Catalysts evaluated in fuel-rich reactants were subjected to run durations of 10 minutes with reactants



at an oxygen/hydrogen weight mixture ratio of 5.33, diluted in gaseous nitrogen to provide an adiabatic reaction temperature of nominally 500 F. The selected combined gas flowrate was such that the theoretical water yield was 0.396 gram for the 10-minute run period.

Catalysts evaluated in oxidizer-rich reactants were subjected to 20-minute run durations with reactants at a mixture ratio of 48, diluted in gaseous nitrogen to provide adiabatic reaction temperatures near 500 F. The theoretical water yield was again adjusted to be 0.396 gram by controlling reactant flowrate for one 20-minute run period.

Provision was made for submerging the reactor in a constant-temperature bath to ensure comparability from catalyst to catalyst of the results of the low environmental temperature reactions. In instances where water was seen to freeze on the catalyst pellets or reactor walls, the reactor was also weighed and the gain in weight during the run added to the gain in weight of the absorber to establish the amount of water formed.

#### Physical Characterization

The physical characterization of the catalysts was generally limited to an elemental analysis (spectrographic), the evaluation of the effects of thermal shock on catalyst structural properties, and analyses of surface area, pore volume, and pore size distribution.



### Elemental Analysis

The elemental analyses of the various catalysts were made by Pacific Spectrochemical Laboratories by conventional emission spectroscopy techniques.

### Thermal Shock Treatment

The thermal shock tests (modified sauna treatment) were conducted by means of a modified Engelhard procedure. The catalyst pellets were cooled in liquid nitrogen to thermal equilibrium, placed in a muffle furnace operating at 1000 C (1832 F) for 10 minutes, and then plunged into liquid nitrogen. Damage to the catalyst was observed visually and by means of succeeding activity measurement.

Surface Characteristics. The characterization of surfaces for the various catalysts was accomplished by use of an Engelhard Isorpta Analyzer. With this instrument, nitrogen adsorption isotherms may be obtained from which the surface area, pore volume, average pore diameter, and pore size distribution can be computed. The analytical technique is somewhat lengthy and, for a comprehensive explanation of the procedure, refer to the manufacturer's instruction manual (Ref. 9 ). From a preliminary analysis, however, it is seen that the measurement of surface characteristics is a function of the amount of nitrogen adsorbed by a catalyst under conditions of given temperature and nitrogen partial pressure. Both the technique of application and manner of calculation are based on classical BET (Brunauer, Emmett, Teller) theory (Ref. 10).



Crush Strength. Catalyst crush strength was measured with the device previously described. In general, the catalyst samples were placed on the tester plate and compressed by increasing pressure on the hydraulic jack piston. Compression was increased until the pellet was crushed. The pressure was noted at which the catalyst failed, multiplied by the area of the piston (0.1 sq in.), and recorded as the crush strength of the catalyst. Multiple runs (5 to 10) were made to provide representative sampling results.

#### Catalyst Screening

Catalyst screening with chilled gaseous propellants was conducted in the 1-inch-diameter hardware, using the gaseous propellant systems previously described. The catalyst to be screened was placed in the reactor and chilled to the target temperature by heat exchange with liquid nitrogen flowing through the reactor jacket. Once the catalyst sample reached the desired temperature, gaseous hydrogen flow was initiated. Gaseous hydrogen was dumped overboard during the propellant chilldown cycle, and diverted through the engine once the desired fuel temperature was reached (normally -270 F). Gaseous oxygen, at ambient temperature, was introduced when it was desired to start the test run, the mixture of ambient oxygen and chilled hydrogen producing the desired propellant environmental temperature (Fig. 19).

#### CATALYST LIFE STUDIES

The catalyst life study task was originally designed to provide a measure of the selected catalyst's ability to resist degradation in repeated ignitions with the catalyst starting at -400 F, then being subjected



to 1000 F steady-state combustion, and then undergoing rapid chilling back to -400 F. However, program complications, which are discussed later, arose which resulted in a change in overall program objectives and associated experimental procedures. Additional effort was incorporated into this task to allow for selected reactor parameter variations.

#### Catalyst Life Evaluation

The catalyst life evaluations were conducted in the 1-1/2-inch reactor previously described and illustrated in Fig. 6. A 4-inch-long bed of the catalyst to be evaluated was placed in the reactor with the upstream end of the catalyst bed a fixed distance from the injector face. Liquid hydrogen was passed through the injector and thrust chamber to prechill the catalyst and hardware to nominally -400 F. Once the target temperature was reached, liquid oxygen was injected to effect ignition and sustain combustion for 10 seconds at a constant mixture ratio of approximately 1.25, equivalent to the combustion chamber temperature of approximately 1800 F. The runs were repeated at less than 1-minute intervals until a catalyst failure was evidenced by an ignition failure. Temperature measurements were taken at 1/4-inch intervals along the length of the catalyst bed to provide information on the transient ignition characteristics within the catalyst bed, to define the point of combustion initiation, and by comparison from run to run, to define the rate at which the catalyst deactivates. Pressure measurements were taken across the catalyst bed to aid in defining the manner in which a catalyst physically degrades in service.



### Reactor Parameter Variations

The procedure employed during the previous life evaluation studies was also employed in the analysis of the effects of reactor parameter variations. The significant differences between these operations were the manner in which the catalyst was placed in the reactor, and in the manner in which reactor geometry was varied. Specific reactor geometry variations incorporated with the previously mentioned experimental procedures were changes in mixing zone length between the injector and the catalyst bed, changes in void mixing volume between the injector and the catalyst bed, introduction of catalyst admixes in the first inch of catalyst bed length, and insertion of antichannelling rings which extended from the reactor wall into the catalyst bed for the purpose of redirecting propellant flow from the reactor wall into the catalyst bed.

During the course of these runs, parameter measurements were made as previously discussed.

### PARAMETRIC ENGINE EVALUATIONS

This program task was originally designed to evaluate the effects of changes in engine chamber pressure and mixture ratio on engine ignition delay along with fixed igniter conditions and constant oxidizer ramp rate, the effects of varying oxidizer ramp rate on engine ignition delay with fixed igniter and engine conditions, and the effects of varying igniter chamber temperature and propellant flowrate on engine ignition delay with constant engine conditions and oxidizer ramp rate. For reasons discussed in a later portion of this report, the phase dealing with the evaluation of the effects of oxidizer ramp rate was deleted, and the other two phases were minimized in scope. The two remaining phases were conducted in virtually identical fashion, and are described herein as a single operation.



The initial step in conducting the experimental runs during the parametric engine evaluation was the installation of the catalyst bed. A 3-inch-long by 1.4-inch-diameter catalyst chamber was inserted in the igniter reactor illustrated in Fig. 13, spaced  $3/4$  inch from the face of the injector. A thermocouple was then placed in the combustion chamber downstream of the catalyst bed to sense the temperature generated by the combustion of the igniter reactants. Prior to the initiation of the experimental run, the catalytic reactor, catalyst bed, and associated hardware were chilled to a temperature of approximately -250 F by passing liquid nitrogen through the annulus surrounding the catalytic reactor. In initiating the run, ambient gaseous hydrogen was charged through the catalyst bed with ambient gaseous oxygen injection occurring approximately 1 second later. The timing of this operation is not critical, as long as a fuel lead is employed.

Once the catalytic reaction between the igniter fuel and oxidizer had been initiated, and the igniter allowed to reach a steady-state reaction temperature of nominally 1500 F, liquid hydrogen flow to the engine was initiated. Approximately 1250 milliseconds were allowed for the liquid hydrogen flow to stabilize prior to the injection of liquid oxygen. On sequence, the liquid oxygen was charged to the engine for a period of 250 to 300 milliseconds, a period of time sufficient to obtain ignition data. An oxidizer bleed was used to prime the oxidizer system prior to opening the oxidizer main valve. At the end of this period of time, the oxidizer main valve was closed and the oxidizer purge was turned on. After approximately 50 milliseconds, the liquid hydrogen flow ceased, and the fuel purge was turned on. Finally, the oxidizer to the igniter was stopped, the igniter oxygen system downstream of the igniter main valve was purged to remove oxygen, and the igniter fuel valve was closed. The igniter fuel manifold was then purged and the run was terminated.



The igniter was, in all cases, operated manually, both during the ignition cycle and at run termination. All other operations were sequenced electrically.





## RESULTS

### CATALYST SELECTION AND EVALUATION

A total of 28 noble metal and metal oxide catalysts was evaluated for relative activity during this program task, some in fuel-rich reactants, some in oxidizer-rich reactants, and some in both. Selected catalysts, chosen on the basis of good relative activity, were subjected to analyses for measuring surface characteristics, elemental analysis, resistance to thermal shock, and crush strength. The results of these analyses and discussions of the significance of these results are presented in the following paragraphs.

#### Catalytic Activity

The results of the relative activity measurements of noble metal and metal oxide catalysts in oxidizer-rich reactants are presented in Table 4, with similar results for catalytic activity measurements in fuel-rich reactants presented in Table 5. The results presented in Table 4 illustrate that only three of the metal oxide catalysts offer real potential for accelerating the oxidizer-rich oxygen/hydrogen reaction, and even so, only at near ambient environmental temperatures. These catalysts, Engelhard Industries, Inc. MFP (iron oxide-on-silicon carbide), Girdler Chemical Company T-3 (copper-on-kieselguhr), and Houdry Process Corporation A-25Z (chromia-on-alumina), each show pronounced loss in catalytic activity with reduction in environmental temperature, the MFP retaining only about 4 percent of the ambient temperature activity at an environmental temperature of -320 F, and the A-25Z catalyst retaining only approximately 2 percent over the same



temperature range. The Girdler T-3 catalyst (copper-on-kieselguhr) retains nearly 60 percent of its ambient temperature activity when the environmental temperature is reduced to  $-320^{\circ}\text{F}$ , but even so, the relative activity is only about 11 percent of the theoretical reactant conversion to water. In general, this relative activity level is insufficient to accelerate appreciably the low temperature oxygen/hydrogen reaction. Consequently, none of the metal oxide catalysts evaluated is considered adequate to the task of accelerating the low-temperature oxidizer-rich oxygen/hydrogen reaction. It is significant, however, that at least three of these catalysts are sufficiently active to justify consideration in special applications wherein the oxidizer-rich reactants are at an elevated temperature or only slightly below normal ambient ( $77^{\circ}\text{F}$ ). The same metal oxide catalysts, when subjected to relative activity analyses in fuel-rich reactants (Table 5), show negligible conversion, even in an ambient temperature environment, with one exception. The single exception to this is the Engelhard MFP catalyst. This material gives adequate conversion of oxygen to water (59.5 percent) in an ambient temperature environment, but provides negligible conversion at reduced temperatures of  $-113$  and  $-320^{\circ}\text{F}$  (3.3 and 2.3 percent, respectively). On the basis of these results, and of those presented in Table 4, the Engelhard MFP catalyst offers potential as a dual-purpose catalyst (i.e., oxidizer-rich or fuel-rich reactants) in specialty applications with near ambient temperature reactants.

The noble-metal catalysts, when subjected to relative activity measurements in fuel-rich reactants, gave the results presented in Table 5. Many of these results were extracted from Ref. 3, and are presented for comparison. The noble-metal catalysts, with the exception of the Houdry A-100S and B-100S catalysts and the Sundstrand catalyst, give very high levels of conversion with ambient temperature reactants in an ambient temperature environment.



In an intermediate temperature environment ( $-114^{\circ}\text{F}$ ), the same catalysts provide relative activities which are entirely adequate for acceleration of the fuel-rich oxygen/hydrogen reaction, the lowest recorded relative activity being 66 percent for the Houdry A-200SR. At an environmental temperature of  $-320^{\circ}\text{F}$ , the Houdry A-200SR catalyst is not considered to be capable of adequately accelerating the fuel-rich oxygen/hydrogen reaction because of the reduced relative activity. The remainder of the noble-metal catalysts shown in Table 5 are considered adequate to the task of promoting the low-temperature gaseous phase reaction of fuel-rich oxygen and hydrogen.

The Houdry A-100S and B-100S catalysts are clearly inadequate for promoting the fuel-rich oxygen/hydrogen reaction, and are eliminated from consideration. The Sundstrand catalyst evaluation in laboratory hardware was generally inconclusive. From a theoretical consideration, this catalyst should have been adequate for the efficient low-temperature reaction of oxygen and hydrogen. The relative activity level reported for the environmental temperature of  $-320^{\circ}\text{F}$  (5.0 percent) is not considered adequate for promotion of the liquid propellant reaction, at least in the configurations of interest in this program. One argument which appears to explain the apparent anomaly is the fact that the Sundstrand catalyst was provided in the form of 5/16-inch-diameter spheres, and was evaluated in laboratory glassware designed for use with nominally 1/8-inch pellets. Conceivably, propellant channelling through the catalyst bed without adequate contact with the catalyst may have been such that insufficient contact was made to promote the reaction. A second possible explanation may be that the Sundstrand catalyst may have deactivated in storage. (This problem of general interest will be discussed in more detail in a succeeding section of this report.) Both of these arguments are considered to be possible explanations for the apparent anomaly, because relative activities for the Sundstrand catalyst



are uniformly low for all environmental temperatures. Furthermore, because in general, noble-metal catalysts in ambient fuel-rich reactant mixtures either have activities on the order of 90 percent or higher, or are less than 5 percent, it appears unlikely that a high noble-metal-content catalyst such as the Sundstrand formulation would have an activity in the range of 31 percent.

A significant feature of the Engelhard MFSA and 4X-MFSA catalysts is demonstrated in Table 5. Both of these catalysts retain a very high level of catalytic activity at an environmental temperature of -320 F. The MFSA catalyst is seen to retain nearly 80 percent of its ambient temperature activity (97.0 percent) at -320 F, whereas the 4X-MFSA catalyst retains in excess of 97 percent of its ambient temperature activity (74.5 percent) at -320 F. These results indicate that catalytic activity for this general catalyst composition and method of manufacture is not a strong function of environmental temperature, and further indicate that these catalysts would have a far greater than average probability for continued promotion of the fuel-rich oxygen/hydrogen reaction at cryogenic environmental temperatures.

The results presented in Table 4 illustrate that most of the noble-metal catalysts are capable of promoting the ambient temperature oxidizer-rich oxygen/hydrogen reaction. At an environmental temperature of -114 F, only the Engelhard catalysts and the Houdry A-200SR catalysts provide relative activities sufficiently high to adequately promote the oxidizer-rich oxygen/hydrogen reaction. A possible exception to this is the Shell 405 catalyst. The first batch of this material received showed a relative activity at -114 F of only 9.7 percent, whereas the second batch provided an activity of 34.5 percent under identical conditions. The apparent difference probably results from slight differences in the manufacturing procedure, or, perhaps, from catalyst improvement between batches. At



an environmental temperature of  $-320^{\circ}\text{F}$ , only the Engelhard MFSA and Houdry A-200SR catalyst provide sufficient activity for adequate promotion of the oxidizer-rich oxygen/hydrogen reaction, the relative activity levels being 50.4 and 26.2 percent, respectively.

A summary chart of the most active catalysts is presented in Table 6 for both noble-metal and metal-oxide catalysts in fuel-rich and oxidizer-rich reactants. From this table, it is seen that the Engelhard MFSA and Houdry A-200SR noble-metal catalysts and the Engelhard MFP metal-oxide catalyst provide potential as dual-function catalysts suitable for use in special applications both in fuel-rich and oxidizer-rich reactant combinations. The Engelhard MFP catalyst activity is too low for applications wherein the environmental temperature may be significantly less than ambient. The Engelhard MFSA and Houdry A-200SR would probably be satisfactory at environmental temperatures of  $-300^{\circ}\text{F}$  or perhaps lower. The primary disadvantage to the use of noble-metal catalysts, in oxidizer-rich reactants is the possibility of catalyst damage because of oxidation of the catalytic surface, which may not be a severe problem; however, an insufficient amount of experimentation has been conducted to confirm multiple reignition capability with noble-metal catalysts in oxidizer-rich reactants.

#### Surface Characterization

Surface characterization was conducted on a representative sample of the most active catalysts, and in some instances on catalysts of a type and preparation different from those evaluated and reported in Ref. 3. In general, the results presented in Table 3 indicate the catalysts to fall into two categories. With notable exceptions, the noble-metal



catalysts have surface areas in the range from 200 to 250 square meters per gram, whereas the oxidizer metal catalysts have surface areas from 50 to 100 square meters per gram. Specific exceptions are the Engelhard MFSA, 4X-MFSA, and MFP catalysts, Sundstrand's AAMT-88R, Davison's SMR 55-1097-1, Girdler's 49B, T-893, and T-1205, and Houdry's A-100S. Engelhard's MFSA catalyst was specifically designed as a high-surface-area material in an effort to provide maximum active area for the oxygen/hydrogen reaction. The 4X-MFSA catalyst uses the same substrate as the MFSA, but suffers a very large decrease in surface area because of the impregnation of large quantities ( $\sim 2$  weight percent) of noble metals. This loss in surface area is perhaps characteristic of catalysts having unusually high active-metal contents. The third Engelhard catalyst, the MFP, has an extremely low surface area, primarily caused by the fact that this catalyst is manufactured with a silicon carbide substrate. The silicon carbide, while highly resistant to high-temperature damage, is extremely difficult to prepare in a high-surface-area form. In this particular instance, the manufacturer was concerned primarily with high-temperature resistance, and recognized that surface area would be sacrificed. The Sundstrand AAMT-88R catalyst has a low surface area primarily because of the unusually large (approximately 10 weight percent) noble-metal content.

The Davison SMR 55-1097-1 is high in surface area, but not unduly so for catalysts manufactured on a silica gel substrate. These materials characteristically have surface areas on the order of 500 to 600 square meters per gram. The Houdry A-100S catalyst was intentionally designed by the vendor as a nominally 100 square meter per gram surface area catalyst.

Pore volumes for the various catalysts are approximately as anticipated. From a very general standpoint, pore volume in magnitude is normally equal to about 0.1 to 0.15 percent of the surface area. Certain notable



exceptions are the Houdry A-25Z, Girdler G-67RS and T-893, and Davison SMR 55-1097-1 catalysts. No explanation is given for the large pore volume exhibited by the Houdry A-25Z catalyst or for the low pore volume of the Girdler T-893, an experimental catalyst. The large pore volume of the Girdler G-67RS undoubtedly results from the reduction and stabilization operation conducted after manufacture of the cobalt oxide catalyst. The Davison SMR 55-1097-1 catalyst is prepared on a silica gel substrate, and as such is not considered under the "0.1 to 0.15 percent" rule of thumb. The indicated pore volume of 0.25 ml/gram is consistent with other silica gel-based catalysts.

The average pore diameter presented for the various catalysts is calculated from the surface area and pore volume measurements, and is consistent for the listed catalysts.

#### Chemical Analysis

Based on activity measurements, only eight of the most promising catalysts were submitted for spectrographic analysis in this program. These catalysts were Engelhard's DS, DSS, MFSS, 4X-MFSA, MFSA, and MFP; and Houdry's A-200SR and A-25Z. The results of these analyses are shown in Table 2.

Reviewing the data presented in Table 2, it is noted that the major difference between the DS and DSS catalysts is the amount of sodium present. Because alkali metals are known to promote catalyst sintering with resultant loss in surface area and activity, it is conceivable that the DSS formulation would have greater reignition capability than the DS formulation. The MFSS catalyst is seen to be different from the DS and



DSS catalysts in noble-metal content. The catalytic agents in the MFSS formulation are platinum and rhodium. The vendor contends that rhodium is more active in promoting the reaction of oxygen and hydrogen than either platinum or palladium. Rhodium, however, is reportedly difficult to deposit on a substrate; hence, platinum is used as a base on which to deposit rhodium. Some synergistic effects may result from use of bi-metallic catalyst, but such was not the purpose in the original formulation.

The fourth catalyst shown in Table 2 , MFSA, is seen to be similar to MFSS in the use of platinum and rhodium, but the analysis indicated an absence of any appreciable quantity of silicon, reduced platinum and rhodium content, and the presence of lead as a third metal. The virtual absence of sodium should make this catalyst capable of repeated use without appreciable loss in activity.

The Engelhard 4X-MFSA catalyst has the same nominal composition as the MFSA with a single exception. The noble-metal content of the 4X-MFSA, while almost equally divided between platinum and rhodium, is about six times that of the MFSA.

The sixth catalyst, A-200SR, appears to be simply a platinum-on-alumina formulation, typical of re-forming catalysts used in the petroleum industry. This particular catalyst is one of a series of sulfur-resistant platinum configurations deposited on, nominally, a 200-square-meter-per-gram surface area substrate. The term "sulfur-resistant" refers to resistance to poisoning by the action of sulfur compounds, a property not important in the present application.

The MFP catalyst, manufactured by Engelhard is essentially free of alumina, the indicated 1.1 weight percent probably resulting from impurities in the silicon or iron used in preparing the catalyst. No carbon is shown





in the analysis; however, it is known that the substrate was silicon carbide, and that carbon appears in the catalyst in stoichiometric proportion with the silicon.

The final catalyst, Houdry's A-25Z, consists almost exclusively of aluminum and chromium, indicating that a high-grade alumina was used in its manufacture, and further that no activity-promoting agent was used. The very low alkali metal content of this catalyst should make it highly resistant to activity loss in repeated service.

#### Resistance to Thermal Shock

The resistance to thermal shock, as measured by the procedure previously described, of most of the noble-metal catalysts has been documented in Ref. 3. The results of similar analyses with the remainder of the noble-metal and of the metal-oxide catalysts is presented in Table 7. Disappointingly, the oxidation-type catalysts do not exhibit adequate activity after treatment. It is of interest that the silicon carbide support incurred least damage. The silicon carbide-supported catalyst (MFP), however, was completely inactive after the thermal shock treatment, as shown in the final column of Table 7. Next to the silicon carbide support, kieselguhr appeared to be the most resistant to thermal shock. Most of the oxidation-type catalysts incurred physical damage, however, indicating that the reduction-type catalysts are far superior to the oxidation type insofar as resistance to thermal shock is concerned. This further indicates that the reduction-type catalysts would be superior to the oxidation type, from a structural integrity standpoint, for applications requiring multiple restart capability.



No explanation, other than the fact that the analytical technique becomes less sensitive for activity measurements less than nominally 5 percent, is given for the fact that certain of the catalysts showed an apparent increase in relative activity in oxidizer-rich reactants after the thermal shock treatment.

#### PRELIMINARY CATALYST EVALUATIONS IN REACTOR HARDWARE

In addition to the analyses conducted in laboratory hardware, preliminary experiments were conducted in the 1-inch diameter reactor hardware illustrated in Fig. 3 and previously described. Selected catalysts, chosen on the basis of the results of laboratory analyses, were evaluated and compared at a variety of environmental conditions, in both fuel-rich and oxidizer-rich reactant combinations.

##### Analyses in Fuel-Rich Reactants

The first catalyst analyses in reaction hardware were conducted with the Engelhard MFSA catalyst in fuel-rich (mixture ratio  $\approx 0.8$ ) reactants, to provide a basis for comparison of other catalysts. A summary of the results of these analyses are presented in Table 8 and Fig. 20 through 23. The specific runs, designated as 1 through 4 in Table 8, were conducted under the conditions indicated, utilizing a catalyst bed 1 inch in diameter by 4 inches long. Response characteristics of the Engelhard MFSA catalyst, in terms of the rates of approach of chamber temperature and pressure toward steady-state values, are shown in Fig. 20 and 21. By comparison, it is shown that the approach to steady state is strongly influenced by reactant mass rate. This is consistent with the theoretical prediction previously discussed.



Under conditions comparable to those reported in Table 8 for run 1, the Engelhard MFP produced no ignition, as shown in run 5. In run 6, conducted at a moderately reduced reactant mass rate, and in an ambient (75 F) temperature environment with ambient temperature reactants, the MFP catalyst produced an ignition with an ignition delay time of nominally 2 seconds, defined as the time lag between arrival of the oxidizer in the injector dome and the first indication of temperature in the combustion chamber. At a higher reactant flowrate (run 7), the ignition delay time was reduced to approximately 1 second. The next four runs conducted with the MFP catalyst were conducted for the purpose of defining the minimum environmental temperatures at which this catalyst would produce an ignition. These runs (8 through 11) were all conducted with ambient temperature reactants (81 F), and with progressively colder catalyst and hardware environmental temperatures. Run 8, conducted with a catalyst bed temperature of -100 F, resulted in an ignition after approximately 1 second, but never reached a steady-state condition during a 10-second run. The following run (9) was conducted with a catalyst bed temperature of approximately -150 F, and produced similar results, as did run 10, conducted with a catalyst bed temperature of -190 F. The final run, conducted with a catalyst bed temperature of -225 F, resulted in an ignition failure, illustrating that the Engelhard MFP catalyst is incapable of promoting the desired oxygen/hydrogen reaction under the flow conditions indicated at temperatures below nominally -200 F.

In addition to the extremely long ignition delay times observed with the MFP catalysts, the rates of approach to steady-state conditions were very slow, and ignition was often unstable. In runs 6 and 7 of Table 8, a pressure surge was experienced at the onset of ignition. In run 10, a flashback occurred after approximately 1500 milliseconds. A brief pressure surge was observed, but without apparent damage to the reactor or to the catalyst bed.



### Analyses in Oxidizer-Rich Reactants

A brief series of runs was conducted with the Engelhard MFP (iron-on-silicon-carbide) and MFSA (platinum, rhodium-on-alumina) and Catalyst and Chemicals, Inc. C 13-1 (nickel oxide-on-alumina) catalysts in oxidizer-rich reactant combinations to evaluate the relative capabilities of these materials to promote the oxygen/hydrogen reaction under conditions existing in typical reaction hardware. The significant results of these runs are presented in Table 8 and Fig. 22 and 23. With ambient temperature (75 to 85 F) reactants, in ambient temperature hardware, each of the three catalysts was capable of promoting the desired reaction. Ignition delay times were excessively long with each of the catalysts, as indicated in Table 8 and Fig. 22 and 23. Neither of the metal-oxide catalysts was capable of promoting the oxidizer-rich reaction at environmental temperatures of -250 F. No runs were conducted with reduced temperature reactants. The Engelhard MFSA catalyst was capable of promoting the oxygen-rich (mixture ratio = 93) reaction at a catalyst bed environmental temperature of -206 F (lowest attempted), as shown in Table 7, run 15. At the beginning of this run, however, a pressure surge was noted. A postrun investigation revealed no damage to the catalyst or to the hardware.

Each of the runs conducted with oxygen-rich reactants indicated extremely long response times. Undoubtedly much of this response delay is attributable to the catalyst and reaction system; however, some of the delay must be attributed to the purely pneumatic lag associated with filling the reaction chamber. It should be noted that for the same mass rate, the oxygen-rich reactant combination (mixture ratio = 85) has a density roughly equal to 7.5 times that of a comparable flame temperature fuel-rich combination (mixture ratio = 1.0). Consequently, the purely pneumatic fill time for the oxygen-rich combination would be approximately 7.5 times that for the fuel-rich reactant mixture.



## CATALYST LIFE EVALUATIONS

The original objective of the catalyst life evaluation task was to evaluate the reignition capability of the Engelhard MFSA and MFSS catalysts with liquid phase reactants at an environmental temperature near -400 F, when subjected to repeated experiments for 10 seconds duration at a reaction chamber temperature of approximately 1800 F, and to relate reignition capability to catalyst useful "life." As a result of certain unanticipated difficulties discussed in the succeeding paragraphs, the objectives were modified to an optimization study on liquid oxygen/liquid hydrogen catalytic reactor design, evaluations of the effects of storage environment on catalyst activity, and analyses of means of reactivating partially deactivated catalysts.

### Catalyst Life Studies

During the initial phase of this task, the catalytic reactor illustrated in Fig. 5 through 7 was designed and fabricated on the basis of technology developed in a previous program (Ref. 3). The fundamental design was based on a number of trade-offs. The results of the previous studies with liquid propellants indicated that a certain minimum propellant velocity in the mixing zone between the injector and the catalyst bed is required to eliminate any spiking tendencies. Consequently, the engine diameter must be sufficiently small (for a given propellant mass rate) to ensure that the minimum velocity is equalled or exceeded. On the other hand, a certain minimum liquid hydrogen mass rate is necessary to ensure delivery of liquid hydrogen to the injector. This is dictated by the rate of heat absorption peculiar to the existing liquid hydrogen facility. On these bases, the catalyst life study engine was designed with a 1-1/2-inch-diameter chamber. The catalyst bed length was based on a catalyst/propellant residence time consideration, and was fixed at 4 inches.



The catalysts used initially during this effort were catalysts available from the previous program (Ref. 3) and were approximately 6 months old. The catalyst first selected for evaluation was the Engelhard MFSS formulation. This catalyst was installed in the chamber and preliminary runs with liquid oxygen and liquid hydrogen were conducted. During the initial two runs, reported in Table 9, conducted for a nominally 2-second duration, no satisfactory ignition was observed. The catalyst was then preburned (again) with gaseous propellants, and preparations were made to repeat the liquid propellant runs. During the first run following the catalyst preburn, a delayed ignition resulted, and the catalytic reactor was destroyed. In analyzing the data from this run, it appeared that the explosion resulted from poor mixture ratio distribution. Apparently, ignition occurred at some point in the bed and propagated back to the injector face. Accumulated propellant quantities in the catalytic reactor were such that the explosion resulting from their reaction was sufficient to "balloon" the section of the reactor adjacent to the injector, between the injector face and the catalyst bed. To correct the mixture ratio distribution problem, and thereby eliminate the problem of explosions, the basic injector design was modified to provide a 2-on-1 (oxidizer-on-fuel) triplet pattern, with an impingement distance of  $1/4$  inch, and an included angle of impingement (oxygen-on-oxygen) of 60 degrees. This injector configuration has been used successfully and found to deliver high  $c^*$  efficiency with liquid hydrogen/liquid fluorine propellants, which are not grossly different from liquid hydrogen/liquid oxygen in mixing characteristics. In general, it appeared that the 4-on-1 (hydrogen-on-oxygen) injector did not give optimum mixing, primarily because the liquid hydrogen did not impinge in a theoretical manner, but tended to vaporize, with loss in momentum and



corresponding loss in mixing efficiency. By impinging the two LOX streams, it is thought that atomization occurs, either with or without hydrogen flow, and that thorough propellant mixing occurs when the two propellants impinge.

The catalytic reactor design was also modified for use in the continuing catalyst evaluations, the specific modification being to delete the requirement for removal of steel around the thermocouple bosses in the chamber wall. The new catalytic reactor had a thicker wall, and was correspondingly heavier.

Following fabrication of the 2-on-1 injector and the redesigned reactor, the catalyst life study was reinitiated. The first three runs (4, 5, and 6 in Table 9) were conducted with fresh samples of MFSA catalyst. Difficulties were encountered during runs 4 and 5 in maintaining mixture ratio control because of a gross shift in liquid hydrogen density with small changes in temperature. As a result, the catalyst bed burned out in each of these runs. This problem was resolved, however, during run 6, and with two exceptions, the results appeared visually to be quite satisfactory. The chamber pressure was only about 75 percent of the anticipated value (125 psia), and the combustion chamber temperature thermocouple indicated only 600 F, possible an erroneous figure. It was assumed that performance was lower than anticipated, thereby accounting for the reduced chamber pressure; and runs 7 and 8 were conducted with the same catalyst and under the same conditions as run 6. Run 7 produced results almost identical to those of run 6, and run 8 experienced an internal explosion and loss of the catalyst bed. A more detailed review of the data indicated that the combustion chamber thermocouple had not failed but simply had



not sensed the true flame temperature. It was tentatively concluded that combustion had occurred in runs 6 and 7, but that the flame front was at some point downstream of the thermocouple, perhaps in the convergent section of the nozzle. In retrospect, it is now known that the temperature indicated by the chamber thermocouple was accurate. The reaction between oxygen and hydrogen had occurred in an upstream region of the catalyst bed, probably in the first or second inch of catalyst. The hot reaction products were simply cooled by heat transfer to the remainder of the catalyst pellets and by heat loss to the surroundings. The results from an analysis of run 6 are presented in Fig. 24. From these data analyses, it is seen that the peak reaction temperature occurs at a location 1.5 inches from the front of the catalyst bed and drops progressively through the remaining 2.5 inches of bed. This result explains the reduced chamber temperature and pressure observed during the previous runs.

Following run 8, a smaller-diameter nozzle, equivalent to a chamber pressure of 200 psia for the prescribed flowrate of 0.16 lb/sec and mixture ratio of 1.1, was installed in the engine. This resulted in an increase in characteristic chamber length of 60 percent, with a corresponding increase in propellant residence time in the combustion chamber. Run 9 was conducted with this new nozzle in a manner identical to that of the three previous runs with one exception. Prior to this run, the catalyst was preburned in a fuel-rich atmosphere at a temperature of 850 F for 10 minutes to promote surface reduction and activation. Following this preburn operation, the run was conducted. No ignition was observed, and on termination of the run as the fuel valve closed and the purges were activated, an internal explosion occurred and the catalyst bed was blown out of the chamber. On the basis of these results, it appeared that oxygen might be freezing on the surface of the catalyst, melting and





boiling off into a predominantly gaseous hydrogen atmosphere as the hydrogen flow was terminated, and reacting violently in the presence of the catalyst. On this basis, the valve sequencing was changed to provide a shorter hydrogen lead (1.5 seconds as compared to the previously used 5 seconds) time, and to increase the hydrogen lags. The purges were sequenced to be turned on immediately upon termination of liquid oxygen flow.

Run 10 was conducted with freshly preburned MFSA catalyst, and with the new valve sequencing schedule. The results were encouraging in the sense that no explosion occurred, but was unsuccessful in that no ignition occurred. In run 11 the Shell Development Company's 405 catalyst was used and the procedure of run 10 repeated. The results of run 11 were largely similar to those of run 10 except that a low level detonation appeared to occur at the end of the run. A visual observation of the catalyst showed that about 20 percent of the catalyst pellets had been shattered, but that the catalyst was apparently undamaged otherwise. Because of its limited availability, no further runs were conducted with the Shell 405 catalyst.

Runs 12 and 13 were conducted with 1-second hydrogen leads in the manner of runs 10 and 11. The catalyst used individually in each run was the Engelhard MFSA, preburned in a hydrogen atmosphere for 10 minutes at approximately 750 F. The results of these runs were virtually identical to those of runs 6 and 7, previously conducted with a smaller characteristic chamber length. Pressure was evidenced in the combustion chamber at a level of about 75 percent of the anticipated value, but no temperature was recorded. Postrun inspection indicated that combustion had been evidenced in the section of the catalyst bed nearest the injector, but this may have occurred on shutdown.



## CATALYST DEACTIVATION

The previously discussed behaviors were of forms heretofore unexperienced during catalytic investigations of hydrogen/oxygen ignition. It appeared that the difficulties must have their origin with the catalyst activity. Effort was then diverted to examine the activity characteristics of the catalysts used during these first life study evaluations. The catalytic activity of the Engelhard MFSA catalyst which had been used during these runs was found to have a relative activity of only about 10 percent of the "as received from the vendor" value, and the experimental catalyst life study runs were terminated pending evaluation of the specific problems of deactivation. Initially, the activity loss was assumed to be temporary; and efforts were made to recover the lost activity by various environmental treatments such as drying and reducing the catalyst in a hot hydrogen atmosphere.

The relative activity of the treated catalysts was evaluated at an environmental temperature of -320 F, and compared to that of the original catalyst and of the catalyst used during these experiments; the results are presented as follows:

<u>Catalyst Condition</u>	<u>Relative Activity, percent</u>
Newly received from vendor	78.3
6-months old	6.3
Dried	12.8
Calcined	35.9

The 6-month-old catalyst was withdrawn from the laboratory storage container without any form of pretreatment. The dried catalyst was dried in hydrogen for 2 hours at 680 F and the calcined catalyst was maintained in an air environment at 1110 F for 2 hours. It was apparent from these



results that the catalyst had experienced some damage during the nominally 6-month storage cycle since receipt from the vendor. In considering the various effects of loss in catalytic activity, a thermodynamic analysis indicated that liquid hydrogen, under the conditions of the experimental program, has the capability for freezing seven times its weight in liquid oxygen. From a propellant residence time/heat transfer rate analysis, this cannot occur in the propellant mixing zone of the catalytic life study reactor (1-1/2-inch diameter by 1-inch long), but can occur on the surface of the catalyst, previously chilled to liquid hydrogen temperature (-400 F). The reduced catalyst activity could conceivably aggravate the freezing problem because of the reduced level of energy input to the system from the chemisorption of hydrogen on the catalytic surface. As observed, these treatments resulted in a maximum recovery on only about half of the original activity as discussed in the succeeding paragraph; consequently, it appeared that the activity loss was permanent rather than temporary.

The next most obvious source of catalyst damage is moisture from the air. In discussing the problem of catalyst deactivation during storage with Engelhard Industries, Inc., of Newark, New Jersey (Ref. 11), it was suggested that the most likely cause of catalyst deactivation was caused by moisture contamination. It has been well documented (Ref. 12) that water has a detrimental effect on noble-metal catalysts in general, and on platinum-based catalysts in particular, the specific manner of catalyst damage probably being some promotion of platinum crystal growth in the presence of water. It is important to note that catalyst activity loss by this mechanism is irreversible. It is further reported (Ref. 13) that exposure to air may have a detrimental effect on catalysts in much the same manner as water. However, precise definitions of this effect are not available.



## CATALYST REACTIVATION

Subsequent to a review of the problems encountered as a result of the catalyst deactivation caused by some form of contamination or physical and chemical change in shelf storage, a quantity of deactivated catalyst was subjected to a variety of treatments in an effort to reactivate, or reclaim lost activity. Following the respective experiments, conducted on separate catalyst samples, analyses of relative catalyst activity at an environmental temperature (catalyst and reactants) of  $-320^{\circ}\text{F}$  were performed. The results of these analyses are presented in Table 10. In general, it appears that marked catalyst reactivation can be accomplished by subjecting the catalyst to selected high-temperature treatments. Exposure of the catalyst sample to a dry nitrogen environment for 10 minutes at a temperature of  $500^{\circ}\text{F}$  has the effect of reactivating the catalyst to a level of nearly 90 percent of the original activity. Subjecting the catalyst to a hydrogen atmosphere for 10 minutes at  $250^{\circ}\text{F}$ , however, results in a recovery of only 50 percent of the original activity. At  $500^{\circ}\text{F}$  environmental temperature, exposure to the hydrogen environment for 10 minutes resulted in essentially complete recovery of original catalyst activity, and at a reactivation temperature level of  $1000^{\circ}\text{F}$ , subjection of the catalyst to the hydrogen environment for 10 minutes has the effect of enhancing relative activity to a level approximately 30-percent greater than that of the original vendor catalyst. A similar exposure to dry air at  $1000^{\circ}\text{F}$  for 10 minutes resulted in an enhancement of relative activity to a level approximately 15-percent greater than that of the original catalyst. These results refute the previously considered possibly irreversible deactivation caused by the promotion of catalyst crystal growth by moisture contamination, and indicate the possibility of a deactivation mechanism in which a material is strongly adsorbed on the surface of the catalyst. The specific nature of the adsorbed material is unknown, but it is significant that it is preferentially desorbed in the presence of nitrogen or hydrogen. From the results



presented in Table 10, it is evident that the effect of hydrogen on relative activity recovery or enhancement is greater than that of nitrogen, but that the effect of pretreatment temperature is much more pronounced.

#### REACTOR CONFIGURATION OPTIMIZATION

Concurrently with the catalyst reactivation efforts, activity was initiated for evaluating the effects of reactor configuration on reaction characteristics with liquid propellants. The objective of this program subtask was to optimize the reactor configuration and thereby maximize the benefits of whatever activity the catalyst may have. This configuration optimization was conducted with the partially deactivated catalyst pending delivery of new catalyst from the vendor. A total of 68 experimental runs was conducted during the configuration analysis. Of these, 47 runs produced ignition, 7 failed because of a facility malfunction, 5 resulted in no ignition because of gross catalyst damage in the previous run, and the remaining 9 either produced no ignition or were aborted after a nominally 1-second delay to eliminate the possibility of hardware damage caused by excessive pressure surges resulting from ignition of accumulated unburned propellants. A summary presentation of the results of these runs is given in Table 11.

Initial effort was directed toward optimization of the mixing zone length between the point of propellant impingement and the catalyst bed and toward minimization of catalyst bed thermal damage caused by inadequate mixture ratio distribution, and of propellant channeling along the reactor walls. Because of the potential expense of instrument replacement and the possibility of reactor damage caused by excessive chamber temperatures and/or pressures, this phase was conducted in sparsely instrumented hardware, the reactor instrumentation consisting of chamber temperature and pressure measurement devices.



The indicated runs were conducted under a variety of conditions, as discussed in the following paragraphs. In general, propellant flowrate was targeted at 0.16 lb/sec, and mixture ratio at 1:1. In many of the runs, neither propellant flowrate nor mixture ratio remained constant during the run duration. This flowrate instability during certain runs resulted from catalyst bed damage during the ignition transient. In some instances, the catalyst bed became a fused mass, obstructed flow, and increased pressure drop through the catalyst bed, thereby changing the pressure differential available for driving propellant to the reactor. This change in motive differential pressure resulted in a corresponding change in flowrate. Because the propellant (oxygen and hydrogen) system pressure drops are not balanced, changes in motive differential pressures resulted in changes in mixture ratio. In other instances, the catalyst bed was burned out of the reactor. The resulting loss in pressure drop resulted in an increase in propellant flowrate and an associated shift in mixture ratio. The predominant cause of flowrate instability, however, appeared to result from difficulties in delivering pure liquid oxygen to the catalyst bed in a stable manner. During all runs, a hydrogen lead was used. This hydrogen lead was of such a duration (2 seconds) that liquid hydrogen delivery to the catalyst bed was assured prior to the introduction of oxygen. Oxidizer flowrate instabilities invariably resulted in catalyst bed damage.

In conducting the configuration analyses, it was necessary to bear in mind the thermodynamic and kinetic limitations imposed by the use of liquid hydrogen/liquid oxygen in these types of reactors. As indicated earlier, an equilibrium energy balance for a liquid hydrogen/liquid oxygen system operating at a mixture ratio of 1:1 shows that the liquid oxygen will be in a frozen state, a condition which cannot be expected to induce ignition in a catalytic system. Further, if the liquid oxygen



droplets are in a subcooled state with little liquid heat content left when they begin to enter the bed, the bed itself will result in an oxidizer frozen condition. The problem of promoting catalytic ignition in a liquid hydrogen/liquid oxygen system for a given catalyst is then reduced to one of controlling the kinetics of the heat and mass transfer processes of the liquid hydrogen/liquid oxygen mixture as it progresses towards and into the catalyst bed. It is recognized that to do this only the heat content of the oxidizer is available as a working tool if the mixture ratio is to be rigidly retained. In essence, what is required is a mixing zone length and oxidizer droplet distribution which is compatible with having sufficient oxidizer heat capacity available to raise the catalyst bed temperature to an acceptable level to promote ignition.

#### Mixing Zone Length Optimization

With this in mind, the initial mixing zone length was selected as 1.0 inch. With this configuration, two runs (14 and 15) were conducted. Each run produced an ignition, but resulted in moderate catalyst bed damage and a mild pressure surge. Subsequently, the mixing zone length was reduced to 1/2 inch. Two successful ignition runs (16 and 17) were conducted with this configuration, and inspection of the catalyst bed after the runs indicated severe catalyst burning as a result of inadequate mixture ratio distribution. It was then concluded that 1/2 inch was too short, and the mixing zone length was increased to 3/4 inch. Catalyst damage caused by inadequate mixture ratio distribution did not appear to be excessively severe at this mixing zone length, and there was no evidence of pressure surging occurring during run termination. Consequently, it was tentatively concluded that 3/4 inch represented a near optimum mixing zone length between the injector and the catalyst bed. Problems of catalyst bed damage caused by propellant flowrate instabilities and of possible propellant channeling along the reactor walls remained, however.



### Reactor Geometry Optimization

To minimize the effects of propellant channeling, flow constrictors were installed at 1-inch intervals along the catalyst bed length. These constrictors extended 1/8 inch (one pellet diameter) into the catalyst bed and served to redirect the flow path of channeling propellants into the catalyst bed, thereby improving contact efficiency between the catalyst and the propellants.

Concurrently with the installation of the constrictor rings in the catalyst bed, an attempt was made to further minimize catalyst bed burning as a result of inadequate mixture ratio distribution and to modify propellant flowrate instabilities. This effort consisted of mixing approximately 50-percent inert alumina with the catalyst in the upstream inch of reactor space nearest the injector. In theory, this would serve to pilot the combustion reaction and to better distribute propellant flow through the remainder of the catalyst bed. In practice, a definite advantage was observed. During the first two runs (18 and 19) conducted with this configuration, ignition occurred at a low combustion temperature but was not sustained. Further analysis of these runs indicated that the flame front moved out of the reactor (blow-out).

The next series of runs, conducted with the same chamber and admixed catalyst bed configuration, consisted of eight runs. The catalyst was preburned for approximately 2 minutes at 500 F to reduce any oxide layer from the catalytic metals. Following this, two runs (20 and 21) were conducted which resulted in no ignition, later established to be caused by excessively low mixture ratio (due to two-phase oxidizer flow rather than all liquid), which undoubtedly resulted in the oxygen freezing. The next six runs resulted in stable ignition. The first of these six runs (22)





was conducted at a temperature of approximately 1400 F, corresponding to a mixture ratio of approximately 1.0. The remaining five runs (23 through 27) resulted in chamber temperatures in excess of 2280 F. Because the catalyst bed as such was not instrumented, the temperature level reached by the catalyst bed is not known. At the conclusion of the final run, however, the catalyst bed was severely burned, and approximately half of the catalyst was lost from the reaction chamber.

Following these moderately successful runs, four attempted runs were conducted with the same configuration, but with a new charge of the 6-month-old catalyst. For a combination of reasons, these runs were unsuccessful. A facility valve malfunction resulted in a grossly reduced oxygen delivery to the reactor. This situation was corrected, and the fifth run of the series resulted in a stable ignition with a steady-state chamber temperature in excess of 2200 F. Ignition was smooth, and appeared to propagate toward a steady-state condition. However, as the reaction proceeded, oxidizer flowrate again began to cycle. The result was a cycling chamber temperature and pressure, which resulted in the catalyst bed being destroyed.

The next run (28) was conducted with a 3/4-inch-long mixing zone length with constrictor rings located at 1-inch intervals through the length of the catalyst bed. The catalyst used during this run was preburned in a fuel-rich environment at 800 F for 2 minutes prior to use. A stable ignition propagated uniformly to a steady-state condition. The flowrate was approximately half the target value (0.16 lb/sec). The rate of approach to steady-state was extremely low, and required nearly 10 seconds to reach a stable temperature. Reaction occurred near the injector face and required a longer time to heat the catalyst bed and reactor walls to a steady-state temperature because of the reduced flowrate.



### Catalyst Life Studies With Optimum Reactor Configuration

The next eleven runs (29 through 39) were conducted with a single catalyst charge. The 11 indicated runs were conducted in a reactor configuration consisting of a 3/4-inch mixing zone between the injector face and the catalyst bed (1/2 inch between the point of reactant impingement and the catalyst bed), a 4-inch long catalyst bed with antichanneling rings spaced at 1-inch intervals beginning after the first inch of catalyst and extending 1/8 inch into the bed, and a volume downstream of the catalyst bed equivalent to a characteristic chamber length of approximately 25 (throat diameter = 0.5 inch). The catalyst was preburned at approximately 800 F for 5 minutes prior to initiation of run 29. The first four runs (29 through 32) were ignitions of cold gaseous oxygen with liquid hydrogen, and resulted in flame temperatures from 280 to 482 F. It is interesting to note at this point that the volumetric metering system used during this task indicated the flow of sufficient oxygen to produce mixture ratios of approximately 1.1 (o/f), with flame temperatures on the order of 1400 F. A theoretical analysis showed that gaseous oxygen at the temperature and pressure existing at the fluid metering device (turbine flowmeter) has a density of approximately 7.0 lb/cu ft. On this basis, the mass flowrate for liquid oxygen as compared to that of saturated gaseous oxygen at 400 psia, would be equal to  $\sqrt{71/7}$  or 3.16 times as high. It is significant that the combustion chamber temperatures indicated in Table 9 for runs 29 through 32 are consistent with mixture ratios roughly equal to the apparent 1.1 divided by 3.16, the square root of the indicated liquid oxygen/gaseous oxygen density ratio, thereby confirming the ignition of liquid hydrogen with saturated gaseous oxygen. The remaining seven runs (33 through 39) were conducted with liquid reactants and resulted in combustion chamber temperatures of approximately 1500 F. During the termination of the eleventh run, a chamber



temperature surge occurred which resulted in the loss of much of the catalyst from the reactor. This temperature surge was caused by a partial loss of hydrogen flow caused by a leak which occurred at the main valve. The resulting mixture ratio shift produced an excessive temperature in the catalyst bed and caused a catalyst bed burn-out. No major damage was sustained by the reactor, however.

#### CATALYST LIFE EVALUATIONS

Following completion of the above runs, a quantity of fresh, "zero storage," Engelhard MFSA catalyst was placed in an instrumented reactor of the type shown in Fig. 5 through 7, and experimentally tested for evaluation of catalyst life characteristics under conditions similar to those in runs 33 through 39. The results of six successful runs on a single catalyst sample are presented as runs 40 through 45 in Table 9. Figure 25 illustrates the manner in which a typical temperature profile through the catalyst bed exists. It is noted that the temperature in the front portion of the bed is low, and that temperature increases with distance from the injector.

The reactor configuration used during this series of runs consisted of a  $3/4$ -inch mixing zone length, a 4-inch-long catalyst bed with constrictor rings extending  $1/8$  inch into the catalyst bed at intervals of 1, 2, and 3 inches from the front of the catalyst bed, and a combustion zone downstream of the catalyst bed equivalent to a characteristic chamber length of 25 inches.

Each of the six runs (40 through 45) produced satisfactory ignitions. The only difficulty encountered was the "icing" of the tube leading to the chamber pressure transducer, resulting in the loss of the chamber pressure



measurement. Three of the runs (41, 44, and 45) resulted in chamber temperatures of near 2000 F, and undoubtedly caused some damage. The extent of the damage was rendered indeterminate by the fact that during run termination following run 45, an internal explosion blew the catalyst from the reactor. No apparent damage was sustained by the reactor, however, and the runs were continued with a new sample of catalyst.

The next series of runs was conducted with the Sundstrand catalyst under conditions nearly identical to those used in runs 40 through 45. Prior to the runs, attempts were made to preburn this sample with fuel-rich gaseous reactants. Considerable difficulty was encountered in obtaining an ignition of these ambient temperature gaseous reactants. After attempting a variety of start conditions, ranging from fuel-rich to simultaneous fuel/oxidizer injection, an ignition was accomplished. The catalyst was then preburned in a hydrogen-rich environment for 5 minutes at 1100 F prior to the runs with liquid phase reactants.

Following the preburning operation with gaseous reactants, three successive runs (46, 47, and 48) were conducted with liquid phase reactants at a mixture ratio of nominally 1.1 (oxidizer/fuel) in a -400 F environment without ignition. A chamber pressure surge occurred during shutdown after the third run, and blew the catalyst out of the chamber. The pressure surge undoubtedly resulted from ignition of accumulated oxygen and hydrogen as the reactants warmed up following the run, thus indicating that this catalyst will promote the reaction under some environments.

Because from a theoretical consideration the Sundstrand catalyst should be active in promoting the liquid oxygen/liquid hydrogen reaction, some qualification of the results is appropriate. The Sundstrand catalyst was provided in the form of a nominal 5/16-inch-diameter sphere. This



catalyst, under the most optimum conditions, should be evaluated in a reactor having a minimum inside diameter of 2.5 inches, because the generally acceptable criteria of optimum reactor design require that the ratio of catalyst bed diameter-to-catalyst pellet diameter be equal to a value of 8 or larger. At lower diameter ratios, propellant "channeling" along the walls and through the catalyst bed without contacting the catalyst becomes excessively large and contributes to grossly reduced efficiencies (because of reduced stay times). During the experiments conducted and reported herein, the reactor diameter was 1.5 inches. This corresponds to a diameter ratio of less than 5.0. While antichanneling rings extending  $1/8$  inch from the wall into the reactor were used in an effort to minimize channeling along the walls, it is considered entirely possible that channeling through the interstices of the bed may have been excessively high and resulted in ignition failures.

Following the experiments with the Sundstrand catalyst, a fresh sample of the "zero storage" MFSA was placed in the reactor with the same configuration reported for runs 40 through 45. This material was preburned at 1000 F for 2 minutes in fuel-rich reactants, and subjected to an experimental evaluation (run 49) with liquid-phase reactants. During this run, severe flowrate cycling developed, inducing temperature and chamber pressure cycling. The effects of such cycling on the various temperatures within the catalyst bed are presented in Fig. 26. It is noted that the cycling from thermocouple-to-thermocouple is slightly out of phase, illustrating the movement of temperature fronts through the catalyst bed.

Following run 49, a final attempt was made to conduct a similar run with the same catalyst. However, when the fuel main valve opened to initiate the nominal 2-second liquid hydrogen lead, the reactor suffered an



internal explosion of sufficient magnitude to tear the reactor from the thrust mount and to rupture the reactor wall. As a result, the catalyst life studies were terminated.

#### EFFECTS OF STORAGE ENVIRONMENT ON ACTIVITY

To evaluate the effects of various catalyst storage environments on catalyst activity, a brief program was undertaken concurrently with the catalyst life studies. Samples of "zero storage" MFSA catalyst were subjected to the following:

1. Exposure for 1 month to normal daily atmospheric changes (i.e.,  $40 < T < 75$  F, 10-percent  $< RH < 90$ -percent relative humidity)
2. Exposure in an oxygen-rich atmosphere at a controlled temperature of approximately 150 F for 1 week and 1 month
3. Exposure to complete water soaking after thorough evacuation
4. Exposure to controlled dry storage for 1 month
5. Exposure to normal daily variations in temperature, but at a controlled 100-percent relative humidity for 1 month

The results of the five treatments are presented in Table 11. The new vendor catalyst had a relative activity at an environmental temperature of -320 F, under the conditions defined in Table 11, of 48.8 percent. When exposed to normal daily environmental storage for 1 month in a container open to the atmosphere, the relative activity showed a surprising 4-percent increase (to 52.4). These results most probably reflect non-representative sampling rather than an actual enhancement in catalytic activity. After exposure to an oxygen-enriched atmosphere at a temperature



of approximately 150 F for 1 week, the relative activity was 44.2 percent; whereas a separate sample exposed to a similar treatment for 1 month had a relative activity of 55.0 percent. On the basis of the apparently contradictory results, it is considered that the differences in relative activity between the original sample and the treated samples are the results primarily of nonrepresentative sampling.

The results presented for the catalytic activity of a sample of the MFSA catalyst exposed to complete immersion in water following subjection to an evacuated system (43.7 percent) indicates that short-duration soaking in water has little detrimental effect on relative catalyst activity. However, when subjected to normal daily variations in temperature, but in a controlled 100-percent relative humidity for 1 month, a similar catalyst sample showed an activity loss to 36.0 percent. The final catalyst sample was subjected to controlled dry storage conditions for 1 month. An evaluation of the relative activity of this catalyst indicated an activity level of 47.1 percent, demonstrating no loss in activity under these conditions.

It is significant that only one of the catalysts evaluated during the storage environment tests showed an appreciable loss of activity. This sample, when analyzed after exposure to moisture at ambient temperature for one month, tends to confirm the possible theoretically predicted loss in activity caused by noble-metal crystal growth. It must be noted, however, that the treatments described are representative only of accelerated storage, and may not necessarily be representative of actual effects of long-term storage. There are no direct scaling data by which to compare and extrapolate the accelerated storage effects. Consequently, only inferences can be drawn from the experiments. In short, these accelerated storage experiments indicate only that moisture exposure for extended periods of time probably results in catalytic activity degradation; however, the degradation does not appear to be irreversible.



## PARAMETRIC ENGINE EVALUATIONS

Following completion of the catalyst studies in the 1.5-inch-diameter reactor, the program task designed to evaluate the use of a catalytic reactor as an ignition source in a scalable ( $\sim 14,000$ -pound-thrust) liquid oxygen/liquid hydrogen engine was initiated. This program task was divided into two phases, the first designed to evaluate the effects of large-engine parameter variations on ignition delay time under conditions of constant engine operation, both as a primary propulsion system and as a gas generator.

In conducting the experimental evaluations, each run was performed, then repeated for verification. The run summary is presented in Table 12 in groups of two runs each. The second run in each instance is the verifying run.

From the results of this program task, previously presented, it is apparent that the catalytic igniter can be used successfully for ignition of liquid oxygen/liquid hydrogen rocket engines. Ignition delay times are characteristically on the order of 30 to 50 milliseconds for the large engine, with attainment of steady-state pressure within 300 milliseconds after introduction of liquid oxygen. During certain of the runs, those involving liquid propellants in the large engine at mixture ratios on the order of 1.5 (o/f), ignition was not smooth. This is probably characteristic of attempted ignition of only marginally flammable oxidizer/fuel blends. Because the flammability limit for the nominally  $-400^\circ\text{F}$  blend of liquid oxygen and liquid hydrogen corresponds to a mixture ratio of approximately 1.3 (o/f) any inconsistencies in mixture ratio distribution could result in "flame out" or reaction quenching. Under conditions wherein the propellant mixture ratio was maintained at a level near 5.5





(o/f) such quenching did not occur. While no data were obtained for ignition of intermediate mixture ratio blends, it is considered that ignition blends richer in oxygen than the marginally combustible blends would exhibit no problems of ignition instability.

A very significant aspect of the large-engine ignition studies is the fact that such large-scale liquid oxygen/liquid hydrogen engines can be stably ignited under conditions wherein the ratio of engine to igniter thrust level, and hence a measure of energy ratio, is as high as 1000:1 (runs 13 and 14 of Table 12). This corresponds to engine operation during which only 0.1 percent of the main engine propellants are passed through the igniter. Based on information currently available, this is considerably less than is being used in present-day large liquid oxygen/liquid hydrogen engines.





## DISCUSSION OF RESULTS

The results of this program have provided design information on catalytic igniters which is described in terms of basic ignition phenomena. Among these are the phenomena of flashback and propellant flammability in catalytic reactors, catalytic reactor response and stability, catalyst life and relative activity, catalytic reactor design and scaling criteria, and the ignition characteristics of catalytically-ignited liquid oxygen/liquid hydrogen engines. A discussion of the experimental results is presented in the following paragraphs.

## FLAME VELOCITIES AND FLAMMABILITY

A number of interesting runs has been obtained during the catalytic ignition experiments of this program as well as the previous program (Ref. 3) in which the phenomenon of flashback occurred. It has been hypothesized in the theoretical developments of this report that the flashback phenomenon in which damaging flashback through the bed to the injector can be prevented if the local throughput velocities are considerably greater than those given for the turbulent flame speeds in Fig. 27 and 28. Calculated turbulent flame speeds at these temperatures are:

$$V_{77} = 110 \text{ ft/sec}$$

$$V_{-250} = 26 \text{ ft/sec}$$

$$V_{-400} = 4 \text{ ft/sec}$$

For 1-inch-diameter beds, the minimum average velocities for minimum gaseous flowrate runs of  $\sim 0.01$  lb/sec for the above three temperature



conditions are on the order of 21, 7.4 and 2.1 ft/sec respectively, all of which are below the turbulent flame velocities. On re-examination of the data in Ref. 3 it was noted that at ambient temperatures there were only a few flashbacks observed. However, at -250 F flashbacks were more predominately encountered at reduced flowrates. The most probable explanation for flashbacks not being observed on all of the reduced ( $< 0.01$  lb/sec) flowrate runs is associated with the axial momentum distribution of the mixed jet streams.

It is recognized that when the propellant jets enter a flow area of cross-section much larger than the jet cross-section they cannot immediately adjust to the new flow area. Further, this adjustment requires some length of flow before actual adjustment does take place. The ideal average velocity just downstream of the point of impingement for impinging jets may be determined in the following manner. A momentum balance for axial velocities on such jets (4:1 or 2:1) yields for the axial velocity:

$$\bar{U} = \frac{\dot{w}_{H_2} U_{H_2} \cos \frac{\beta}{2} + \dot{w}_{O_2} U_{O_2}}{\dot{w}_T} \quad (1)$$

For mixture ratios of 1:1

$$\bar{U} = 0.5 U_{H_2} \cos \frac{\beta}{2} + 0.5 U_{O_2} \quad (2)$$

Typical hydrogen velocities are on the order of 1000 ft/sec and the liquid oxidizer velocity is on the order of 60 ft/sec. For a  $\beta$  of 60 degrees,  $\bar{U}$  is then on the order of 500 ft/sec. Recent cold-flow injector studies at Rocketdyne have shown at a distance of 4 to 5



impingement lengths off the injector face the velocity will be on the order of  $1/10$  the theoretical velocity, or in this case  $\sim 50$  ft/sec, a value very close to the flashback condition. Four to five impingement lengths nearly equals the usually used ( $3/4$  to 1 inch) upstream mixing zone.

In Ref. 3, it was found that linear mean throughput velocities had to exceed  $\sim 12$  ft/sec to prevent flashback for liquid injection of both propellants. A similar momentum analysis in these cases shows a velocity on the order of 15 ft/sec, a value again close to the flashback. These values, as well as the gaseous results, are quite close to the flame velocities for the low flowrates. Further, any slight misimpingement could result in velocities less than the flame limits.

Using these requirements, the design of the mixer and mixing zone should provide satisfactory operation.

#### CATALYST-LIMITING TEMPERATURES

The results of Ref. 3 and this program fairly well confirm that the alumina-base noble-metal catalysts can be operated in a repeated manner at temperatures up to  $\sim 1500$  F. Beyond this point the catalysts being to sinter and degrade in activity.

#### REACTOR RESPONSE

As has been predicted by the theoretical results, the primary response factor in the use of a catalyst bed appears to be the thermal response. Examination of the data of Ref. 3 and this study for cold initial beds



shows that the response of a catalytic reactor in terms of pressure buildup follow the predicted time constants. Typical runs are shown in Fig. 29 for cases where flashback did not occur. The calculated time constants are also indicated on the curves. The actual times are a little longer, indicating that other heat losses are undoubtedly occurring. In Ref. 3, it was found that the use of contact resistance heat barriers of thin metal foil could almost completely eliminate extraneous heat losses with the result that the calculated time constants almost identically match the predicted results. It is of interest that the catalytic bed acts as a "linear" thermal system, in that irrespective of what the initial bed temperature is, the time constant remains nearly constant for the given system; and apparently the simple assumed thermal model is adequate when the catalytic activity is high enough to promote the reaction to completion in a given bed.

#### CATALYTIC REACTOR STABILITY

This characteristic of the catalyst bed is most important. Analytical results discussed later (Overall Catalytic Bed Stability) show a relationship of the form

$$Q_I = \frac{\frac{r}{3} \rho_\beta a_m \frac{\alpha(\text{Rate})}{k_g}}{1 + \frac{r}{3} \rho_\beta a_m \frac{\alpha(\text{Rate})}{k_g}} = Q_{II}$$

This equation has three solutions, and predicts the possibility of either one or three steady-state flow and chemical reaction conditions. A large amount of the gaseous phase reaction data in Ref. 3 was re-examined to determine if in fact such instabilities had occurred. The check of this is obtained in examining some of the temperature data for a number of runs. During most of these runs there were three thermocouples in a 3- to 4-inch bed. As a measure of instability, an arbitrary temperature



of 400 F was selected as a dividing point. In Fig. 30 the results for a large number of runs for flowrate against thermocouple location for the MFSS catalysts are plotted. The crosses are indicated for the furthestmost upstream thermocouple reading in excess of 400 F in the apparent steady state.

These runs were at initial temperatures of -250 F. It is observed that the 400 F points occur in a random manner as a function of flowrate. Since flows were maintained completely steady and there were no catalyst degradation effects, it may be concluded that certainly some form of steady-state instability has occurred during these runs. This is important because the minimum bed length must be such as to accommodate these instabilities and still ensure that overall repeatable ignition will occur.

The liquid runs have, as a whole, continually resulted in difficulties in maintaining steady states without flow variations occurring. These flow variations have resulted almost invariably in catalyst bed failures of one sort or another. It is felt that these results, coupled with the prediction of the boiling stability model that the liquid hydrogen runs will be extremely sensitive to small perturbations, show that a great deal of effort is still required if catalytic ignition of liquid hydrogen/liquid oxygen propellants is to be carried out in a stable manner.

#### CATALYST LIFE

The environmental runs at -400 F had originally been designed to provide a measure of catalyst resistance to thermal cycling degradation effects. Because of flowrate instabilities encountered during the attempts to maintain overall control to steady state, it was not possible to obtain a large number of cycles from which quantitative data could be extracted to determine effective bed activity loss. The longest set of cycles was 11. Examination of the temperature data from these runs shows that no two runs were ever identical, and that the measured temperatures were varying widely even within the same run.



A very definite measure of catalyst life can be obtained from the data of Ref. 2, 3, and 6. In Ref. 2 the longest series of attempted runs to steady state was 19 on MFSS catalyst from a cold bed at -250 F heated to 1500 F. These runs were not cycled in general; however, they were successive shots, and the catalyst was behaving during the nineteenth run in the same manner as during the first run for the selected run sequence of hydrogen leads and hydrogen lags on shut down. In Ref. 3, a series of 69 runs was performed with MFSS catalyst at environmental starting temperatures of -250 F. In Ref. 6, where blends of hydrogen/oxygen/nitrogen were evaluated, where the hydrogen/oxygen ratio was stoichiometric, pulse mode work was conducted with pulse lengths varying from 20 to 40 milliseconds and dead times of 20 to 285 milliseconds for cold beds, moderately warm beds (~200 to 500 F) and hot beds (1000 to 1200 F). The maximum number of pulses under each one of these conditions was in excess of 1500 and the catalyst was still performing in a completely repeatable manner at the end pulses, indicating that when the mixture ratio and flowrates can be controlled, the catalyst will provide a reliable ignition technique.

#### CATALYTIC ACTIVITY

It has been indicated earlier that there is presently no way to determine the actual chemical activity level for the catalyst bed. The relative activity ratings serve to rank the catalysts in an order which reflects some manner of overall chemical activity. The oxygen/hydrogen reactant combination is representative of a chemical system having well-defined flammability limits, but only moderately defined autoignition temperatures. The catalytic oxygen/hydrogen system, because of inherent thermal limitations of the catalysts employed, is forced to operate within the





range indicated in Fig. 31 to be nonflammable. In order for the oxygen/hydrogen reaction to be self-sustaining, it is necessary that the gas temperature be raised above the diagonal line and then to the autoignition limit. This increase in gas temperature comes about as a result of two phenomena, thermal energy release to the system by the heat of chemical adsorption of hydrogen on the catalytic surface, and the heat of reaction of oxygen and hydrogen in the vicinity of the catalyst. On this basis, it is apparent that for any given environmental temperature and reactant flowrate, a certain minimum catalyst bed mass is required. This minimum catalyst bed can be determined experimentally; however, to minimize the cost of experimentation over the entire range of catalytic reactor sizes and environmental temperatures, it is essential that some correlation be developed relating reactant flowrate and environmental temperature to minimum catalyst mass and ultimately to chemical activity level. For a conventional tubular reactor, catalyst mass can be expressed in terms of catalyst bed length. The minimum catalyst bed length can therefore be defined as the length at which the reactants and reaction products reach the autoignition temperature for the specific mixture. This minimum catalyst bed length is a function of chemical activity which is also a function of the preignition environmental temperature. Experimentally, the relative activity changes with environmental temperature have been defined in laboratory apparatus and the results were presented earlier. Because the relative activity does not change in a linear manner with environmental temperature, it is convenient to develop some sort of analytical scaling criteria to relate the specific change in activity to environmental temperature. Using a value designated as  $\alpha$  as a measure of the specific reactant conversion per unit of bed length, an empirical relationship may be developed to indicate the manner of change of  $\alpha$  with respect to distance through the catalyst bed, because temperature is in



some manner proportional to catalyst bed length. The equation indicating the relationship between reaction rate and temperature is

$$K \sim C_1 T^{n'} e^{-\frac{\Delta E}{RT}} \quad (3)$$

Because the percent conversion in an actual bed,  $\alpha$ , is proportional to  $K$  for an incremental catalyst bed length, Eq. 3 may be rewritten as

$$\alpha \sim C_1' T^{n'} e^{-\frac{\Delta E}{RT}} \quad (4)$$

This conversion must be related to relative activity in some manner and Eq. 4 may then be reduced in terms of the laboratory relative activity conversion percentages.

$$\ln(\text{percent conversion}) = \ln C_1'' + n' \ln T - \frac{\Delta E}{RT} \quad (5)$$

Using the data presented in Table 13, values for  $C_1''$ , a measure of the molecular collision frequency and the fraction of molecular collisions between molecules having sufficient energy to react,  $n'$ , a measure of the manner of change in conversion level with temperature and  $\int(\frac{\Delta E}{R})$ , a function of the activation energy for the catalytic reaction have been calculated for selected catalysts and are presented in Table 13. It is seen that each catalyst has a unique set of constants, and that the effective activation energy varies over a wide range from catalyst to catalyst. The precise meaning of this information is still under investigation; however, certain operations on the data can now be made for extrapolation purposes. Because the values  $C_1''$  and  $C_2''$  are constant for



a given catalyst, the effect of temperature, and hence of catalyst bed position, on reaction promotion relative to some base value may be presented as

$$\frac{\alpha_1}{\alpha_2} = \left(\frac{T_1}{T_2}\right)^n e^{-\frac{\Delta E}{R} \left[\frac{1}{T_1} - \frac{1}{T_2}\right]} \quad (6)$$

The precise manner of evaluation of  $\alpha$  has not been well defined; however, the relationship presented in Eq. 6 enables direct prediction of relative activity over a range of environmental temperatures for a given catalyst operating at a constant reactant/catalyst mass ratio.

It is also of interest as to what minimum relative activity measurement may be acceptable to operating a catalyst bed. As demonstrated in this program extremely low activity levels (~10 percent) will still promote ignition of the liquid hydrogen/liquid oxygen system. For gases, no specific effort along these lines has been carried out; however, it is suspected that a level of 10 to 20 percent is the lower limit at which ignition can still be achieved in a minimum length catalyst bed. It must be recognized that because the hydrogen/oxygen system is spontaneously unstable that very low activity levels may be used to induce reaction, provided the bed is long enough and time of ignition is not of concern.

#### LIQUID PROPELLANTS REACTOR SCALING

On the basis of the data obtained during this program and in Ref. 3, it is not possible to arrive at firm overall scaling criteria for catalytic ignition of liquid oxygen/liquid hydrogen propellants. It is possible,



however, to arrive at the conclusion that flashback with its associated pressure surging and burnout characteristics can be eliminated by satisfying some minimum propellant mixing zone flow velocities as determined simply through a consideration of flame velocity being about 3 to 5 ft/sec at -400 F and designing this zone for a 12 to 15 ft/sec mean velocity (at -400 F). This can be readily accomplished either by contouring the mixing zone or by packing this zone with some inert material to reduce open cross-sectional area and thereby increase propellant linear velocity. It is also possible to conclude, from a consideration of the kinetics of heat and mass transfer on the liquid oxygen droplets in the mixing zone, that the energy of these droplets may be used to raise the temperature of the catalyst bed at the injector end of the reactor sufficiently high to promote the reaction of liquid oxygen with liquid hydrogen. This is possible, however, only as a result of certain tradeoffs. If the mixing zone length is too long, and the contact time between propellants is too long, the liquid oxygen droplets tend to freeze, and thereby virtually eliminate any possibility of reaction. Conversely, if the mixing zone length is too short, reaction occurs before the propellants become homogeneously mixed, and local catalyst burning occurs as a result of nonuniform mixture ratio distribution. For the hardware used in this program, the optimum mixing zone length appeared to be nominally 0.75 inch. In this hardware, the oxidizer/fuel impingement distance was 0.25 inch from the injector face for a 2-on-1 (oxygen-on-hydrogen) injector element design, the liquid oxygen injector pressure drop was 50 psi, and the liquid hydrogen injector pressure drop was 70 psi. On this basis, 0.50 inch was the apparent optimum distance between the point of propellant impingement and the catalyst bed. In considering other possible combinations of injector design and pressure drop characteristics, it must be recognized that the degree of propellant atomization has a pronounced effect on the kinetics of heat and mass transfer.



## GASEOUS PROPELLANT REACTOR SCALING

The available -250 F gaseous data were examined for the MFSS 1/8-inch spherical catalyst in small diameter (1-, 1.5-, and 2.0-inch) hardware for cases of ignition vs no ignition as a function of superficial mass flowrate vs length of the bed. It is recognized that each of the catalytically promoted reaction systems has a minimum catalyst/reactant contact time requirement, and that in heterogeneous flow reactors, this minimum "residence time" is a function of a number of variables, including catalyst activity and reactant environmental temperature, relative homogeneity of reactant mixing, catalyst configuration, and reactor configuration.

It was not possible within the scope of this program to evaluate separately the relative effects of each of these parameters. The evaluation of the minimum residence time required was for a given reactor, injector, catalyst configuration, and environmental temperature. The results of this investigation are presented in summary in Table 14. In each instance, surveys of a large number of runs were made to define the superficial mass velocity at which the catalyst failed to promote the reaction. The three runs presented for each catalyst bed length are representative of two conditions wherein reaction was satisfactorily promoted, and one run during which no reaction was noted. This latter case corresponds to a superficial mass velocity in excess of the maximum allowable for the specific catalyst bed length.

In addition to the tabular presentation of the results of the run survey, the selected runs are corrected such that they may be considered on a comparable basis and plotted in Fig. 30. The theoretical relationship for bed length is given in a later section of this report (Eq. 77), and served as the basis for correction of the individual run data. In general, the data were corrected to a common  $\bar{P}$  and  $\bar{T}$  basis by simply using corrected



ratios of  $\bar{P}_1/\bar{P}_2$  as indicated in Eq. 7. The average temperature was assumed nearly constant for the runs. The result is given in Fig. 31. It is seen that when this is done the curve more nearly fits the predicted form of  $X \sim \dot{w}^{0.41}$ . On this basis, it is felt then that higher mass rate extrapolations may be made by using the simple ratio:

$$\frac{X_2}{X_1} = \frac{\bar{P}_{T_1}}{\bar{P}_{T_2}} \frac{G_{o_2}^{0.41}}{G_{o_1}^{0.41}} \quad (7)$$

where the "1" condition is taken off the upper part of the curve.

For the same activity levels, sizing of catalyst effect extrapolations can also be made but with less confidence because the entrance effects change. For fixed  $G_o$ , this extrapolation gives

$$\frac{X_2}{X_1} = \frac{\bar{P}_{T_1}}{\bar{P}_{T_2}} \left(\frac{a_1}{a_2}\right)^{1.41} \quad (8)$$

For operation at different inlet temperatures it is necessary to consider activity ratios. The scaling parameter here is proportional to the reaction rate constant

$$\alpha \sim T^n e^{-\frac{C}{T}} \quad (9)$$

Therefore for  $G_o$  fixed,

$$\frac{X_2}{X_1} = \frac{\bar{P}_{T_1}}{\bar{P}_{T_2}} \left(\frac{T_1}{T_2}\right)^n e^{-C\left[\frac{1}{T_1} - \frac{1}{T_2}\right]} \quad (10)$$

where the values of  $n$  and  $C$  pertain to a given catalyst of a base reference relative activity.



The extrapolation from one relative activity to another is somewhat more questionable. It can be done through use of the ratios of the approximate rate constant curve fits; however, in general, at this time it would not be recommended. Also, the extrapolations are for a bed of 1-inch diameter with a chamber to pellet ratio of 8. Direct scaling to larger reactors should provide conservative estimates, because there may be some energy loss from the reactor for this data.

Direct scaling to smaller reactors is not recommended. Data from Ref. 2 on small engines equivalent to 1 to 5 pounds of thrust show that a catalyst bed of 1- x 1-inch diameter dimensions is required for the MFSS catalyst.

Of final interest here is that in the range of 10- to perhaps 75-pound-thrust equivalence a rule of thumb for using the 1/8-inch MFSS (and MFSA) catalyst in its fresh state of activity can be obtained from Fig. 31 as

$$\frac{\dot{w}}{A_c V} \sim \frac{0.04 \text{ lb/sq in.-sec}}{\text{cu in. catalyst}}$$

At the low end of the curve it is almost exact, while at the high end it is conservative..

The basic curve is for a mixture ratio of 1:1 and a -250 F inlet propellant condition.

#### OVERALL CATALYTIC IGNITER DESIGN

These studies, coupled together with the previous studies (Ref. 3 ) indicate that igniters operating with gaseous phase oxygen/hydrogen or



liquid oxygen/gaseous hydrogen down to  $-300^{\circ}\text{F}$  can be reliably designed for use in oxygen/hydrogen engine systems. The liquid phase oxygen/hydrogen data indicate that there is still a need for research effort to support design of liquid oxygen/liquid hydrogen catalytic igniters. The primary problem appears to be concerned with phase state control in the catalytic bed. The boiling effects are most pronounced in that the physical properties of liquid hydrogen vary widely with temperature. The theoretical basis for the gaseous propellant design appears to be well founded, except in two areas. First, smaller catalyst sizes have not been experimentally investigated. It is known from the theoretical results that smaller catalyst sizes should promote better reaction; however, they also have attendant higher pressure drops. Second, the effects of bed entrance lengths cannot be predicted at this time. A small amount of research effort here would clear up this deficiency. The combined empirical/theoretical results now available are sufficient for design of igniters from a 10-pound-thrust class to perhaps a 200-pound-thrust class. The supporting data will be nearly exact at the lower level, while at the upper level the designs based on this data will be conservative.

## LARGE-ENGINE IGNITION CHARACTERISTICS

### Phase I: Effects of Engine Parameter Variations

In evaluating the effects of engine parameter variations on ignition delay at constant igniter conditions, it is apparent that under comparable conditions of engine propellant mixture ratio, ignition delay time for a given engine configuration is a function of propellant flowrate. A comparison of runs 1 and 2 of Table 12 with runs 5 and 6, and of 3 and





4 with 7 and 8, indicates that ignition delay time varies to the nominally 1.4 power with changes in propellant flowrate:

$$\frac{\dot{w}_1}{\dot{w}_2} = \left( \frac{\theta_1}{\theta_2} \right)^{1.4} \quad (11)$$

where

$\theta$  = ignition delay time

Similarly, the effect of mixture ratio on ignition delay time, at comparable chamber pressure, is represented by the equation

$$\frac{MR_2}{MR_1} = \left( \frac{\theta_1}{\theta_2} \right)^{1.25} \quad (12)$$

Therefore, for this fixed engine geometry, the relationship between ignition delay time, and mixture ratio and propellant flowrate can be given by

$$\frac{\theta_1}{\theta_2} = K \left( \frac{\dot{w}_1}{\dot{w}_2} \right)^{1/1.4} \left( \frac{MR_2}{MR_1} \right)^{1/1.25} \quad (13)$$

This relationship is based on a limited number of experimental observations and should be considered in this light, pending further confirmation.

During each of the runs 1 through 8 (Table 12) ignition of the mainstage propellants was accomplished with the catalytic igniter operating at nominally 1500 F and a propellant flowrate of approximately 0.16 lb/sec.



Chamber pressure in the igniter was controlled at a target level of nominally 350 psig. During the remaining runs, however, the igniter flowrate was varied at constant mixture ratio to evaluate the effects of ignition energy variations on ignition delay at constant engine conditions. During each run, the igniter chamber pressure was maintained constant and at a level approximately 50-psi higher than the target engine chamber pressure.

#### Phase II: Effects of Igniter Parameter Variations

During runs 9 through 14 and 21 and 22, the igniter flowrate was varied from 0.18 to 0.067 lb/sec while the engine steady-state condition was maintained at a flowrate of approximately 45 lb/sec and a mixture ratio between 5.4 and 6.3. The results show that the lower igniter propellant flowrate is adequate for ignition of the large engine at the indicated conditions of operation, and that the ignition delay time is an inverse function of igniter flowrate, as shown in Fig. 32.

The results illustrated in this figure demonstrate the dependence of ignition delay time on ignition source intensity. Because the igniter hot-gas temperature was the same during each run, the interaction effects of temperature and mass flowrate can be ignored. The fundamental variable then becomes mass flowrate through the igniter relative to the large engine. In the limit (i.e., a case in which the igniter flowrate grossly exceeds the engine flowrate), the ignition delay time for the engine is zero milliseconds. At the other end of the scale, as the igniter flowrate approaches zero, the ignition delay time theoretically approaches infinity. In practice, however, a condition would probably be encountered in which a "hard start" of sufficient magnitude to destroy the engine would result. In any event, the results presented in Fig. 32 demonstrate the range of igniter parameter variations studied to be within the limits of satisfactory operation.



Under the conditions shown in Table 12 for runs 15 through 20, wherein the igniter flowrate was varied from 0.175 to 0.067 at constant igniter mixture ratio, it was demonstrated that the lower flowrate is adequate for ignition of the large engine propellants. During these runs, designed to evaluate the effects of igniter parameter variations on ignition delay characteristics for a liquid oxygen/liquid hydrogen engine operating as a gas generator, the propellant flowrate was controlled at approximately 10 lb/sec and a mixture ratio of 1.5. During each experiment, ignition occurred after an approximately 40-millisecond delay, indicating that, for this mode of engine operation, ignition delay is not particularly controlled by igniter energy level. In comparing the results of these runs with those reported for runs 9 through 14, 21, and 22, it is apparent that the controlling factor, insofar as ignition is concerned, is not the energy level of the igniter, but instead is the temperature/mixture ratio/mass flowrate relationship existing with the mainstage propellants. At the reduced temperature level (near -400 F), the low-mixture-ratio oxygen/hydrogen propellant combination is only marginally flammable, and consequently would have a longer ignition delay time. Conversely, at the reduced mass flowrate, relative to runs 9 through 14, 21, and 22, the ignition delay time would be reduced. Apparently, these compensating factors combined to create a limit condition which controls ignition delay time regardless of the ignition energy level provided. Undoubtedly, some ignition energy and temperature level exists below which ignition would become erratic, occur after excessive periods of ignition delay, and, under the most severe conditions, result in destruction of the engine. This, however, is not limited to catalytic igniters alone, and would be true with any ignition technique.



Under certain conditions, the engine propellant reaction showed a tendency to quench following the ignition cycle. This was generally caused by the marginal flammability of the low-mixture-ratio liquid oxygen/liquid hydrogen propellant combination. However, to illustrate the specific manner of the quenching tendency, typical chamber pressure traces for normal ignition and for erratic ignition are presented in Fig. 33. Even under conditions wherein the tendency to quench existed, no apparent tendency for chamber pressure spikes was noted.

During the course of the parametric engine evaluations, no major hardware damage was observed. It is worthy of note, however, that moderate large-engine injector discoloration occurred as a result of overheating. This was anticipated on the basis of the injector design. Because performance was not an objective of this program, no special effort was devoted to optimization of large-engine injection characteristics. Consequently, the injector was designed as a "workhorse" device, with injector elements considerably larger than those that would be selected on the basis of optimum performance and durability characteristics.



## THEORETICAL CONSIDERATIONS

For completeness of understanding of the overall catalytic process and its application in rocket engine ignitors certain theoretical hypotheses and results are presented. The optimum design of catalytic reactors for use in the ignition systems of  $H_2/O_2$  rocket engines requires consideration of several fundamental aspects of a catalytically promoted heterogeneous reaction. For such an application the propellants are premixed upstream of the catalyst bed and then flowed through the bed where reaction is promoted to a sustained and completed state upon leaving the catalyst bed. Among the fundamental parameters affecting the overall design of these reactors are the propellant mix flammability limits, flame velocity envelope, catalyst pellet limiting temperatures, the magnitude of the chemical, pneumatic, and thermal time response characteristics of the bed, overall reactor scaling criteria including bed length, diameter, effective catalytic activity, and pressure drop, and overall reactor stability. In addition to these characteristic parameters, the nature of the selected catalyst is quite important to the design. The design parameters and catalyst enables reaction to take place in the absence of sustained combustion. The flammability limits of  $H_2/O_2$  under widely varying conditions of temperature and pressure are not too well defined. However, some data are available which may be used to define catalytic requirements.

## LITERATURE SURVEY

The literature is meager as to the effects of temperature and pressure of the gas mixture on the flammability limits of  $H_2/O_2$ , and most experimenters appear to be convinced that pressure effects are not significant except at ultra low pressures or very high pressures. Zabetakis of the Bureau of Mines, whose values of flammability are accepted by the Liquid Propellant Information Agency (Ref. 14), states that their studies of



flammability limits of various combustible gases indicate that the flame temperature remains nearly constant at both the upper and lower flammability limits, in a manner independent of pressure. With this as an assumed basic characteristic of the  $H_2/O_2$  system, calculations may be made to determine the change in flammability limits with a change in either  $O_2$  or  $H_2$  inlet temperature, while maintaining the flame temperature constant through changes in mixture ratio. Using Zabetakis' experimental results of the flame temperatures being 1078 F and 2290 R respectively at 4 and 94 percent  $H_2$  in  $O_2$  at 522 R, the flammability limits at the lower and upper limits have been determined (Ref. 15) and the results are given in Fig. 35 for a range of  $H_2$  and  $O_2$  inlet temperatures. The results of this calculation show the flammability limits to be insensitive over a wide range of  $O_2$  temperatures at the upper limit (fuel-rich). If the thermodynamic reasoning of this calculation is correct, these results can also be assumed valid for heterogeneously mixed propellants (liquid oxidizer, vaporized oxidizer, and hydrogen gas). On the other hand, the results at the lower limit (Fig. 34) show a very strong dependence on the inlet environmental conditions. The engine ignitor research reported herein is primarily associated with fuel-rich mixtures. For conditions beneath the flammability curve, the system will not support a reaction in the normal sense, that is when it is exposed to an ignition source whose temperature is above the autoignition temperature for the  $H_2/O_2$  mixture.

Little data is available on the limiting autoignition temperature; however, it is felt that it is on the order of 1000 F and reasonably constant over a wide range of mixture ratios (Ref. 16). The actual flammability limits and autoignition temperatures appear to be influenced by the type of the experiment, and apparently no detailed experiments have been carried out to determine the limiting ignition behavior of various ignition source sizes and strengths on premixed gas mixtures ( $H_2/O_2$ ) in varying sizes of experimental containers.



Because this type of limiting flammability behavior has not been investigated, it is thus difficult to exactly determine the nature of a catalytic promoted heterogeneous reaction in the zone beneath the flammability curves. At this time, the theoretical results are hypothesized to mean that for a given size catalytic bed, the energy release characteristics must be such that the temperature of the flowing mixture of  $O_2$ ,  $H_2$ , and  $H_2O$  products will be raised above the autoignition limit by following a path generally as indicated in Fig. 34, in order that sustained combustion may occur. For a given flowrate and bed diameter, there must therefore be a minimum bed length which will promote the reaction in a sustained manner. Any bed lengths shorter than this critical bed length result in a reaction temperature less than that necessary for sustained reaction.

#### FLAME VELOCITY EFFECTS

A consideration of flame velocity is important in a catalytic reactor even though the reaction may be proceeding without the presence of actual flame initially in the bed. Actual flame may be established further downstream in the bed, and should there exist local nonhomogeneous mixture ratios upstream in the bed which tend towards stoichiometry, the possibility of flashback along such nonhomogeneities becomes quite strong. Flashback to the injector mixer usually occurs with resultant bed burnout as well as mixer damage.

For overall igniter reliability such a situation is undesirable, and a knowledge of flame velocity characteristics is needed for the proper design of the catalytic reactor. Quantitative data on flame velocities under a wide variation in temperature and pressure and conditions of turbulent flow are even less available than flammability data. The results presented here partly follow the survey discussion in Ref. 17.



Most of the laminar flame speed data in the literature (Ref. 17) have been obtained either with strongly oxidizer-rich mixtures or at near stoichiometric conditions. For laminar velocities, the highest velocities are observed for slightly fuel-rich mixtures (Ref. 18 and 19). For pressures ranging between 0.5 and 15 atmospheres, the laminar velocities correlate quite well with the following expression:

$$S_u \text{ (cm/sec)} = 1200 + 315 \ln P_{\text{atm}} \quad (14)$$

Flame speeds at 90 atmospheres exceed the prediction of Eq. 14 by ~75 percent. Flame speeds obtained at these higher pressures correlate better with the following expression:

$$S_u = a P^b \quad (15)$$

where  $b$  is a measure of order of reaction. The laminar burning velocities of Ref. 18 and 19 are shown in Fig. 28.

Very little turbulent flame speed data are available for  $O_2/H_2$  mixtures; however, a minimum of isolated data (Ref. 20 and 21) obtained with turbulent stream conditions are presented in Fig. 28. These data correspond quite well with air/hydrogen data in Ref. 22, as far as the relative values of  $S_{ut}$  and  $S_u$  are concerned.

It is known that the percent of turbulence affects the turbulent flame velocity. A theory of flame propagation in turbulent gases developed by Karlovitz and reported in Ref. 23 attempts to account for stream turbulence and is expressed as follows:

$$S_{ut} = S_u + \sqrt{2 S_u u'} \quad (16)$$





The value of  $u'$  to be used in Eq. 16 is not the approach stream value, nor necessarily the value in the flame zone, but is probably some intermediate value. Use of  $u'$  values from the flame zone will generally result in conservative (high) values of  $S_{ut}$ , and is recommended for that reason. However, accurate measurement of flame zone turbulence is quite difficult. The turbulence velocity  $u'$  is known to be a function of local Reynolds number, approaching asymptotic values for large Reynolds numbers (Ref. 24).

From a qualitative standpoint, the relative values of turbulent and laminar flame speed for  $O_2/H_2$  are presented in Fig. 27. These values were obtained with ambient or near ambient gases. Using the theoretical flame speed expression of Mallard and Le Chatelier, as shown below, an approximate temperature correction may be made to obtain qualitative design data.

$$S_u = \bar{k} (T_b - T_{ig}) / [(T_{ig} - T_u) p \bar{C}_p \Delta X_b] \quad (17)$$

In this equation,  $T_{ig}$  may be taken as the flammability limiting temperature for  $O_2/H_2$ , and  $T_u$  as the premix temperature. The extrapolation procedure is to take the ratio of  $S_u$  at two different temperatures,  $T_u$ , for a fixed pressure.

$$\frac{S_u(T_1)}{S_u(T_2)} \approx \left( \frac{T_{u1}}{T_{u2}} \right)^{3/2} \left( \frac{T_{b1} - T_{ig1}}{T_{b2} - T_{ig2}} \right) \left( \frac{T_{ig2} - T_{u2}}{T_{ig1} - T_{u1}} \right) \quad (18)$$

Assuming  $\bar{C}_p$  and  $\Delta X_b$  are roughly constant and the conductivity,  $k$ , being with a further approximation of  $T_b - T_{ig}$  roughly constant, Eq. 18 can be reduced to

$$\frac{S_u(T_1)}{S_u(T_2)} \approx \left( \frac{T_{ig2} - T_{u2}}{T_{ig1} - T_{u1}} \right) \left( \frac{T_{u1}}{T_{u2}} \right)^{3/2} \quad (19)$$



Because the ratio  $(T_{ig2} - T_{u2})/(T_{ig1} - T_{u1})$  remains nearly constant,

$$S_u(T_2) \simeq S_u(T_1) \frac{T_{u2}}{T_{u1}}^{3/2} \quad (20)$$

Belles (Ref. 22) has empirically investigated the effects of temperature on air/H<sub>2</sub> mixture flame velocities over a limited range and found the exponent that most nearly fits the data to be approximately 1.41 in place of the above theoretical value of 1.5. There are no available O<sub>2</sub>/H<sub>2</sub> data at various initial temperatures to which this result may be compared. However, there are some hydrocarbon/air data of Dugger available for propane (Ref. 25) through which Eq. 20 can be checked. Dugger's data show  $S_u$  rises from approximately 2 ft/sec at 84 F to 6.3 ft/sec at 650 F. Using Eq. 20, the predicted upper limit velocity would be 5.6 ft/sec.

The ambient results of Fig. 27 have been corrected to lower inlet temperatures in Fig. 28 by the use of Eq. 20. It is pointed out that these velocities may not necessarily be the maximum possible for consideration in the catalytic reactor. Flashback caused by nonhomogeneous mixture ratio distribution may conceivably result in flame velocities in excess of those previously considered. Belles (Ref. 22) has stressed that selection of values of  $S_{ut}$  for design purposes to prevent flashback must be made with extreme caution because of the lack of ability to accurately measure and interpret turbulent flame speeds. It has been shown (Ref. 22) that flame speeds are strongly affected by boundary velocity gradients. Under certain conditions, the laminar flashback boundary velocity gradient may be as high as 10,000 ft/sec/ft for the air/H<sub>2</sub> mixture. It is further shown (Ref. 22) that the ratio of the turbulent to laminar boundary velocity gradient is approximately 2.8. Therefore, the turbulent flashback boundary velocity gradient may be as high as 28,000 ft/sec/ft. These values are strongly affected by mixture ratio, and fall drastically as hydrogen concentration increases from approximately 40 volume percent.



It is difficult to explain why the ratio of turbulent to laminar flashback boundary velocity gradients is as high as 2.8. Since the flashback boundary velocity gradient is a function of the laminar burning velocity rather than the turbulent burning velocity, the turbulent burning velocity cannot be used in any way to explain this fact. It is tentatively concluded that the explanation lies in the penetration of the flame into the laminar sublayer at the burner wall and that the flame approaches the wall more closely in turbulent than in laminar flow.

Seemingly, some advantage may be gained in the design of a catalytic reactor by virtue of certain geometrical design considerations which tend to promote quenching. Because flames are quenched by excessive loss of heat or active specie or both, to the adjacent walls, design of the reactor walls to maximize heat losses within the mixing zone may tend to minimize flashback to the injector face. Experiments have shown that flames in a mixture of given temperature, pressure, and composition cannot pass through openings smaller than some minimum size. Considerable effort has been expended, and is summarized in Ref. 22, on the evaluation of various materials and size ranges for use as "flame traps." In general, it is reported that  $O_2/H_2$  flames are extremely difficult to arrest, and further that the quenching distance is proportional to the system pressure to some exponential value. For the range of hydrogen concentrations of interest in this program, the value of the exponent is approximately -1.0. In the event that flame traps are to be considered in the design of a catalytic reactor, certain words of caution are given. The quenching distance for turbulent flashback is only about one-fourth that of laminar flashback, and calculations of this value must be based on turbulent burning velocity considerations. Furthermore, the flame traps designed on the basis of turbulent flashback considerations are flame stoppers, and may not be effective against detonation.



In addition, to the problem of potential flashback, consideration must be given to the possibility of formation of a detonation wave. Under certain conditions, an ordinary flame traveling through a vessel containing a combustible mixture can transform into a detonation. The detonation wave then advances at a velocity equivalent to a Mach level of approximately 4 or 5 in the unburned mixture. In the case of such a detonation wave, the ratio of pressure behind the wave, in the burned gas, to that ahead of the wave may be as high as 18, depending on the mixture ratio (Ref. 16). In addition, a strong convective flow of burned gas follows the detonation wave, and when such a pressure wave meets an obstacle, the momentum of the burned gas is added to the pressure effect, and very large forces may be exerted. Under certain conditions, these forces may be sufficient to rupture the catalyst retainers and blow the catalyst from the reactor. In practical applications, the flame must travel a considerable distance before detonation occurs, the run-up distance being a function, among other factors, of surface roughness, reactor diameter, reactant mixture ratio, and system pressure. Furthermore, the onset of detonation can be delayed by making the reactor walls of an acoustically attenuating material, or by providing a sudden enlargement in the reactor. These factors would be well considered in the design of a catalytic reactor, with some thought given to the potential advantages of a contoured mixing zone between the catalyst bed and the injector, and of antichannelling rings within the catalyst bed. A more satisfactory approach, however, is to ensure that the reactants are homogeneously mixed in the mixing zone. For oxygen/hydrogen mixtures, the detonation limits are from 15 to 90 volume percent hydrogen (Ref. 16). For the catalytic oxygen/hydrogen system, the maximum recommended mixture ratio (o/f) is 1.1, corresponding to approximately 96 volume percent hydrogen, well beyond the detonation limit. Therefore, homogeneous mixing of reactants in the mixing zone should eliminate any possibility of detonation within the catalytic reactor.



From these considerations of flame speeds and flashback characteristics, it can be seen that the propellant mixing sections of the igniter hardware must be designed very conservatively regarding through put velocities to ensure the prevention of flashing or detonation in the mixing chambers.

#### CATALYST PELLET LIMITING TEMPERATURES

It has been found in previous catalytic ignition research programs on  $H_2/O_2$  that the commercially available noble metal catalysts begin to sinter if the reaction temperature is higher than 1500 F (Ref. 2 ). Further, it has been found that the catalytic igniter exhaust temperature must be at least  $\sim 1000$  F to ignite a  $H_2/O_2$  engine, and the higher the temperature the more reliable the igniter. Because the catalyst promotes the reaction in a heterogeneous manner, the surface temperatures will be higher than 1500 F. It is of interest to determine the magnitude of the difference between the catalyst and effluent temperatures to appreciate the probable temperatures at which sintering takes place.

As reported elsewhere in this report, an estimate of the amount of 1/8-inch spherical MFSA catalyst required to promote the  $H_2/O_2$  reaction to completion in a small reactor can be obtained from

$$\frac{\dot{W}}{A_c V} \sim 0.04 \quad (21)$$

where

$A_c, V$  in inch units

The average bed density of the typical random packed 1/8-inch spherical catalyst particles is 0.025 lb/cu in. The actual particle density is  $\sim 0.033$  lb/cu in. The external projected particle surface per unit weight



of catalyst and per unit volume of catalyst is needed to make the temperature calculations. The projected surface area per unit weight is given by

$$a_m = \frac{\pi D^2}{\frac{\pi D^3}{6} \rho_p} \quad (22)$$

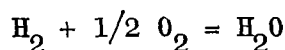
and is  $\sim 14.5$  sq ft/lbm in this case. The external surface area per unit bed volume is then given by

$$\bar{a} = a_m \rho_{\text{bed}} \quad (23)$$

and is  $626 \text{ ft}^{-1}$  for the 1/8-inch catalysts of interest here. Of interest are approximate values for 1/16 inch catalyst. The value  $a$  is  $\sim 20.4$  feet, and  $a_m$  is  $\sim 980 \text{ ft}^{-1}$ . To estimate the temperature difference between the catalyst pellet surface and the free stream, it is necessary to obtain a measure of the various species flux at the catalytic pellet surface, which can be done through the relation

$$\dot{N}_{i0} = \dot{N}_{\text{H}_2\text{O}} \left( \frac{R_i}{R_{\text{H}_2\text{O}}} \right) / a_m \quad (24)$$

In Eq. 24 the ratio  $R_i/R_{\text{H}_2\text{O}}$  is the ratio of moles of species "i" produced per mole of water vapor. Considering the basic reaction



the ratios are given as follows:

<u>species, i</u>	<u><math>R_i/R_{\text{H}_2\text{O}}</math></u>
$\text{H}_2$	-1.0
$\text{O}_2$	-0.5
$\text{H}_2\text{O}$	<u>1.0</u>
	-0.5



$\dot{N}_{H_2O}$  is the rate of water production in moles/sec-sq ft. Next consider a 1 cu in. of catalyst material with a cross section of 1 sq in. At a mixture ratio of 1:1 (o/f) the water conversion is ~56.3 percent of the total propellant flowrate. Using Eq. 23 and 24 the molar rate of production of water is 0.0392 moles water/sec/lb of catalyst. For this example Eq. 24 becomes

$$\begin{aligned}\dot{N}_{io} &= 0.0382 \left( \frac{R_i}{R_{H_2O}} \right) / 14.5 \\ &= 0.00271 \frac{R_i}{R_{H_2O}} \text{ moles/sec-sq ft}\end{aligned}\tag{25}$$

The molar flux of water is then 0.0027 moles/sec-sq ft. Considering the heat of reaction, the energy generation at the catalyst surface is ~101 Btu/sec-sq ft. To obtain the temperature difference, an estimate of the effective film coefficient is needed. To do this, a packed bed heat transfer relation is needed. A currently acceptable relationship is the following (Ref. 26):

$$J_H = 0.91 \text{ Re}^{-0.51} \psi, \text{ Re} < 50\tag{26}$$

$$J_H = 0.61 \text{ Re}^{-0.41} \psi, \text{ Re} > 50\tag{27}$$

The Reynolds number is defined here as

$$\text{Re} = \frac{G_o}{a_m u_f \psi}\tag{28}$$

For spheres  $\psi$  is approximately unity (Ref. 26). For the example of interest the Re number is approximately 200 for 500 to 1000 F gases composed predominately of water vapor and hydrogen.



$$\therefore J_H = 0.0506$$

The heat transfer  $J_H$  factor is defined as

$$J_H = \frac{h}{C_p G_o} Pr^{2/3} \quad (29)$$

For the gases of interest,  $h$ , the film coefficient, is determined from Eq. 29 to be  $\sim 0.584$  Btu/sq ft-sec-F. The temperature difference is then given by

$$\Delta T = \frac{Q}{h} = \frac{101}{0.584} = 173 \text{ F}$$

In summary, the catalyst pellet surface temperature on the average will be on the order of 200 F higher than the local gas stream. Upon the surface of the pellet, the individual catalytic active sites may be considerable hotter than the average calculated value, because the areas of the active sites on a local basis are considerably less than the projected surface areas and, consequently, for the same energy generation rate, the temperature difference must be larger. Therefore, a 1500 F bulk stream temperature in a reacting catalyst system will have catalyst pellet surface temperatures at least as high as 1700 F, with a strong probability of local surface temperature being considerably higher. This is important to the use of platinum-type catalysts because temperatures higher than this may be enough to result in catalytic activity destruction for restart purposes. Further, sintering may also begin to occur. Smaller catalyst ( $\sim 1/16$  inch) may have even higher temperatures.





## ANALYTICAL PREDICTION OF CATALYTIC REACTOR RESPONSE CHARACTERISTICS

Research studies carried out to date at Rocketdyne on the catalytic reactor system indicate that the overall response of a packed bed catalytic reactor can be determined through the consideration of three rate processes: (1) the heterogeneous chemical reaction, (2) the pneumatic filling of the catalytic reactor chamber, and (3) the effective rate of energy loss from the bulk stream flow. The theoretical determination of the magnitude of each of these processes is presented below.

### Heterogeneous Chemical Reaction

For the overall reaction, to proceed it is necessary for  $H_2$  and  $O_2$  to diffuse to the active sites and for the reaction products to diffuse away from the catalyst particles. The limiting species diffusion will be the oxygen species because of its higher molecular weight.

On the assumption that the rate-limiting step in the catalytic reaction sequence is the diffusion of oxygen from bulk stream through a stagnant film of the hydrogen to the surface of the catalyst, and further assuming that the products of the surface reaction desorb and diffuse into the bulk stream instantaneously, the rate of the chemical reaction can be calculated by use of the relationship

$$\frac{dN_A}{dt} = \frac{D_{AB} P_A}{RTZ \Delta P_{BM}} (P_{A1} - P_{A2}) \quad (30)$$

The diffusivity,  $D_{AB}$ , can be estimated from the equation (Ref. 27)



$$D_{AB} = \frac{0.000929 T^{3/2} \left( \frac{1}{M_A} + \frac{1}{M_B} \right)^{1/2}}{P \sigma_{AB}^2 f (kT/\epsilon_{AB})} \quad (31)$$

$D_{AB}$  is calculated as

$$D_{AB} = \frac{0.000929 (1090)^{3/2} \left( \frac{1}{32} + \frac{1}{2} \right)^{1/2}}{10.2 (3.20)^2 (0.315)}$$

$$= 0.81 \text{ cm}^2/\text{sec}$$

for the reaction system operating at 150 psia and 1500 F.

On the basis of the foregoing assumptions, the concentration of oxygen at the catalytic surface is negligible; consequently, for an overall propellant mixture ratio of 1.1, the mole fraction hydrogen in the bulk stream is 0.94 and at the catalyst surface is 1.0. The mean partial pressure of hydrogen is therefore

$$\Delta P_{Bm} = (10.2) \frac{(0.94 - 1.00)}{\ln \frac{0.94}{1.00}}$$

Assuming the effective diffusion film thickness to be equal to several hydrogen mean free paths ( $5.9 \times 10^{-6}$  centimeter at 1500 F, 150 psia) and the diffusion area equal to one mean free path cross section, the diffusion rate,  $dN_A/dt$ , calculated from Eq. 30, equals  $\sim 10^{-12}$  molecules/second. This indicates a diffusion time per oxygen molecule of less than  $10^{-12}$  seconds; consequently, the chemical heterogeneous reaction response times may be ignored in considering overall response times and attention may be focused on the pneumatic and thermal response times if the catalyst possesses sufficiently high activity to promote the reaction.



### Pneumatic Filling Response

To obtain an order of magnitude calculation on the pneumatic filling response, several assumptions may be made.

1. The catalyst bed pressure drop is ignored.
2. The gas is uniformly heated to  $T_g$  in the bed.
3. The energy losses are negligible.
4. The gaseous propellant input and output to the reactor are sonic at all times.

Of these assumptions, the latter three are most restrictive. To be rigorously correct, a set of equations involving the continuity, momentum, and energy equations should be solved simultaneously. The assumptions that the gas is heated uniformly to  $T_g$  does not account for some pneumatic delay effects caused by a reduced temperature for some early parts of the pneumatic filling operation; however, it will be shown in the next section that the error attributable to this effect may be ignored when compared to the overall response. The injector flow is not sonic throughout its flow condition, but this assumption enables a simple solution to be obtained which allows an order of magnitude analysis to be made of the pneumatic response time.

The pneumatic response time is obtained by considering a simple transient mass balance on the overall combustion volume. With the assumption of sonic flows, the flowrates into and out of the chamber are given by

$$\dot{w}_1 = \frac{C_1 P_1 A_1}{\sqrt{T_1}} \left( \frac{M_1}{29} \right)^{1/2} \quad (32)$$



$$\dot{w}_2 = \frac{C_2 P_c A_t}{\sqrt{T_g}} \left( \frac{M_2}{29} \right)^{1/2} \quad (33)$$

Using the perfect gas law

$$PV = wRT \quad (34)$$

and letting  $P$  and  $w$  be variables of time,

$$\frac{dP}{dt} = \frac{RT}{V} \frac{dw}{dt} \quad (35)$$

Approximating  $\frac{dw}{dt}$  by  $\dot{w}_1 - \dot{w}_2$

$$\frac{dP_c}{dt} = \left[ \frac{C_1 P_{c1} A_{t1}}{\sqrt{T_{g1}}} \left( \frac{M_1}{29} \right)^{1/2} - \frac{C_2 P_c A_t}{\sqrt{T_g}} \left( \frac{M_2}{29} \right)^{1/2} \right] \frac{RT_g}{V} \quad (36)$$

Eq. is integrated to obtain

$$P_c(t) = \frac{C_1 P_{c1} A_{t1}}{C_2 P_{cs} A_t} \left( \frac{M_1}{M_2} \right)^{1/2} \frac{1}{\sqrt{T_{g1} T_g}} \left[ 1 - \exp - \left\{ \frac{R \sqrt{T_g} C_2 A_t}{V} \left( \frac{M_2}{29} \right)^{1/2} t \right\} \right] \quad (37)$$

Overall engine response percentage is obtained by dividing  $P_c(t)$  by the steady-stage value of  $P_{cs}$ :

$$\frac{P_c(t)}{P_{cs}} = 1 - \exp - \left[ \frac{RC_2 A_t}{V} \left( \frac{M_2 T_g}{29} \right)^{1/2} t \right] \quad (38)$$

The quantity  $V/A_t$  is a rocket combustor is normally the definition of the characteristic combustion chamber length and is a parameter indicative of the combustion dwell time in the chamber. In the catalytic reactor, the same definition may apply if the volume is taken as the free



volume in the chamber, including the catalytic bed interstices. The final form for the response of the chamber to pneumatic filling is given by

$$\frac{P_c(t)}{P_{cs}} = 1 - \exp - \left[ \frac{RC_2}{L^*} \left( \frac{M_c T_g}{29} \right)^{1/2} t \right] \quad (39)$$

By definition, the time constant (the time for the ratio of  $P_c(T)/P_{cs}$  to reach 63 percent of its steady-stage value) is found by

$$1 - \frac{P_c(t)}{P_{cs}} = e^{-t/\tau} \quad (40)$$

Comparing Eq. 39 with 40, it is seen that the time constant  $\tau$  is given by

$$\tau = \frac{L^*}{RC_2} \left( \frac{29}{M_c T_g} \right)^{1/2} \quad (41)$$

The time to 95 percent of steady state is approximately

$$t_{95} \approx 3\tau = \frac{3L^*}{RC_2 P_{cs}} \left( \frac{29}{M_c T_g} \right)^{1/2} \quad (42)$$

For a perfect exhaust nozzle (no discharge losses) Eq. 42 reduces to

$$t_{95} \approx 3.09 \left( \frac{L^{*2}}{M_c T_g} \right)^{1/2} \text{ ms} \quad (43)$$

With  $L^*$  in inches and  $T_g$  in R, Eq. 43 is plotted in Fig. 35 for various effective  $L^*$  and  $T_g$  values. A typical catalytic reactor might have an  $L^*$  of 100 inches. At an exhaust temperature of 2000 F, the response time would be on the order of 3.8 milliseconds. As will be shown in the next section, this response time may be considered to be virtually instantaneous and is not the major contributor to overall reactor response time. The bed pressure drop effects are considered later in this report.



### Thermal Response

The thermal response of the catalytic bed may be examined in two ways. First the response of the individual pellets may be determined. Secondly, the response of the bed as a heat sink may be found. The one which shows the largest time will then be the controlling factor in determining the catalytic bed thermal response.

Individual Pellet Response. The individual particle response is found by considering a single pellet suddenly exposed to a hot gas with a constant film coefficient. The formulation of this situation is as follows:

$$\frac{\partial T_p}{\partial t} = \alpha' \left( \frac{\partial^2 T_p}{\partial r^2} + \frac{2}{r} \frac{\partial T_p}{\partial r} \right) \quad (44)$$

The following boundary conditions apply:

$$T_p(r, 0) = 0 \quad (45)$$

$$\frac{\partial T_p}{\partial r}(r = a, t) = \frac{h}{k} (T_o - T_{p,a}) \quad (46)$$

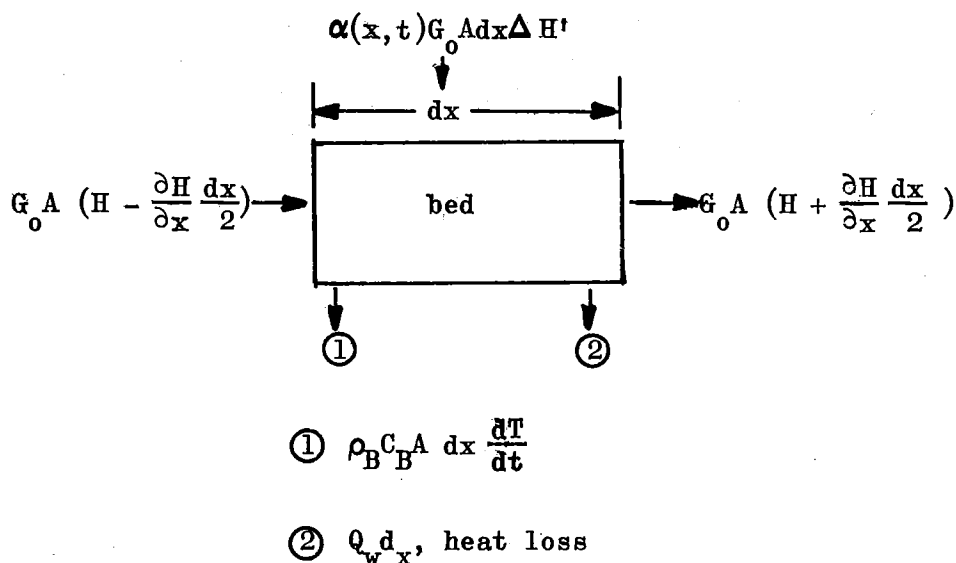
$$\frac{\partial T_p}{\partial r}(0, t) = 0 \quad (47)$$

A solution to this classical conduction problem is given in Ref. 28 in terms of the dimensionless Biot and Fourier numbers,  $hR/k$  and  $\alpha t/R^2$ .

Using the previously determined film coefficient of  $\sim 0.5$  Btu/sec-sq ft-F for alumina pellets, the heat transfer results indicate that the 1/8-inch pellet responds nearly instantaneously to all temperature variations of the bulk stream.



Overall Bed Response. By assuming that the bed is effectively infinitely conductive as indicated in the previous section, and therefore in thermal equilibrium with the bulk stream gas, a new thermal equilibrium analytical model may be described as shown below:



The energy balance yields:

$$\alpha(x,t)G_o dx A \Delta H' - G_o A dx \frac{\partial H}{\partial x} = \rho_B C_B A dx \frac{\partial T}{\partial t} + Q_w dx \quad (48)$$

where  $GA$  is the total propellant flowrate. The factor  $\alpha(x,t)$  is a measure of catalytic bed activity (more will be said about this factor in later sections).  $\Delta H'$  is the heat of reaction in the bed.

To obtain a measure of thermal response several simplifying assumptions may be made at this time.



1. The enthalpy term may be replaced by

$$\frac{dH}{dx} = \bar{C}_p \frac{dT}{dx} \quad \text{in} \quad (49)$$

This is not strictly correct for a reacting mixture unless  $\bar{C}_p$  is defined as given in Appendix A.

2. The  $\alpha$  factor is constant and the bed is long enough that all reaction occurs in the bed, providing an instantaneous rise to the final reaction temperature,  $T_o$ .
3. No wall losses exist.

With these assumptions Eq. 48 may be reduced to

$$\dot{w} \bar{C}_p (T_D - T) dt = \dot{M}_B C_B dt \quad (50)$$

where

$$T = T_1 \quad \text{at } t = 0 \quad (51)$$

The integration result is

$$\frac{T_o - T}{T_o - T_1} = \exp - \left[ \frac{\dot{w} \bar{C}_p t}{\dot{M}_B C_b} \right] \quad (52)$$

The thermal time constant,  $\tau_H$ , for 95 percent thermal response is

$$\tau_H \approx 3000 \frac{\dot{M}_B C_B}{\dot{w} C_p} \text{ ms} \quad (53)$$





For the experimentally determined mass loading factor of

$$\frac{\dot{w}}{A_c V} \approx 0.04 \frac{\text{lb/cu in.-sec}}{\text{cu in.}}$$

for 1/8-inch catalyst spheres and a 0.025 lb/cu in. catalyst,  $\tau_H$  is ~150 milliseconds. Clearly,  $\tau_H$  is much larger than any of the other response times; and therefore, it may be considered to be the dominating factor in considering overall catalytic reactor response characteristics. For 1/16-inch catalysts,  $\tau_H$  may be expected to be considerably smaller.

#### CATALYTIC REACTOR SCALING CRITERIA

Scaling criteria for a gaseous propellant catalytic reactor can be derived in terms of the bed length, bed diameter, effective catalytic activity, and pressure drop effects for a given mass rate. Criteria for these parameters are presented in the following sections.

##### Bed Length

The bed length functional form will be determined only for the steady-state case. To do this, it is assumed that the chemical reaction steps are controlled by mass transfer to the catalyst surfaces. This being the case, the reaction rate is related directly to the diffusional flux. It has previously been determined that the flow is turbulent in most cases of interest, and further that the oxidizer species transport is the limiting factor for reaction.



The mass transfer coefficient may be defined in terms of the mass fractions of oxygen in the free bulk stream and at the catalytic wall:

$$\dot{m}_{O_2} = \rho h_D (W_\infty - W_W) \quad (54)$$

where  $\rho$  is the total gas density. For a fluid of constant properties,  $\rho$  is nearly constant. It has been previously shown that the catalyst surface temperature is only  $\sim 200$  F higher than the bulk stream. At 1500 F, the assumption of constant density involves an error of only  $\sim 9$  percent in the density. The mass fractions may be converted to partial densities to give

$$\dot{m}_{O_2} = h_D (\rho_{\infty, O_2} - \rho_{W, O_2}) \quad (55)$$

If it is then assumed that the effects of local temperature differences are small (as indeed they are for only a 200 F difference) and the perfect gas law is applied, Eq. 55 may be reduced to

$$\dot{m}_{O_2} = \frac{h_D}{R_{O_2} T} (P_{O_2, \infty} - P_{O_2, W}) \quad (56)$$

It is assumed that all oxidizer species that diffuse to the wall are instantaneously consumed, leaving  $P_{O_2, W}$  being zero. Therefore,

$$\dot{m}_{O_2} = \frac{h_D P_{O_2, \infty}}{R_{O_2} T} \quad (57)$$

To proceed further, a relation is needed for  $h_D$ . The Lewis relation deriving the analogy between mass and heat transfer yields (Ref. 28)

$$h_D = \frac{h}{\rho c_p} \quad (58)$$



as a working relation for  $h_D$ . Therefore, the turbulent heat transfer relationship used earlier for determining the catalyst surface temperature may be used for  $h_D$ , simply by dividing the result by the local specific heat. Using Eq. 27

$$h_D = \frac{0.61}{\bar{p}} G_o \text{Re}^{-0.41} \text{Pr}^{-2/3} \quad (59)$$

Substituting for the Re number,

$$h_D = \frac{0.61}{\bar{p}} G_o \left( \frac{G_o}{a\mu_f \psi} \right)^{-0.41} \text{Pr}^{-2/3} \quad (60)$$

Substituting this result in Eq. 57, the mass flux of  $O_2$  species is

$$\dot{m}_{O_2} = \frac{0.61}{R_{O_2} T} \frac{P_{O_2, \infty}}{\bar{p}} G_o \left( \frac{G_o}{a\mu_f \psi} \right)^{-0.41} \text{Pr}^{-2/3} \quad (61)$$

Because the oxygen species is being used up and the temperature is increasing, both  $P_{O_2, \infty}$  and  $T$  are functions of distance along the catalyst bed. The rate given in Eq. 61 is per sq ft of projected catalyst surface. The catalyst surface per unit volume is given by Eq. 23 as

$$\bar{a} = a_m \rho_{bed} \quad (23)$$

Multiplying this by the volume  $A_c x$  gives the cumulative surface area

$$a_c = a_m \rho_{bed} A_c x \quad (62)$$

The surface distribution per unit length is then

$$a' = a A_c \quad (63)$$

The mass flux or reaction rate per unit length of bed is obtained by multiplying  $a'$  times  $\dot{m}_{O_2}$



$$\text{Rate} = \frac{0.61 a A_c}{R_{O_2} T} \frac{P_{O_2, \infty}}{\bar{\rho}} G_o \left( \frac{G_o}{a \mu_f \psi} \right)^{-0.41} \text{Pr}^{-2/3} \quad (64)$$

Maintaining an overall species mass balance requires this quantity to be equal to the decrease in oxygen species in the bulk stream. To obtain the relation for this term, consider a small differential element of length  $dx$  and write a mass balance on it for the oxidizer species. The result is

$$\frac{-dG_{O_2}}{dx} = \text{Rate} \quad (65)$$

The oxidizer rate through the bed is

$$A_c G_{O_2} = \frac{\rho_{O_2}}{\rho T} G_o A_c \quad (66)$$

Using the perfect gas law:

$$A_c G_{O_2} = \frac{P_{O_2} \bar{R}}{R_{O_2} P T} G_o A_c \quad (67)$$

$$\therefore -A_c \frac{dG_{O_2}}{dx} = A_c \frac{\bar{R} G_o}{R_{O_2} P T} \frac{dP_{O_2}}{dx} \quad (68)$$

Setting this result equal to the rate equation, the final differential form for the partial pressure distribution of oxidizer species is obtained.

$$\frac{dP_{O_2, \infty}}{dx} = \frac{-0.61 a P_T P_{O_2, \infty}}{\bar{R} T \bar{\rho}} \left( \frac{G_o}{a \mu_f \psi} \right)^{-0.41} \text{Pr}^{-2.3} \quad (69)$$

Separating and integrating:



$$0.61 \int_0^x \frac{P_T}{RT} \left( \frac{G_o}{a\mu_f \psi} \right)^{-0.41} \frac{Pr}{\bar{\rho}}^{-2/3} dx = \int_{P_{O_2, \infty, out}}^{P_{O_2, \infty, in}} \frac{dP_{O_2, \infty}}{P_{O_2, \infty}} \quad (70)$$

To proceed further in the analysis,  $P_T$ ,  $\bar{R}$ ,  $T$  must be known as functions of  $x$ . As a first approximation, they must be assumed nearly constant to yield:

$$x = 1.64 \frac{RT\bar{\rho}}{P_T a} \left( \frac{G_o}{a\mu_f \psi} \right)^{0.41} Pr^{2/3} \ln \frac{P_{O_2, \infty, in}}{P_{O_2, \infty, out}} \quad (71)$$

where the quantities denote appropriate averages for the integration of the left side of Eq. 70. It is observed that an infinite catalyst length is necessary to remove all the oxidizer. Practically,  $P_{O_2, \infty, out}$  may be selected as  $\sim 0.05$  of  $P_{O_2, \infty, in}$  say. Then

$$x = \frac{4.92}{\bar{\rho}} \frac{\bar{RT}}{\bar{P}_T a} \bar{\rho} \left( \frac{G_o}{a\mu_f \psi} \right)^{0.41} Pr^{2/3} \quad (72)$$

It is suggested for simplicity that the average values be taken at the arithmetic average values; i.e.,

$$\bar{T} = (T_{in} + T_{out})/2 \quad (73)$$

$$\bar{P} = (P_{in} + P_{out})/2 \quad (74)$$

$$\bar{R} = \left( \frac{R}{M_{in}} + \frac{R}{M_{out}} \right)/2 \quad (75)$$

As is seen on examining Eq. 75, the distance  $x$  to achieve a given percentage of the total reaction is proportional to the mass flux to the 0.41 power and inversely proportional to the mean total pressure in the catalyst bed. However, the average density  $\bar{\rho}$  also appears and tends to largely cancel this effect. This relationship will be used later to provide a means of interpolating data for igniter design with gaseous propellants. This relationship is not adequate for liquid propellants as it stands.

Effective Bed Catalytic Activity

Equation 72 would be exactly true if each catalytic surface had a sufficiently high catalytic activity that each molecule of  $O_2$  that diffused to the surface reacted. However, this may not be the case; and it is necessary to account for reduced catalytic activity. If the bed activity per unit length is denoted by  $\alpha(x, t)$  as before and only the steady-state value is used,  $\alpha(x)$ , the effect of reduced activity may be introduced into Eq. 72 as an approximate correction for reaction less than completion.

$$\text{Rate} = \frac{0.61 a A_c}{R_{O_2} T} P_{O_2, \infty} \frac{G_o}{\rho} \alpha(x) \left( \frac{G_o}{a \mu_f \psi} \right)^{-0.41} Pr^{-2/3} \quad (76)$$

If  $\alpha(x)$  is nearly constant, the required length of bed for 95-percent reaction is

$$x = \frac{4.92 \overline{RT}}{\alpha \overline{P}_a} \frac{G_o}{\rho} \left( \frac{G_o}{a \mu_f \psi} \right)^{0.41} Pr^{2/3} \quad (77)$$

High values of  $\alpha$  are suggested to minimize the required bed length.

It is noted that Eq. 77 will over estimate the required length if at any point in the bed the bulk temperature exceeds the flammability temperature, at which point the reaction will sustain itself. The exact nature of  $\alpha$  cannot be determined theoretically, an appeal to experiment must be made to obtain some insight as to the behavior of  $\alpha$ .

Bed Diameter

There is no completely logical manner to theoretically obtain the required catalyst bed diameter to prevent bed fluid channelling. Instead, the proper bed diameter is determined empirically by measuring bed pressure



drop for a fixed bed length and mass flux for varying ratios of reactor diameter to pellet diameter. When this is done, it is found that channeling is negligible (Ref. 26) when

$$R_D = \frac{D_R}{D_P} > 8 \quad (78)$$

This relationship was not investigated in this program but was assumed adequate for design purposes.

### Bed Pressure Drop

Balanced catalytic reactor bed design calls for not only matching  $D_p$  to  $D_R$  and fixing the length,  $x$ , but it is also necessary to usually keep the bed pressure drop within prescribed limits. There are a large number of empirical relations for the pressure drop across a packed bed. The one selected here for illustration is taken from Ref. 26 and is given as

$$g_c \left( \frac{\Delta P \bar{\rho}_D}{G_o^2 L} \right) \left( \frac{\epsilon^3}{1-\epsilon} \right) = 150 \frac{(1-\epsilon)}{\left( \frac{D_P G_o}{\mu_f} \right)} + 1.75 \quad (79)$$

This is the Ergun equation for turbulent flow.  $\bar{\rho}$  is taken as the average bed gas density, and  $\epsilon$  is the bed void fraction (usually  $\sim 0.3$ ). Equation 79 has been used with remarkable success in packed column work. In addition to this frictional pressure loss, an additional pressure loss caused by acceleration must be included in obtaining the total bed pressure drop.



## OVERALL CATALYTIC BED STABILITY

The catalytic bed stability is concerned with whether or not a reaction will proceed in a repeatable manner at a given bed location for a variety of flow conditions for both gaseous and liquid propellants. Theoretical arguments as to the nature of some possible modes of instability are presented here. In the first case, the gaseous propellant system is examined. In the second case, liquid propellants are examined.

### Gaseous Propellants

It is of interest to the application of catalytic ignition to  $H_2/O_2$  gaseous systems that the catalytic bed may exhibit an unusual type of instability. This instability manifests itself in a manner characterized by the fact that for given flow and initial propellant and catalyst temperatures there may exist the possibility for several steady-state reaction regimes in the bed. Barkelew (Ref. 29) has made an extensive numerical study for a packed bed reactor to arrive at empirical generalizations. Wagner (Ref. 30) has studied the stability of single catalytic particles, and Cannon and Denbigh (Ref. 31) have examined the thermal stability of single reaction promoting particles. Wicke and Vortmeyer (Refs. 32, 33, 34, 35) have examined the packed bed reactor in some detail with regards to stability. A quite simple but meaningful model has been examined by Lin and Amundson (Ref. 36), and the nature of that model is presented here.

The reactor is assumed to be adiabatic in that no radial heat flow or mass flow occurs, and axial transport of these flows occurs only by overall gross mass distribution. Velocity is assumed uniform.





The particle heat and mass transfer characteristics are combined at the catalytic surface as was done in the previous theoretical discussion in this report.

The general transient equations describing mass and energy balances in the bed may be written as follows:

Mass conservation of interstitial fluid,

$$\frac{-G_o}{P_T \bar{M}} \frac{\partial P_{O_2, \infty}}{\partial x} - a k_g (P_{O_2, w} - P_{O_2, \infty}) = \frac{\epsilon \bar{\rho}}{\bar{M} P_T} \frac{\partial P_{O_2, \infty}}{\partial t} \quad (80)$$

where to a first approximation,  $G_o/P_T \bar{M}$  may be taken as a constant.

Continuity of interstitial fluid,

$$G_o = \epsilon \bar{\rho} u \quad (81)$$

Heat balance,

$$G_o \bar{C}_p \left( \frac{\partial T}{\partial x} + \frac{1}{u} \frac{\partial T}{\partial t} \right) = a h (T_p - T) \quad (82)$$

Two transfer units may be defined:

$$H_M = \frac{G_o}{\bar{M} P_T a k_g} \quad (83)$$

$$H_H = \frac{G_o \bar{C}_p}{a h} \quad (84)$$



The conservation equations may be rewritten as:

$$H_M \frac{\partial P_{O_2, \infty}}{\partial x} + \frac{1}{u} \frac{\partial P_{O_2, \infty}}{\partial t} = P_{O_2, w} - P_{O_2, \infty} \quad (85)$$

$$H_H \frac{\partial T}{\partial x} + \frac{1}{u} \frac{\partial T}{\partial t} = T_P - T \quad (86)$$

Consider a single particle of radius of radius  $r$ , and surface area per unit mass of catalyst as  $a_m$ . Let  $\alpha$  (rate) be the rate of disappearance of the oxidizer species per unit surface area of catalyst. The transient mass balance on  $O_2$  at a single surface is then

$$P_{O_2, \infty} - P_{O_2, w} - \frac{r}{3} \frac{\rho_{P_m} a \alpha(\text{Rate})}{k_g} = \frac{r}{3} \frac{\bar{\epsilon} \rho}{\bar{M}_P k_g} \frac{\partial P_{O_2, \infty}}{\partial t} \quad (87)$$

The energy balance at the particle is

$$T - T_P + \frac{r}{3} \frac{\rho_{P_m} a \alpha(\text{Rate})}{h} (-\Delta H^1) = \frac{r}{3} \frac{\rho_P C_P}{h} \frac{\partial T_P}{\partial t} \quad (88)$$

In the steady state these equations may be reduced to the following:

$$H_M \frac{dP_{O_2, \infty}}{dx} = P_{O_2, \infty} - P \quad (89)$$

$$H_H \frac{dT}{dx} = T_P - T$$

$$P_{O_2, \infty} - P_{O_2, w} = \frac{r}{3} \frac{\rho_{P_m} a \alpha(\text{Rate})}{k_g} P_{O_2, w} \quad (90)$$

$$T_P - T = \frac{r}{3} \frac{\rho_{P_m} a \alpha(\text{Rate})}{h} P_{O_2, w} (-\Delta H^1) \quad (91)$$



It is of interest that when the factor  $\alpha$  is considered (the case where all diffused  $O_2$  does not react at the catalyst pellet surface) a finite oxidizer partial pressure must exist at this surface.

An energy balance taken at any section of the bed from the bed entrance gives

$$\frac{-\Delta H'}{MP_T} (P_{O_2, \text{inlet}} - P_{O_2, \infty}) = C_p (T - T_{\text{inlet}}) \quad (92)$$

The local partial pressure is then

$$P_{O_2, \infty} = P_{\text{inlet}} + (T - T_{\text{inlet}}) \frac{MP_T C_p}{\Delta H'} \quad (93)$$

Equation 90 may be rewritten as

$$P_{O_2, w} = \frac{P_{O_2, \infty}}{1 + \frac{r}{3} \frac{\rho_{\text{bed}} a_m \alpha(\text{Rate})}{k_g}} \quad (94)$$

Substituting this into Eq. 91

$$Q_I = \frac{T_P - T}{-\Delta H' \frac{k_g}{h} P_{O_2, \infty}} = \frac{\frac{r}{3} \frac{\rho_{\text{bed}} a_m \alpha(\text{Rate})}{k_g}}{1 + \frac{r}{3} \frac{\rho_{\text{bed}} a_m \alpha(\text{Rate})}{k_g}} \quad (95)$$

Using Eq. 95, the final result of interest is



$$Q_I = \frac{T_P - T}{(P_{O_2, \text{inlet}} + (T - T_{\text{inlet}}) \frac{M_P C_P}{\Delta H'} - \Delta H' \frac{k_g}{h}} + \frac{\frac{r}{3} \rho_\beta a_m \frac{\alpha(\text{Rate})}{k_g}}{1 + \frac{r}{3} \rho_\beta a_m \frac{\alpha(\text{Rate})}{k_g}} = Q_{II} \quad (96)$$

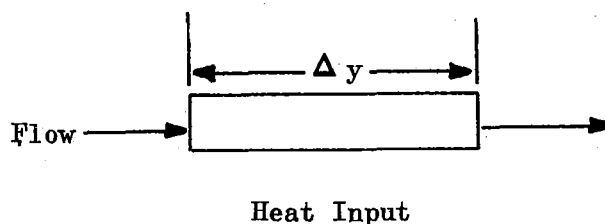
For a given value of  $T$ , with the other parameters specified, this equation may have one or three solutions for  $T_P$ . When  $Q_{II}$  is plotted as a function of  $T_P$ , the nature of the curve is as shown in Fig. 36 for  $Q_{II}$ . When  $Q_I$  is plotted for fixed  $T$ , linear functions result in which there may be as many as three intersections with the  $Q_{II}$  curve. Each intersection is a legitimate steady state. Because of this, a multiplicity of steady-state temperatures and concentrations in the reactor may occur. The "stability" of any one of these may be examined by perturbing the solution about the steady-state solutions. When this is done (Ref. 37), the transient behavior is predicted to follow the steady-state prints in order from  $a_0$  to  $a_1$  to  $a_2$  in a series of undefined jumps. Whether or not all three will be encountered is dependent upon the initial conditions in the bed and fluids.

### Liquid Propellants

When liquid propellants are introduced into a catalyst bed in which vaporization and gas phase reaction will occur, a new form of instability is possible, in addition to that previously described. This instability is primarily attributable to the boiling phenomenon in the catalyst bed.



In analyzing the effects of local flow perturbations on overall catalytic bed stability when liquid propellants are introduced to a catalytic bed and heterogeneous reaction is promoted, resulting in propellant boiling and vaporization, consider the interstitial flow zones as a flow conduit with heat input of  $hA\Delta T$ , and the surface area as  $\pi Dy$ . Consider an element  $\Delta y$  as below and write an energy balance on it



The energy balance gives

$$\dot{W} [h_f + x(y)h_{fg}] = h\pi D\Delta T \Delta y - \dot{W} [h_f + x(y + \Delta y)h_{fg}] \quad (97)$$

Evaluating  $x(y + \Delta y)$  in a Taylor series and substituting into Eq. 97 yields:

$$\dot{W}h_{fg} \frac{dx}{dy} = h\pi D\Delta T \quad (98)$$

By continuity,

$$\dot{W} = \rho Au$$

$\rho$  = average density

The acceleration pressure loss  $\Delta P$  is

$$\Delta P = \frac{\dot{W}}{g} \frac{\Delta u}{A} \quad (99)$$



and

$$\Delta u = \frac{\partial u}{\partial y} \Delta y \quad (\text{to the first order}) \quad (100)$$

Substituting for  $\Delta u$  in Eq. 99 gives

$$\frac{\Delta P}{\Delta y} = \frac{\partial u}{\partial y} \frac{\dot{w}}{g} \quad (101)$$

The differential  $\partial u / \partial y$  may be obtained by the following:

$$u(y) = \frac{\dot{w}}{\rho(y)A}, \quad u(y + \Delta y) = \frac{\dot{w}}{\rho(y + \Delta y)A} \quad (102)$$

The density at  $y$  is given by

$$\rho(y) = \frac{1}{v_f + x(y)v_{fg}} \quad (103)$$

The velocity change  $\Delta u$  is

$$\Delta u = \frac{du}{dy} \Delta y = \frac{\dot{w}}{A} \left[ \frac{1}{\rho(y + \Delta y)} - \frac{1}{\rho(y)} \right] \quad (104)$$

Further,

$$\frac{du}{dy} = \frac{\partial u}{\partial x} \left( \frac{\partial x}{\partial y} \right) \quad (105)$$

The velocity  $u$  is

$$u = \frac{\dot{w}}{A} (v_f + xv_{fg}) \quad (106)$$

$$\therefore \frac{\partial u}{\partial x} = \frac{\dot{w}}{A} v_{fg} \quad (107)$$



Substituting Eq. 98 and 106 into Eq. 101 gives

$$\frac{\Delta P}{\Delta y} = \frac{\dot{w}^2}{A_g^2} v_{fg} \frac{h \pi D \Delta T}{h_{fg}}$$

Now consider the actual boiling itself. Let  $y(t_b)$  be the distance for boiling to occur, and let  $z(t)$  be the distance from  $y(t)$  to the location of interest. Let  $z'(t)$  be  $y(t) + z(t)$ , and let  $L(t)$  be the total distance for vaporization.

Assume constant heat flux,

$$\phi = h(T_w - T)$$

where

$$T_w = \text{catalyst wall temperature}$$

the heat balance on the fluid is approximately

$$\dot{w} C_p \frac{dT}{dy} = h \pi D (T_w - T) \quad (108)$$

Integrating Eq.

$$\frac{T_w - T}{T_w - T_i} = \exp - \frac{h \pi D y}{\dot{w} C_p}$$

where

$$T_i = \text{inlet temperature at } y = 0.$$



Solving for  $y(t_b)$  and substituting for  $\dot{w}$ :

$$y(t_b) = \ln \left( \frac{T_w - T_i}{T_w - T_b} \right) \frac{C_{pl} \rho_l A}{\pi D h} V_o(t) \quad (109)$$

The time for the onset of boiling,  $t_b$ , is

$$t_b = \frac{y(t)}{V_o(t)} \ln \left( \frac{T_w - T_i}{T_w - T_b} \right) \frac{C_{pl} \rho_l A}{\pi D h} \quad (110)$$

The volume of mass in the boiling element is

$$N = w (v_f + x v_{fg}) \quad (111)$$

The evaporation rate is given by

$$\frac{\phi N \pi D}{A h_{fg}}$$

The quality rate change is

$$\frac{dx}{dt} = \frac{\phi \pi D}{A h_{fg}} (v_f + x v_{fg}) = \left( \frac{v_f}{v_{fg}} + x \right) \gamma \quad (112)$$

where

$$\gamma = \frac{\phi D v_{fg}}{A h_{fg}}$$

Integration of Eq. 112 gives

$$x(t, t_b) = \frac{v_f}{v_{fg}} [e^{\gamma(t-t_b)} - 1], \quad t > t_b \quad (112a)$$





$$x(t, t_b) = 0 \quad t \leq t_b$$

For times greater than  $t_b$ , the point of reference will be transferred to the  $z$ -coordinates.  $z$  moves with  $y(t)$  as the lower boundary. The volume flow into the element is

$$\frac{dv_o}{dt} = A(V_o - \frac{dy}{dt}) \quad (113)$$

and the volume flow out is

$$\frac{Adz}{dt}$$

The volume generated by boiling is  $A\gamma_z$

$$\therefore \frac{dz}{dt} = \gamma_z + V_o - \frac{dy}{dt} \quad (114)$$

Using Eq. 113

$$\frac{dz}{dt} = \gamma_z + V_o - \beta V_o \quad (115)$$

with

$$\beta = \ln \frac{T_w - T_i}{T_w - T_b} \frac{\bar{C}_p \rho_l A}{\pi D h_1}$$

The fluid velocity at  $z'(t)$  is

$$u = \frac{\partial y}{\partial t} + \frac{\partial z}{\partial t} = \gamma_z + V_o \quad (116)$$



But

$$z = z' - y$$

$$\therefore u = \gamma_z' + V_0 [1 - \gamma\beta] \quad (117)$$

The fluid acceleration at  $z'$  is

$$\begin{aligned} \ddot{u} &= \frac{\partial^2 y}{\partial t^2} + \frac{\partial^2 z}{\partial t^2} = \frac{dz}{dt} + \dot{V}_0 \\ &= \gamma^2_{z'} + V_0 [\gamma - \gamma^2\beta] + \dot{V}_0 (1 - \gamma\beta) \end{aligned} \quad (118)$$

The density  $\rho(t, t_b)$  is then

$$\rho(t, t_b) = \rho_f e^{-(t-t_b)} \quad (119)$$

The distance  $L$  for total vaporization is

$$L = y(t_b) + z\ell \quad (120)$$

where  $z\ell$  is distance for vaporization. The time for complete vaporization is

$$t_0 = t_b + \frac{1}{\gamma} \ln \frac{V_{fg} + V_f}{V_f} \quad (121)$$

Now let the flow perturbations be given by

$$u(t) = V_0 + u'' e^{st} \quad (122)$$

$$\therefore y_1(t) = \beta(V_0 + u'' e^{st}) \quad (123)$$



$dz/dt$  is given by

$$\frac{dz}{dt} = \gamma_z + \left( V_0 + u'' e^{s(t-t_b)} \right) - \beta \left( \dot{V}_0 + s u'' e^{s(t-t_b)} \right) \quad (124)$$

If  $\dot{V}_0$  is small

$$\frac{dz}{dt} = \gamma_z + V_0 (1 - \beta s) u'' e^{s(t-t_b)} \quad (125)$$

The solution for  $z$  at  $t > t_b$  is

$$z_1 = \left( \frac{1 - \beta s}{s - \gamma} \right) u'' e^{(s-\gamma)t - \gamma t_b} - \frac{V_0}{\gamma} C_1 e^{\gamma t} \quad (126)$$

where  $C_1$  is determined by

$$z(t-t_b) = 0$$

$$\therefore z = \frac{V_0}{\gamma} \left[ e^{\gamma(t-t_b)} - 1 \right] + \left( \frac{1 - \beta s}{s - \gamma} \right) u'' \left[ e^{s(t-t_b) - \gamma t} - e^{\gamma t - \gamma t_b} \right] \quad (127)$$

The velocity  $u$  at  $z'$  is

$$u(z) = V_0 e^{\gamma(t-t_b)}, \quad t_b \leq t \leq t_0 \quad (128)$$

Let

$$s = iw, \quad z = z_R + iz_I$$



With a step function input to the velocity perturbation, the real part of  $z$  is

$$z_R = \beta V_0 + \beta u'' + \frac{V_0}{\gamma} \left[ e^{\gamma(t_0 - t_b)} - 1 \right] + \frac{u''}{\gamma} \left[ e^{\gamma(t_0 - t_b)} - e^{-\gamma t_0} \right] \quad (129)$$

To prevent liquid carryover a distance  $L$ , the velocity perturbation  $u''$  to  $u_0$  ratio must then satisfy

$$\frac{u''}{u_0} \leq \frac{\frac{\gamma L}{u_0} - \gamma \beta - \left[ e^{\gamma(t_0 - t_b)} - 1 \right]}{\gamma \beta + e^{\gamma(t_0 - t_b)} - e^{-\gamma t_0}} \quad (130)$$

where

$$\gamma = \phi Dv_{fg}/Ah_{fg}$$

with  $\phi$  as the particle surface heat flux.

$$\beta = \ln \left( \frac{T_w - T_i}{T_w - T_b} \right) \frac{\bar{C}_{pl} \bar{\rho}_l A}{\pi Dh_1} \quad (131)$$

$t_b$  = time for boiling to occur

$t_0$  = time

Equation 130 is a somewhat surprising relation because it shows that the greater the average throughput velocity  $V_0$  is, the smaller  $u''$  must be to prevent either liquid carry over or flash back in the bed. Near saturation  $t_b = 0$ , and  $u''/V_0$  must be less than  $\gamma L/zu_0$ . The pressure oscillations (and indirectly, the temperature oscillations) will be directly related to the velocity oscillations if there is negligible chemical reaction lag. In a catalyst bed with such perturbations, there is



essentially no damping present to reduce the oscillations. For a fluid like  $\text{LH}_2$ , the specific volume change  $v_{fg}$  is very large, whereas the latent heat,  $h_{fg}$ , is relatively small. It is then observed that in the limit near saturation that the allowable perturbation  $u''$  must be very small to achieve any semblance of stable bed reaction.

### CATALYST CHARACTERISTICS

In considering optimal catalysts for use in the  $\text{H}_2/\text{O}_2$  environment there are a number of factors to consider. Of primary importance is the ability of the catalyst to promote the overall reaction in an efficient and repeated manner. The factors affecting this overall reaction which are of most interest to igniter designs are size and shape, surface characteristics, nature of the substrate, attrition and shock resistance, and active metal content and configuration of the active metal and activity. Each of these is discussed briefly below.

#### Size and Shape

There are a large number of sizings and shapes in which catalysts may be obtained. Among these are spheres, cylinders, and random shapes. In a previous program (Ref. 2) it was determined that spheres offered better reproducibility for ignition than did cylinders. This presumably occurs because uniform spheres tend to pack in nearly an identical way each time a bed is poured. No experience is available on the use of random sizes and shapes. It is felt that such materials may not be of optimum use when efforts are made to minimize the amount of catalyst required to promote the reaction in a repeatable manner. From an overall reaction standpoint, the theoretical results show that minimum bed lengths result, all other parameters being constant, for the smallest spheres, because



the parameter,  $a$ , surface area per unit volume, is largest for smallest sizes. Also, the smaller sizes influence the necessary overall bed diameter requirements by making it possible to minimize the bed diameter to particle ratio. However, small sizes do have higher pressure drop unit of bed length.

### Surface Characteristics

The factors of most importance here are total surface area per unit mass of catalyst, catalyst pore volume, and average pore diameter. The actual active surface area of a catalyst is virtually impossible to measure; however, active surface area is known to be proportional to total surface area, and is commonly used as a measure of relative activity for comparable catalyst. It is apparent that the greater the catalyst surface area, the higher the rate of collision between reactant and catalyst; hence, large surface area in a catalyst is desirable.

Catalyst pore volume and average pore diameter are equally important to overall catalyst activity. They are certainly necessary characteristics for high surface area. The pore volume is a general measure of catalyst porosity and is indicative of the ease with which reactants may pass into the catalyst interstices and reach the less active metal sites. Average pore size serves as an indication of the relative availability of catalyst pores for reaction. For example, in a reaction between chemical species having molecular diameters of  $5A$ , a catalyst having a mean pore size of only  $4A$  would not be expected to promote the reaction as well as a similar one having a pore diameter of  $10A$ . Pore size distribution serves as a measure of activity and durability, because catalyst damage may result from pore closure during the reaction sequence. It is not possible to predict a priori that a wide pore size distribution is beneficially better than a narrow size.



### Nature of the Substrate

A primary criteria for the substrate is that it be thermally resistant to high temperatures, which at the same time exhibiting high crush strength and resistance to attrition. It is well known, however, that the selected substrate is important to overall catalytic activity, particularly with the noble metals. Further, some substrates can be produced with better surface characteristics than others.

### Active Metal Content, Metal Site Sizing, and Activity

On the basis of results presented in Ref. 3 it has been felt that high metal contents are desirable for high activity. It appears that high metal content can be beneficial as long as it can be laid on the substrate in a discrete, crystalline form. If the content is so high as to preclude this, the overall surface area is reduced along with loss in catalytic activity. The maximum sizing of the diameter crystals for good activity is reportedly to be ~30 to 50A.

With regards to activity, there is no absolute means to measure activity. Instead, it is only possible to determine a relative activity rating among catalysts. For  $H_2/O_2$ , this can be done by comparing actual  $H_2O$  yields to theoretical yields in flowing systems for fixed quantities of catalysts.

1. The first part of the document is a list of the names of the persons who were present at the meeting.

2. The second part of the document is a list of the names of the persons who were absent from the meeting.

3. The third part of the document is a list of the names of the persons who were present at the meeting.

4. The fourth part of the document is a list of the names of the persons who were absent from the meeting.

5. The fifth part of the document is a list of the names of the persons who were present at the meeting.

6. The sixth part of the document is a list of the names of the persons who were absent from the meeting.

7. The seventh part of the document is a list of the names of the persons who were present at the meeting.

8. The eighth part of the document is a list of the names of the persons who were absent from the meeting.

9. The ninth part of the document is a list of the names of the persons who were present at the meeting.

10. The tenth part of the document is a list of the names of the persons who were absent from the meeting.

11. The eleventh part of the document is a list of the names of the persons who were present at the meeting.

12. The twelfth part of the document is a list of the names of the persons who were absent from the meeting.

13. The thirteenth part of the document is a list of the names of the persons who were present at the meeting.

14. The fourteenth part of the document is a list of the names of the persons who were absent from the meeting.

15. The fifteenth part of the document is a list of the names of the persons who were present at the meeting.

16. The sixteenth part of the document is a list of the names of the persons who were absent from the meeting.

17. The seventeenth part of the document is a list of the names of the persons who were present at the meeting.

18. The eighteenth part of the document is a list of the names of the persons who were absent from the meeting.

19. The nineteenth part of the document is a list of the names of the persons who were present at the meeting.

20. The twentieth part of the document is a list of the names of the persons who were absent from the meeting.

21. The twenty-first part of the document is a list of the names of the persons who were present at the meeting.

22. The twenty-second part of the document is a list of the names of the persons who were absent from the meeting.

23. The twenty-third part of the document is a list of the names of the persons who were present at the meeting.

24. The twenty-fourth part of the document is a list of the names of the persons who were absent from the meeting.

25. The twenty-fifth part of the document is a list of the names of the persons who were present at the meeting.

26. The twenty-sixth part of the document is a list of the names of the persons who were absent from the meeting.

27. The twenty-seventh part of the document is a list of the names of the persons who were present at the meeting.

28. The twenty-eighth part of the document is a list of the names of the persons who were absent from the meeting.

29. The twenty-ninth part of the document is a list of the names of the persons who were present at the meeting.

30. The thirtieth part of the document is a list of the names of the persons who were absent from the meeting.



APPENDIX A

## EQUILIBRIUM SPECIFIC HEATS FOR REACTING MIXTURES

The equilibrium specific heats for a reacting mixture of thermally perfect gases in equilibrium are derived in this section. The basic fundamentals of this derivation are given in Ref. 38.

To begin the analysis, assume the specific entropy to be a function of pressure, temperature, and species present

$$s = s(p, T, c^k) \quad (A-1)$$

$$ds = \left( \frac{\partial s}{\partial T} \right)_{p, c^k} dT + \left( \frac{\partial s}{\partial p} \right)_{T, c^k} dp + \sum_K \left( \frac{\partial s}{\partial c^k} \right)_{T, p, c_i^k} dc^k \quad (A-2)$$

$$Tds = T \left( \frac{\partial s}{\partial T} \right)_{p, c^k} dT + T \left( \frac{\partial s}{\partial p} \right)_{T, c^k} dp + T \sum_k \left( \frac{\partial s}{\partial c^k} \right)_{T, p} dc^k \quad (A-3)$$

Since  $s = \sum_K s_c^k$

$$\frac{\partial s}{\partial c^k} = s_c^k \quad (A-4)$$



$$Tds = T\left(\frac{\partial s}{\partial T}\right)_{P, c^k} dT + T\left(\frac{\partial s}{\partial P}\right)_{T, c^k} dP + \sum_K s^k dc^k \quad (\text{A-5})$$

The coefficient of  $dT$  is found from the Maxwell relation (Ref. )

$$T\left(\frac{\partial s}{\partial T}\right)_{P, c^k} = c_{pf} = \sum c^k c_p^k \quad (\text{A-6})$$

which is the frozen specific heat.

The coefficient of  $dP$  in Eq. A-5 is recognized as the specific volume.

$$T\left(\frac{\partial s}{\partial P}\right)_{T, c^k} = -V \quad (\text{A-7})$$

To proceed from this point requires the last term in Eq. A-5 to be put in terms of pressure and temperature. Begin with the differential form of the Gibbs' function.

$$dg = -sdT + vdP + \sum_K \mu^k dc^k \quad (\text{A-8})$$

Also

$$g = \sum_K \mu^k c^k \quad (\text{A-9})$$

$$dg = \sum_K \mu^k dc^k + \sum_K c^k d\mu^k \quad (\text{A-10})$$



where the chemical potential  $\mu^k = g^k$

Comparing Eq. C-11 with Eq. C-9 shows that

$$\sum c^k d\mu^k = -sdT + vdP \quad (A-11)$$

Further, the mass fraction change  $dc^k$  can be shown to be, in terms of the equilibrium constant,

$$dc^k = \frac{\nu^k}{n^k} \frac{n}{N} d\xi = \frac{\frac{\nu^k}{n^k} d \ln k_x}{\sum \frac{(\nu^k)^2}{x^k} - (\Delta \nu)^2} \quad (A-12)$$

where  $\nu^k$  are the stoichiometric coefficients for the reaction.

With the aid of Eq. C-13, the term  $T \sum_k s^k dc^k$  becomes

$$T \sum_k s^k dc^k = \frac{nT d \ln k_x}{\sum \frac{(\nu^k)^2}{x^k} - (\Delta \nu)^2} \sum_k \frac{s^k \nu^k}{n^k} \quad (A-13)$$

The Gibbs' function for a single species  $k$  is

$$g^k = h^k - Ts^k \quad (A-14)$$

$$\therefore s^k = \frac{h^k - g^k}{T} \quad (A-15)$$



The summation term of Eq. A-13 is, therefore,

$$\sum_k s^k \frac{\nu^k}{n^k} = \sum_k \frac{\nu^k}{n^k} \left( \frac{h^k - g^k}{T} \right) \quad (\text{A-16})$$

But 
$$\sum_k \frac{\nu^k}{n^k} h^k = \Delta H \quad (\text{A-16a})$$

$$\sum_k \frac{\nu^k}{n^k} g^k = \Delta G \quad (\text{A-16b})$$

For equilibrium  $\Delta G = 0$ . With  $\Delta G = 0$  and Eq. A-16a, Eq. A-16 becomes

$$\sum_k s^k \frac{\nu^k}{n^k} = \frac{\Delta H}{T} \quad (\text{A-17})$$

Returning to Eq. A-12 and using Eq. A-17

$$T \sum_k s^k d c^k = \frac{n \Delta H d \ell_{n k_x}}{\sum_k \frac{(\nu^k)^2}{x^k} - (\Delta \nu)^2} \quad (\text{A-18})$$

Let  $\ell_{n k_x}$  be a function of  $T, P$ .

$$\therefore d \ell_{n k_x} = \left( \frac{\partial \ell_{n k_x}}{\partial T} \right)_P dT + \left( \frac{\partial \ell_{n k_x}}{\partial P} \right)_T dP \quad (\text{A-19})$$



The relationships for the coefficients of  $dT$  and  $dP$  are well known, i.e.,

$$\left( \frac{\partial \ln k_x}{\partial \ln T} \right)_P = \frac{\Delta H}{RT} \quad (A-20)$$

$$\left( \frac{\partial \ln k_x}{\partial \ln P} \right)_T = -\Delta \nu \quad (A-21)$$

Substitution of Eq. A-20 and A-21 in Eq. A-19 which in turn is substituted in Eq. A-18, gives

$$T \sum s^k_{dc^k} = \left[ \frac{n \Delta H}{\sum \frac{(\nu^k)^2}{x^k} - (\Delta \nu)^2} \right] \left[ \left( \frac{\Delta H}{RT^2} \right) dT - \left( \frac{\nu \Delta \nu}{nRT} \right) dP \right] \quad (A-22)$$

Rewriting Eq. A-5 using Eq. A-6, A-7, and A-21 gives

$$Tds = \left[ \sum_k c^k_p c^k + \frac{\left( \frac{\Delta H}{RT} \right)^2 nR}{\sum \frac{(\nu^k)^2}{x^k} - (\Delta \nu)^2} \right] dT + \left[ -\nu - \frac{\nu \Delta \nu \left( \frac{\Delta H}{RT} \right)}{\sum \frac{(\nu^k)^2}{x^k} - (\Delta \nu)^2} \right] dP \quad (A-23)$$



A comparison of coefficients of  $dT$  between Eq. A-5 and A-22 gives the following:

$$T \left( \frac{\partial s}{\partial T} \right)_{P, c^k} = c_{pf} = \sum_k c^k c_p^k$$

$$T \left( \frac{\partial s}{\partial T} \right)_P = c_{pe}, \text{ the equilibrium specific heat}$$

where  $c_{pe}$  is given by

$$c_{pe} = \sum_k c^k c_p^k + \frac{\left( \frac{\Delta H}{RT} \right)^2 nR}{\sum_k \frac{(\nu_k)^2}{x_k} - (\Delta \nu)^2} \quad (\text{A-23})$$

A similar argument with independent variable  $V$  and  $T$  lead to the equilibrium specific heat at constant volume as

$$c_{ve} = T \left( \frac{\partial s}{\partial T} \right)_V = \sum_k c^k c_v^k + \frac{\left( \frac{\Delta U}{RT} \right)^2 nR}{\sum_k \frac{(\nu_k)^2}{x_k}} \quad (\text{A-24})$$

where  $\sum_k c^k c_v^k$  is the frozen specific volume.



## NOMENCLATURE

$A$	= diffusion area, sq cm
$A_c$	= reactor cross-sectional area, sq in.
$C_D$	= discharge coefficient
$C_P$	= heat capacity, Btu/lb F
$\bar{C}_P$	= mean heat capacity, Btu/lb F
$C$	= constant
$D$	= pellet diameter, inch
$D_{AB}$	= diffusivity of specie A through stagnant film of B, sq cm/sec
$\Delta E$	= energy of activation, Btu/lb-mole, F
$G$	= superficial mass velocity, lb/in. <sup>2</sup> -sec
$H$	= enthalpy, Btu/lb
$H_M$	= mass transfer unit
$H_H$	= heat transfer unit
$J_H$	= heat transfer factor
$K$	= reaction rate constant
$L$	= length
$L^*$	= characteristic chamber length
$M$	= molecular weight
$\dot{M}$	= mass







$\dot{N}$	= rate of specie production
$N$	= volume of mass in boiling element
$P$	= pressure
$Pr$	= Prandtl number
$Q$	= heat transferred, Btu/sec
$Q_I, Q_{II}, Q_{III}$	= solutions to the steady-state equation
$R$	= molar gas constant
$R_M$	= moles of specie
$Re$	= Reynolds number
$S$	= entropy, Btu/lb F
$S_u$	= laminar flame speed
$S_{ut}$	= turbulent flame speed
$T$	= temperature
$V$	= volume
$X$	= catalyst bed length, inch
$a$	= empirical constant
$a_B$	= specific bed area
$\bar{a}$	= external surface area per unit bed volume, ft <sup>-1</sup>
$b$	= empirical constant
$g$	= gravitational constant
$h$	= film coefficient, Btu/sec in. <sup>2</sup> F
$h_D$	= mass transfer coefficient





$\bar{k}$	= thermal conductivity, Btu/sec in. <sup>2</sup> F/in.
$k$	= Boltzmann constant = $1.38 \times 10^{-6}$ erg/K
$M$	= mass transferred
$N$	= empirical exponent
$r$	= pellet radius
$t$	= time, seconds
$u$	= velocity
$\bar{u}$	= average velocity
$u'$	= turbulence velocity
$u''$	= boiling perturbation velocity
$\dot{W}$	= mass flowrate, lb/sec
$x$	= distance along x-coordinate
$x_b$	= thickness of flame front
$y$	= distance along y-coordinate
$z_f$	= film thickness
$z$	= distance along z-coordinate
$\alpha$	= percent conversion of oxygen to water
$\beta$	= impingement angle
$\epsilon$	= bed void fraction
$\epsilon_{AB}$	= viscosity
$\phi$	= heat flux, Btu/sec-in. <sup>2</sup>
$\rho$	= density, lb/cu ft
$\sigma_{AB}$	= molecular separation at collision, Å
$\psi$	= sphericity
$\tau$	= time constant, sec <sup>-1</sup>





#### REFERENCES

1. RR 63-9, Hydrogen/Oxygen Catalytic Ignition, C. Bendersky, Rocketdyne, a Division of North American Aviation, Inc., Canoga Park, California, January 1963.
2. RR 64-2, Hydrogen/Oxygen Catalytic Ignition for Application to the J-2 Engine, R. Roberts, Rocketdyne, a Division of North American Aviation, Inc., Canoga Park, California, January 1964.
3. CR-54086, Investigation of Catalytic Ignition of Oxygen/Hydrogen Systems, R. Roberts, Rocketdyne, a Division of North American Aviation, Inc., Canoga Park, California, August 1964.
4. RR 64-61, An Investigation of Catalytically-Ignited Oxygen/Hydrogen Attitude Control Engines, M. Hilario and R. Roberts, Rocketdyne, a Division of North American Aviation, Inc., Canoga Park, California.
5. RR 65-8, Feasibility Investigation of Catalytic Ignition of Premixed Oxygen, Nitrogen, and Hydrogen Propellants, E. Prono, R. Roberts, G. Falkenstein, and H. Burge, Rocketdyne, a Division of North American Aviation, Inc., Canoga Park, California, March 1965.
6. RR 65-25, Investigation of Catalytic Ignition of a Premixed Oxygen, Nitrogen, and Hydrogen Blend for Use in Attitude Control Systems, E. Prono and R. Roberts, Rocketdyne, a Division of North American Aviation, Inc., Canoga Park, California, June 1965.
7. ASME Paper No. 50A-45, Orifice Meters With Supercritical Compressible Flow, R. G. Cunningham, Transactions of the ASME, July 1951, 625-637.
8. ASME, Fluid Meters, Their Theory and Application, Fifth Edition, New York, 1959.
9. Instruction Manual, Isorpta Analyzer Model 2A, Engelhard Industries, Inc., Newark, New Jersey.



10. Brunauer, S., Emmett, P. H., and Teller, E., "Adsorption of Gases in Multimolecular Layers," Journal of the American Chemical Society 60, 309 (1938).
11. Personal Communication with Philip Romeo of Engelhard Industries, Inc., Newark, New Jersey, 5 February 1965.
12. Askey, W. E., Platinum Catalyst Reforming, The Pace Company, Houston, Texas, September 1959.
13. S-13917, Development of Catalysts for Monopropellant Decomposition of Hydrazine, W. E. Armstrong, et al., Shell Development Company, Emeryville, California, March 1965, CONFIDENTIAL.
14. TR 60-141, WADD, Research on the Hazards Associated With the Production and Handling of Liquid Hydrogen, M. Zabetakis and D. Burgess, Bureau of Mines, United States Department of the Interior, June, 1960.
15. Constantine, M., "Flammability Limits of Hydrogen in Oxygen," Rocketdyne Internal Memo of 30 October 1962.
16. Lewis, B., and von Elbe, G., Combustion, Flames, and Explosion of Gases, Academic Press, Inc., 1951.
17. RR 64-29, Steady State Rocket Combustion of Gaseous Hydrogen and Liquid Oxygen, Part II: Analysis for Coaxial Jet Inspection, L. Combs and M. Schuman, Rocketdyne, a Division of North American Aviation, Inc., Canoga Park, California, March 1965.
18. Agnew, J. and Graiff, L., "The Pressure Dependence of Laminar Burning Velocity by the Spherical Bomb Method," Combustion and Flame, Vol. 5, No. 3, September 1961.
19. Strauss, W., and Edse, R., "Burning Velocity Measurements by the Constant-Pressure Bomb Method," Seventh Symposium (International) on Combustion, Butterworths Scientific Publications, London, 1959.



20. Edse, R., Bull. Engr. Exper. Sta., Ohio, Vol. 149, 1952, 441; quoted by G. A. McD. Cummings: "Stationary Flames at Pressures Above One Atmosphere," Combustion Researches and Reviews, 1957, Butterworths Scientific Publications, London, 1957.
21. RR 64-24, Steady State Rocket Combustion of Gaseous Hydrogen and Liquid Oxygen, Part I: Experimental Investigation, L. Combs and F. Hoehn, Rocketdyne, a Division of North American Aviation, Inc., Canoga Park, California, June 1964.
22. NACA Report 1383, Survey of Hydrogen Combustion Properties, I. Drell and F. Bellis, 1958.
23. Gaydon, A., and Wolfhard, H., Flames, Their Structure, Radiation, and Temperature, Chapman & Hall LTD, London, 1960.
24. Schlichting, H., Boundary Layer Theory, Mc-Graw-Hill 4th Edition, 1960.
25. Dugger, G., and Heimel, S., NACA Tech. Note, No. 2624.
26. Bird, R. Stewart, W., and Lightfoot, E., Transport Phenomena, John Wiley & Sons, 1960.
27. Hirschfelder, J., Curtiss C., and Bird, R., Molecular Theory of Gases and Liquids, John Wiley & Sons, 1954.
28. Carslaw, H., and Jeager, J., Conduction of Heat in Solids, Oxford Press, 1959.
29. Barkelew, C., Chem. Engr. Progr, Symposium Series 55, 1959.
30. Wagner, C., "Stationary State of Catalysts in Heterogeneous Reactions," Chem.-Tech. 18, 1945.
31. Cannon, K., and Denbigh, K., "Gas-Solid Reactions, Causes of Thermal Instability," Chem. Engr. Sci., 6, 1957.
32. Wicke, E., and Vortmeyer, D., Alta Technologia Chimica, Accademia Nazionale dei Lincei, Varese, 1960.



33. Wicke, E., and Vortmeyer, C., "Steady-State Conditions in Exothermic Gas Reactions on Porous Catalysts," Chem. Eng.-Tech 29, 1957.
34. Wicke, E., and Vortmeyer, D., "Stable and Unstable Reaction States in Exothermic Reactions," Zeitschrift Elektrochem., 65, 1961.
35. Wicke, E., and Vortmeyer, D., "Ignition Zones of Heterogeneous Reactions in Granular Beds," Zeitschrift Elektrochem., 63, 1959.
36. Liu, S., and Amundsen, N., "Stability of Adiabatic Packed Bed Reactors, An Elementary Treatment," Industrial Engineering Chemistry Fundamentals, 1, 1962.
37. Eckert, E., and Drake, R., Heat and Mass Transfer, Mc-Graw-Hill Book Co., 1959.
38. Knuth, E., Notes on Aerothermochemistry, Revised-Spring Semester 1961, Department of Engineering, University of California at Los Angeles.
39. Denbigh, K., Principles of Chemical Equilibrium, Cambridge University Press, London, 1957.





TABLE 1

TABULATION OF CATALYSTS EVALUATED WITH  
THE OXYGEN/HYDROGEN SYSTEM

Code	Type	Substrate	Size and Shape	Manufacturer
DS	Palladium	Alumina	1/8-inch spheres	Engelhard Industries, Inc.
DSS	Palladium	Alumina	1/8-inch spheres	Engelhard Industries, Inc.
MFSS	Platinum/Rhodium	Alumina	1/8-inch spheres	Engelhard Industries, Inc.
MFSA	Platinum/Rhodium/ Lead	Alumina	1/8-inch spheres	Engelhard Industries, Inc.
4X-MFSA	Platinum/Rhodium/ Lead	Alumina	1/8-inch spheres	Engelhard Industries, Inc.
MFP	Iron Oxide	Silicon Carbide	3/16- by 3/16-inch cylinders	Engelhard Industries, Inc.
SMR55-1097-1	Platinum	Silica Gel	1/16-inch granules	Davison Chemical Company
Oxidizer 903	Metal Oxide	Unknown	1/8- by 1/8-inch cylinders	Davison Chemical Company
SMR 55-8182	Metal Oxide	Unknown	1/8- by 1/8-inch cylinders	Davison Chemical Company
C12-3	Iron Oxide, Chromium Oxide	Alumina	1/4- by 1/4-inch cylinders	Catalysts and Chemicals, Inc.
C13-1	Nickel Oxide	Alumina	1/4- by 1/4-inch cylinders	Catalysts and Chemicals, Inc.
C20-6	Cobalt Oxide, Molybdenum Oxide	Alumina	1/8-inch extrudate	Catalysts and Chemicals, Inc.
A-100S	Platinum	Alumina	1/8-inch extrudate	Houdry Process Corporation
B-100S	Palladium	Alumina	1/8-inch extrudate	Houdry Process Corporation



TABLE 1  
(Concluded)

Code	Type	Substrate	Size and Shape	Manufacturer
G-13	Nickel Oxide	Alumina	1/8- by 1/8-inch cylinders	Girdler Chemical Company
G-22	Copper Chromate	None		
G-49B	Nickel	Kieselguhr		
G-62	Cobalt Oxide	"Special Base"		
G-67	Cobalt Oxide	Kieselguhr		
G-67RS	Cobalt	Kieselguhr		
T-3	Copper Oxide	Kieselguhr		
T-893	Zirconia, Nickel	"Refractory" Oxide	1/4- by 1/4-inch cylinders	
T-1205	Nickel Oxide	Kieselguhr	1/8- by 1/8-inch cylinders	
None	Zirconia, Chromia	None	1/4- by 1/4-inch cylinders	Harshaw Chemical Company
405	Noble Metal	Alumina	1/8- by 1/8-inch cylinders	Shell Development Company
None	Palladium	Alumina	5/16-inch spheres	Sundstrand Aviation



TABLE 2  
SPECTROGRAPHIC ANALYSIS OF CATALYSTS

Catalyst Metal	Composition*, weight percent							
	DS	DSS	MFSS	MFSA	4X-MFSA	A-200SR	MFP	A-25Z
Aluminum	47	48	48	52	52	52	1.1	45
Silicon	4.0	3.6	4.0	0.096	0.089	0.053	68	0.11
Palladium	<u>0.29</u>	<u>0.27</u>	0.001	Nil	Nil	Nil	Nil	Nil
Platinum	Nil	Nil	<u>0.26</u>	<u>0.13</u>	<u>0.94</u>	<u>0.14</u>	Nil	Nil
Rhodium	Nil	Nil	<u>0.58</u>	<u>0.14</u>	<u>0.88</u>	Nil	Nil	Nil
Sodium	<u>0.92</u>	<u>0.61</u>	0.23	Trace	Nil	Trace	Nil	Nil
Calcium	<u>0.023</u>	0.021	0.027	0.001	0.053	0.003	0.14	0.003
Lead	Nil	Nil	Nil	<u>0.13</u>	Nil	Nil	Nil	Nil
Nickel	Nil	Nil	Nil	Nil	Nil	Nil	0.006	Nil
Magnesium	Nil	Nil	Nil	Nil	0.001	Nil	0.044	0.003
Manganese	Nil	Nil	Nil	Nil	0.012	Nil	Nil	Nil
Iron	Nil	Nil	Nil	Nil	0.015	Nil	<u>0.24</u>	0.021
Silver	Nil	Nil	Nil	Nil	0.004	Nil	Nil	Nil
Chromium	Nil	Nil	Nil	Nil	Nil	Nil	Nil	10

\*The difference between the sum total percentages shown and 100, represent the amount of oxygen and trace impurities contained within the catalyst. This oxygen exists in the form of metal oxides (e.g.,  $Al_2O_3$ ,  $SiO_2$ , rather than Al or Si).

NOTE: The underlined numbers represent items which contribute significantly to the performance of the catalyst.



TABLE 3

## CATALYST SURFACE CHARACTERISTICS

Catalyst	Type	Surface Characteristic		
		Surface Area, m <sup>2</sup> /gm	Pore Volume, ml/gm	Average Pore Diameter, angstroms
Engelhard Industries, Inc.				
DS	Pd	230	0.24	42
DSS	Pd	224	0.30	54
MFSS	Pt/Rh	251	0.28	44
MFSA	Pt/Rh/Pb	460	0.58	50
4X-MFSA	Pt/Rh/Pb	18	0.018	41
MFP	Fe <sub>2</sub> O <sub>3</sub>	0.3	*	*
Houdry Process Corporation				
A-100S	Pt	120	0.13	43
A-220SR	Pt	238	0.32	53
A-25Z	Cr <sub>2</sub> O <sub>3</sub>	81.2	0.135	66
Girdler Chemical Company				
G-22		30.4	0.032	42
G-49B	Ni	255	0.135	21
G-62	CoO	62	0.062	40
G-67	CoO	86.7	0.092	43
G-67RS	Co	49.4	0.134	108
T-3	Cu	57	0.035	25
T-893	Ni	184	0.077	17
T-1205	Ni	237	0.174	29
Davison Chemical Company				
SMR 55-1097-1	Pt	566	0.25	18
Shell Development Company				
405	--	228.3	0.19	33
Sundstrand				
AAMT-88R	Pt	1.9	0.003	67



TABLE 4

RESULTS OF CATALYTIC ACTIVITY EVALUATIONS WITH OXIDIZER-RICH PROPELLANTS

Vendor	Vendor Designation	Catalyst Type	Relative Activity		
			At 77 F	At -113 F	At -320 F
Catalysts and Chemicals, Inc.	C12-3	Fe <sub>2</sub> O <sub>3</sub> , Cr <sub>2</sub> O <sub>3</sub> on alumina	13.9	—	—
	C13-1	NiO on alumina	1.2	—	—
	C20-6	CoO, MoO <sub>3</sub> on alumina	0.0	—	—
Davison	Oxidizer 903	—	2.5	—	—
	SMR 55-8182	—	0.3	—	—
	SMR 1097-1	Pt on silica gel	87.5	—	—
Engelhard Industries, Inc.	DS	Pd on alumina	88.1	37.2	0.2
	DSS	Pd on alumina	75.5	59.9	5.3
	MFP	Fe <sub>2</sub> O <sub>3</sub> on silicon carbide	59.5	3.3	2.3
	MFSS	Pt, Rh on alumina	80.8	63.5	5.3
	MFSA	Pt, Rh, Pb on alumina	71.3	60.6	50.4
	4X-MFSA	Pt, Rh, Pb on alumina	72.1	37.5	0.0
	G-13	—	0.0	—	—
	G-22	Ba-promoted copper chromite	2.8	—	—
Girdler Chemical	G-49B	Ni on dieselguhr	3.2	—	—
	G-62	CoO on "special base"	13.5	—	—
	G-67	CoO on kieselguhr	3.7	—	—
	G-67RS	Co on dieselguhr	2.9	—	—
	T-3	Cu on kieselguhr	19.2	17.3	11.4
	T-893	ZrO <sub>2</sub> -promoted nickel	6.3	—	—
	T-1205	ZrO <sub>2</sub> -promoted nickel	8.3	—	—
	—	Zirconia/Chromia	0.0	—	—
Harshaw Chemical	—	—	—	—	—
	—	—	—	—	—

TABLE 4  
(Concluded)

Vendor	Vendor Designation	Catalyst Type	Relative Activity		
			At 77 F	At -113 F	At -320 F
Houdry Process Corp.	A-25Z	Cr <sub>2</sub> O <sub>3</sub> on alumina	57.3	7.5	1.4
	A-100S	Pt on alumina	1.8	---	---
	B-1005	Pd on alumina	2.3	---	---
	A-200SR	Pt on alumina	99.8	77.7	26.2
Shell Chemical Company Sundstrand	405	---	65	34.5	1.9
		Pt on alumina	57.4	26.6	4.8

## Conditions of test:

Catalyst charge, 5 grams  
Oxygen/hydrogen mixture ratio, 48:1 (diluted in gaseous nitrogen)  
Run duration, 20 minutes  
Theoretical water yield, 0.396 gram



TABLE 5  
RESULTS OF CATALYTIC ACTIVITY EVALUATIONS WITH FUEL-RICH PROPELLANTS

Vendor	Designation	Catalyst Type	Relative Activity		
			At 77 F	At -113 F	At -320 F
Engelhard Industries, Inc.	DS	Pd on alumina	93.5	86.3	19.0
	DSS	Pd on alumina	94.5	92.7	22.7
	MFSS	Pt-Rh on alumina	92.2	87.5	24.2
	MFSA	Pt-Rh-Pb on alumina	97.0	96.0	78.3
	4X-MFSA	Pt-Rh-Pb on alumina	74.5	73.5	72.8
	MFP	Fe <sub>2</sub> O <sub>3</sub> on silicon carbide	59.5	3.3	2.3
Catalysts and Chemicals, Inc.	Cl2-3	Fe <sub>2</sub> O <sub>3</sub> , Cr <sub>2</sub> O <sub>3</sub> on alumina	0.2	---	---
	Cl3-6	NiO on alumina	3.6	---	---
Girdler Chemical Company	G-22	Ba-promoted copper chromite	0.2	---	---
	G-49B	Ni on kieselguhr	0.8	---	---
	G-62	CoO on "special base"	3.1	---	---
	G-67	CoO on kieselguhr	1.5	---	---
	G-67RS	Co on kieselguhr	4.7	---	---
	T-3	Cu on kieselguhr	2.5	---	---
	T-893	ZrO <sub>2</sub> -promoted nickel	7.2	---	---
	T-1205	ZrO <sub>2</sub> -promoted nickel	4.4	---	---
Houdry Process Corporation	A-100S	Pt on alumina	3.3	---	---
	B-100S	Pd on alumina	2.7	---	---
	A-200SR	Pt on alumina	85.6	66.0	9.6
	A-25Z	Cr <sub>2</sub> O <sub>3</sub>	2.3	---	---
Shell Development Company	405	---	51.2	38.7	8.4
		Pt on alumina	30.9	14.9	5.0
Sundstrand					

Conditions of test:

Oxygen/hydrogen mixture ratio, 0.33  
Catalyst charge, 5 grams  
Run duration, 10 minutes  
Theoretical water yield, 0.396 gram



TABLE 6  
SUMMARY RESULTS OF CATALYST EVALUATIONS IN BOTH FUEL-RICH  
AND OXIDIZER-RICH SERVICE EXTRACTED FROM TABLES 3 AND 4

Catalyst	Vendor	Percentage Conversion							
		Fuel-Rich System				Oxygen-Rich System			
		77 F	-114 F	-320 F	77 F	-114 F	-320 F	77 F	-320 F
Hydrogenation-type									
DS	Engelhard Industries, Inc.	93.5	86.3	19.0	88.1	37.2	0.2		
DSS	Engelhard Industries, Inc.	94.5	92.7	22.7	75.5	59.9	5.3		
MFSS	Engelhard Industries, Inc.	92.2	87.5	24.2	80.8	63.5	5.3		
MFSA	Engelhard Industries, Inc.	97.0	96.0	78.3	71.3	60.6	50.4		
4X-MFSA	Engelhard Industries, Inc.	74.5	73.5	72.8	72.1	37.5	0.0		
405	Shell Development Co.	89.5	83.2	28.3	36.4	9.7	2.9		
A-200SR	Houdry Process Corp.	85.6	66.0	9.6	99.8	77.7	26.2		
Oxidation-type									
MFP	Engelhard Industries, Inc.	59.5	3.3	2.3	80.1	10.5	3.3		
A-25Z	Houdry Process Corp.	4.2	---	---	57.3	7.5	1.4		
T-3	Girdler Chemical Co.	2.5	---	---	19.2	17.4	11.4		





TABLE 7  
RESULTS OF THERMAL SHOCK TREATMENT\* ON  
PHYSICAL STRUCTURE AND RELATIVE ACTIVITY

Catalyst	Size and Support	Effect of Treatment		Relative Activity at 77 F	
		Pellet Cracking	Color Change	Before Treatment	After Treatment
MFP	3/16-inch cylindrical silicon carbide	None	None	80.1	0.0
C-13-1	1/4-inch cylindrical alumina	Slight	Grey-brownish	1.2	6.8
G-22	1/8-inch cylindrical copper chromite	Visible	Black-greenish	2.8	1.6
T-1205	1/8-inch cylindrical kieselguhr	None	Black-greenish	8.3	2.5
C-12-3	1/4-inch cylindrical alumina	Visible	Brown-dark brown	13.9	0.9
G-67RS	1/8-inch cylindrical kieselguhr	Visible slight	Black-grey	2.9	3.9
G-49B	1/8-inch cylindrical kieselguhr	Visible slight	Black-greenish	3.2	4.1
T-893	1/4-inch cylindrical refractory	None	Black-greenish	6.3	1.0
G-62	1/8-inch cylindrical "special base"	Visible slight	Black-blue green	13.5	0.5
T-3	1/8-inch cylindrical kieselguhr	Slight	Black-reddish	3.1	2.3
A-25Z	1.8-inch extruded alumina	Slight	- - - - -	57.3	3.9
G-67	1/8-inch cylindrical kieselguhr	----	Black-brownish	3.7	6.7
4X-MFSA	1/8-inch spherical alumina	None	None	74.5	72.0
Sundstrand	5/16-inch spherical alumina	None	None	30.9	26.3

\*Catalyst prechilled in liquid nitrogen to -320 F, placed in a furnace operating at 1832 F for 10 minutes, then reimmersed in liquid nitrogen



TABLE 8

SUMMARY OF RESULTS WITH GASEOUS REACTANTS

Run No.	Catalyst	Environmental Temperature, F		Total Flowrate, lb/sec	Mixture Ratio, o/f	Chamber		Ignition Lag, milliseconds										Remarks
								Chamber Pressure					Chamber Temperature					
		Catalyst	Propellant			Temperature, F	Pressure, psig	First Indication	63.2 Percent of Steady State	90 Percent of Steady State	First Indication	63.2 Percent of Steady State	90 Percent of Steady State	First Indication	63.2 Percent of Steady State	90 Percent of Steady State		
1	MFSA	-250	-246	0.0238	0.713	1122	60	20	100	1100	23	330	1,460	No ignition Delayed ignition; pressure surge Delayed ignition; pressure surge Flashback No ignition Pressure surge				
2	(MFSA)	-250	-250	0.0151	0.831	1280	67	20	310	1300	25	450	1,550					
3	(MFSA)	-250	-258	0.0346	0.65	1400	95	13	250	1450	20	280	1,010					
4	(MFSA)	-250	-250	0.0510	0.73	1280	155	15	140	800	20	185	750					
5	MFP	-175	-240	0.0239	0.74	-100	3	No Ignition										No ignition
6	(MFP)	75	75	0.0213	0.63	1229	54	20	6000	9000	2000	8900	10,500	Delayed ignition; pressure surge				
7	(MFP)	75	75	0.0293	0.66	2315 <sup>1</sup>	58 <sup>1</sup>	45	70	7400	900	6400	8,600	Delayed ignition; pressure surge				
8	MFP	-100	75	0.0330	0.52	1084 <sup>1</sup>	46	10	1500	3600	1050	2400 <sup>2</sup>	4,300 <sup>2</sup>	Flashback				
9	(MFP)	-150	75	0.0366	0.54	1242 <sup>1</sup>	55	15	4600	7500	1100	5700 <sup>2</sup>	7,500 <sup>2</sup>					
10	(MFP)	-190	75	0.0292	0.78	1825 <sup>1</sup>	44 <sup>1</sup>	15	2500	4500	1200	3600 <sup>2</sup>	5,800 <sup>2</sup>					
11	MFP	-225	75	0.0336	0.62	-225	25	No Ignition										No ignition
12	C13-2	75	75	0.0254	143 <sup>3</sup>	1122	35	100	2200	9000	200	4600	8,800	Pressure surge				
13	MFP	85	85	0.0173	172 <sup>3</sup>	873	16	150	4500	5400	200	7000	10,400					
14	MFSA	76	83	0.0185	92 <sup>3</sup>	1186	15	200	950	4000	200	4500	9,400					
15	MFSA	-206	76	0.0188	93 <sup>3</sup>	1349	16	20	900	2700	20	4200	8,800					

( ) Parentheses indicate the same catalyst used in the previous run

<sup>1</sup>Transient measurement

<sup>2</sup>Times are to 63.2 and 90 percent of maximum value attained

<sup>3</sup>Data questionable because of the inaccuracies in measuring very small hydrogen flows



TABLE 9  
SUMMARY OF RESULTS OF CATALYST LIFE STUDIES

Run No.	Catalyst	Environmental Temperature, F			Total Flowrate, lb/sec	Mixture Ratio, o/f	Chamber		Remarks
		Catalyst Bed	Liquid Hydrogen	Liquid Oxygen			Temperature, F	Pressure, psig	
1	MFSS	-409	-409	-302	0.135	1.25	-300	5	4(Liquid hydrogen)-on-1 (liquid oxygen) injector; no ignition; 5-second liquid hydrogen lead
2	MFSS	-405	-405	-300	0.128	1.19	B.O.	200*	4-on-1 injector; delayed ignition; bed burnout
3	MFSS	-405	-405	-300	0.104*	0.50*	B.O.	3	4-on-1 injector; liquid oxygen flow erratic; catalyst preburned at 500 F; delayed ignition; reactor destroyed
4	MFSA	-410	-410	-300	0.069	1.02*	2280+	200+	Liquid hydrogen flow erratic; bed burned out
5	MFSA	-403	-403	-302	0.134	0.75*	2280+	200+	Liquid hydrogen flow erratic; delayed ignition; bed burned out
6	MFSA	-408	-408	-305	0.074	1.32	600	85	Liquid hydrogen flow stable; catalyst preburned at 250 F for 1 minute
7	(MFSA)	-408	-408	-305	0.084	1.33	700	68	Reaction quenched

\*Transient measurement

NOTE: Parentheses indicate same catalyst as in preceding run

TABLE 9  
(Continued)

		Environmental Temperature, F			Total Flowrate, lb/sec	Mixture Ratio, o/f	Chamber		Remarks
		Catalyst Bed	Liquid Hydrogen	Liquid Oxygen			Temperature, F	Pressure, psig	
8	(MFSA)	-410	-410	-303	0.082	1.28	B.O.	300+	Internal explosion; bed blown out of reactor
9	MFSA	-413	-413	-300	0.158	1.26	-300	12	Catalyst preburned at 850 F for 2 minutes; internal explosion at run termination
10	MFSA	-408	-408	-300	0.133	1.22	-240	12	1.5-second liquid hydrogen lead; catalyst preburned at 850 F for 1 minute
11	405	-402	-402	-301	0.149	1.26	-120	75*	Catalyst preburned at 780 F for 6 minutes; reaction quenched; postrun detonation
12	MFSA	-405	-405	-305	0.105	1.23	557	126	Catalyst preburned at 750 F for 10 minutes; reaction zone near injector
13	MFSA	-410	-410	-303	0.131	1.21	482	105	Catalyst preburned at 750 F for 10 minutes; reaction zone near injector

\*Transient measurement

NOTE: Parentheses indicate same catalyst as in preceding run



TABLE 9  
(Continued)

Run No.	Catalyst	Environmental Temperature, F		Total Flowrate, lb/sec	Mixture Ratio, o/f	Chamber		Remarks
		Catalyst Bed	Liquid Hydrogen			Temperature, F	Pressure, psig	
14	MFSA	-405	-405	0.100	1.13	1186	60	1-inch mixing zone length; pressure surge
15	(MFSA)	-408	-408	0.114	1.33	1400	90	1-inch mixing zone length; moderate catalyst burning; pressure surge
16	MFSA	-412	-412	0.100	1.00	1100	55	1/2-inch mixing zone length
17	(MFSA)	-412	-412	0.098	1.05	1200	55	1/2-inch mixing zone length; severe catalyst burning
18	MFSA	-408	-408	0.116	1.00	962	50	Al <sub>2</sub> O <sub>3</sub> mixed with first inch of catalyst; constrictor rings at 1-inch intervals; reaction quenched
19	MFSA	-415	-415	0.249	1.09	1400	92	Al <sub>2</sub> O <sub>3</sub> mixed with first inch of catalyst; constrictor rings at 1-inch intervals; reaction quenched

NOTE: Parentheses indicate same catalyst as in preceding run

TABLE 9  
(Continued)

Run No.	Catalyst	Environmental Temperature, F			Total Flowrate, lb/sec	Mixture Ratio, o/f	Chamber		Remarks
		Catalyst Bed	Liquid Hydrogen	Liquid Oxygen			Temperature, F	Pressure, psig	
20	MFSA	-403	-403	-240	0.092	0.48	-250	15	Configuration same as run 19; two-phase liquid oxygen flow; catalyst preburned at 600 F for 2 minutes
21	(MFSA)	-403	-403	-240	0.110	0.57	-250	10	Configuration same as run 20; two-phase liquid oxygen flow
22	(MFSA)	-410	-410	-305	0.123	0.95	1370	108	Configuration same as run 21
23	(MFSA)	-403	-403	-304	0.089	1.23	2280+	66	Configuration same as run 22; pressure surge
24	(MFSA)	-420	-420	-305	0.084	1.21	2280+	60	Configuration same as run 23
25	(MFSA)	-420	-420	-305	0.085	1.13	2280+	100	Configuration same as run 24
26	(MFSA)	-420	-420	-305	0.090	1.00	2280+	70	Configuration same as run 25
27	(MFSA)	-420	-420	-305	0.085	1.36	2280+	45	Configuration same as run 26; catalyst severely burned
28	MFSA	-420	-420	-300	0.081	1.08	1444	30	Catalyst preburned at 800 F for 2 minutes

NOTE: Parentheses indicate same catalyst as in preceding run

TABLE 9  
(Continued)

Run No.	Catalyst	Environmental Temperature, F			Total Flowrate, lb/sec	Mixture Ratio, o/f	Chamber		Remarks
		Catalyst Bed	Liquid Hydrogen	Liquid Oxygen			Temperature, F	Pressure, psig	
29	MFSA	-410	-410	-240	0.081	0.45	482	65	Gaseous oxygen flow to injector; 3/4-inch mixing zone length; constrictor rings at 1-inch intervals
30	(MFSA)	-415	-415	-250	0.075	0.36	325	63	Gaseous oxygen flow to injector
31	(MFSA)	-405	-405	-240	0.078	0.39	325	40	Gaseous oxygen flow to injector
32	(MFSA)	-410	-410	-230	0.069	0.35	280	35	Gaseous oxygen flow to injector
33	(MFSA)	-415	-415	-305	0.212	1.19	1460	60	Liquid oxygen flow to injector
34	(MFSA)	-410	-410	-305	0.217	1.13	1482	60	Liquid oxygen flow to injector. New, "zero storage" MFSA catalyst, pressure transducer iced closed
35	(MFSA)	-410	-410	-300	0.213	0.68	1000	45	
36	(MFSA)	-405	-405	-300	0.206	0.93	1665	75	
37	(MFSA)	-410	-410	-305	0.220	1.02	1470	80	
38	(MFSA)	-415	-410	-305	0.123	1.56	1444	45	
39	(MFSA)	-415	-415	-305	0.112	1.33	1554	45	
40	MFSA	-415	-415	-305	0.123	1.16	1293	ND	

NOTE: Parentheses indicate same catalyst as in preceding run

TABLE 9  
(Concluded)

Run No.	Catalyst	Environmental Temperature, F			Total Flowrate, lb/sec	Mixture Ratio, o/f	Chamber		Remarks
		Catalyst Bed	Liquid Hydrogen	Liquid Oxygen			Temperature, F	Pressure, psig	
41	(MFSA)	-410	-410	-305	0.122	1.18	2280+	ND	
42	(MFSA)	-415	-415	-305	0.128	1.13	1250	ND	
43	(MFSA)	-412	-412	-302	0.134	0.20	1366	ND	
44	(MFSA)	0410	-410	-300	0.129	1.30	1964	ND	
45	(MFSA)	-415	-415	-302	0.130	1.24	1894	ND	
46	Sundstrand	-400	-400	-305	0.124	1.14	-230	15	Sundstrand catalyst preburned at 1100 F for 2 minutes
47	(Sundstrand)	-400	-400	-305	0.124	1.10	-240	12	
48	(Sundstrand)	-400	-400	-302	0.118	1.27	2280+	60*	Temperature and pressure surge at run termination
49	MFSA	-415	-415	-305	0.111	1.28	920*	48*	Temperature pressure and flowrate cycling; "zero storage" MFSA

\*Transient measurement

NOTE: Parentheses indicate same catalyst as in preceding run





TABLE 10

EFFECTS OF VARIOUS TREATMENTS ON CATALYTIC  
ACTIVITY FOR THE ENGELHARD MFSA CATALYST

Treatment Conditions*		Percent Conversion at -320 F
Temperature, F	Atmosphere	
500	Nitrogen	59.4
250	Hydrogen	35.6
500	Hydrogen	67.6
1000	Hydrogen	84.0
1000	Air	75.4

\*10-minute treatment duration

## Run Conditions:

Oxygen/hydrogen mixture ratio, 0.33

Run duration, 10 minutes

Theoretical water, 0.396 gram

Catalyst charge, 5 grams

Catalyst, Engelhard MFSA

Original activity at -320 F, 78.3 percent

Activity at -320 F after storage, 12.3 percent



TABLE 11

EFFECTS OF STORAGE ENVIRONMENT ON ACTIVITY  
FOR THE ENGELHARD MFSA CATALYST

Storage Environment	Duration	Percent Conversion at -320 F
Normal Daily Atmospheric Changes	1 Month	52.4
Oxygen-rich at 150 F	1 Week	44.2
	1 Month	55.0
Evacuated, water soaked	---	43.7
Controlled Dry Storage	1 Month	47.1
Normal Daily Temperature Changes, controlled 100-percent relative humidity	1 Month	36.0

## Run Conditions:

Oxygen/hydrogen mixture ratio, 0.53

Run duration, 10 minutes

Theoretical water, 0.396 gram

Catalyst charge, 5 grams

Catalyst, Engelhard MFSA

Original Activity at -320 F, 48.8 percent



TABLE 12

SUMMARY OF RESULTS OF PARAMETRIC ENGINE EVALUATIONS

Run No.	Catalyst	Igniter					Engine				Time, milliseconds			
		Environmental Temperature, F			Total Flowrate, lb/sec	Mixture Ratio, o/f	Chamber Temperature, F	Propellant Temperature, F		Total Flowrate, lb/sec	Mixture Ratio, o/f	Target Chamber Pressure, psig	To Ignition	To 90-Percent Chamber Pressure
		Catalyst Bed	Hydrogen	Oxygen				Hydrogen	Oxygen					
1	MFSA	-250	68	68	0.160	0.89	1463	-410	-248	44.7	5.8	250	30	150
2	MFSA		68	68	0.160	0.89	1488	-410	-253	45.0	5.6	250	28	150
3	MFSA	-250	68	68	0.171	0.90	1470	-410	-271	22.0	1.61	250	80	300
4	MFSA		68	68	0.171	0.90	1448	-410	-271	22.3	1.62	250	80	270
5	MFSA	-250	68	68	0.159	0.92	1435	-400	-278	20.2	5.2	100	14	130
6	MFSA		68	68	0.159	0.92	1457	-400	-280	21.7	5.3	100	16	127
7	MFSA	-250	69	69	0.161	0.87	1589	-405	-280	10.1	1.46	100	40	130
8	MFSA		69	69	0.161	0.87	1580	-405	-280	9.8	1.58	100	40	140
9	MFSA	-250	68	68	0.180	0.86	1466	-410	-249	45.3	5.4	250	20	250
10	MFSA		68	68	0.180	0.86	1464	-408	-253	44.8	5.8	250	22	150
11	MFSA	-250	68	68	0.099	0.91	1457	-408	-250	44.2	6.3	250	30	280
12	MFSA		68	68	0.099	0.91	1448	-408	-250	44.3	6.2	250	40	100
13	MFSA	-250	72	72	0.067	0.90	1431	-409	-251	44.7	5.9	250	60	200
14	MFSA		72	72	0.067	0.90	1475	-408	-253	44.3	5.8	250	50	230
15	MFSA	-250	66	66	0.175	0.89	1549	-405	-270	9.9	1.54	100	43	130
16	MFSA		66	66	0.175	0.89	1558	-408	-274	9.7	1.62	100	45	120
17	MFSA	-250	70	70	0.094	0.84	1405	-410	-270	9.8	1.58	100	40	230
18	MFSA		70	70	0.094	0.84	1400	-410	-270	10.2	1.43	100	40	150
19	MFSA	-250	69	69	0.067	0.86	1383	-405	-274	9.9	1.54	100	40	150
20	MFSA		69	69	0.067	0.86	1392	-407	-270	10.3	1.40	100	30	130
21	MFSA	-250	72	72	0.072	0.88	1435	-403	-263	44.7	5.8	250	50	240
22	MFSA		72	72	0.107	0.88	1400	-410	-265	45.0	5.6	250	32	430



TABLE 13

EXPERIMENTAL CONSTANTS FOR CATALYTIC REACTION RATE  
ANALYSES WITH FUEL-RICH AND OXIDIZER-RICH REACTANTS

Catalyst	Reactant Condition	Constants*		
		$C_1''$	n	$f \left( \frac{\Delta E}{R} \right)$
MFSA	Fuel-rich	-1220	-200	-1,380,000
MFSS	Fuel-Rich	- 135	- 39	- 257,000
4X-MFSA	Fuel-rich	67	1.4	- 8,900
MFSA	Oxidizer-rich	- 550	94	19,400
MFSS	Oxidizer-rich	- 131	35	5,600
4X-MFSA	Oxidizer-rich	1850	290	- 58,800
A-200SR	Oxidizer-rich	1460	-200	64,000
MFP	Oxidizer-rich	1515	-200	65,000

\*Constants used in the equation

$$\ln (\text{percent conversion}) = \ln C_1'' + n \ln T - \frac{\Delta E}{RT}$$



TABLE 14

SUMMARY OF RESULTS OF CATALYTIC REACTOR  
DESIGN CRITERIA INVESTIGATIONS\*

Run No.	Reactant Flowrate, lb/sec	Mixture Ratio (o/f)	Reaction Temperature, F	Catalyst Volume, cu in.	Catalyst Mass, pounds	Ratio of Reactant Flowrate to Catalyst Volume, lb/sec-sq in. cu in.
1	0.0282	1.0	1510	0.785	0.0196	0.046
2	0.0334	1.0	1505	0.785	0.0196	0.055
3	0.0371	1.07	Cold	0.785	0.0196	0.061
4	0.0464	1.00	1519	1.18	0.0295	0.050
5	0.0496	1.00	1466	1.18	0.0295	0.054
6	0.0514	0.94	Cold	1.18	0.0295	0.056
7	0.0469	0.93	1390	1.57	0.0393	0.038
8	0.0594	1.05	1545	1.57	0.0393	0.049
9	0.0678	0.92	Cold	1.57	0.0393	0.055
10	0.0661	1.04	1490	2.36	0.0590	0.036
11	0.0753	0.95	1427	2.36	0.0590	0.041
12	0.0867	0.97	Cold	2.36	0.0590	0.047

\*Data extracted from previous studies (Ref. 3) conducted under NASA Contract NAS 3-2565.

Run Conditions:

Catalyst, Engelhard MFSS  
Environmental Temperature  
Catalyst, -250 F  
Reactants, -250 F

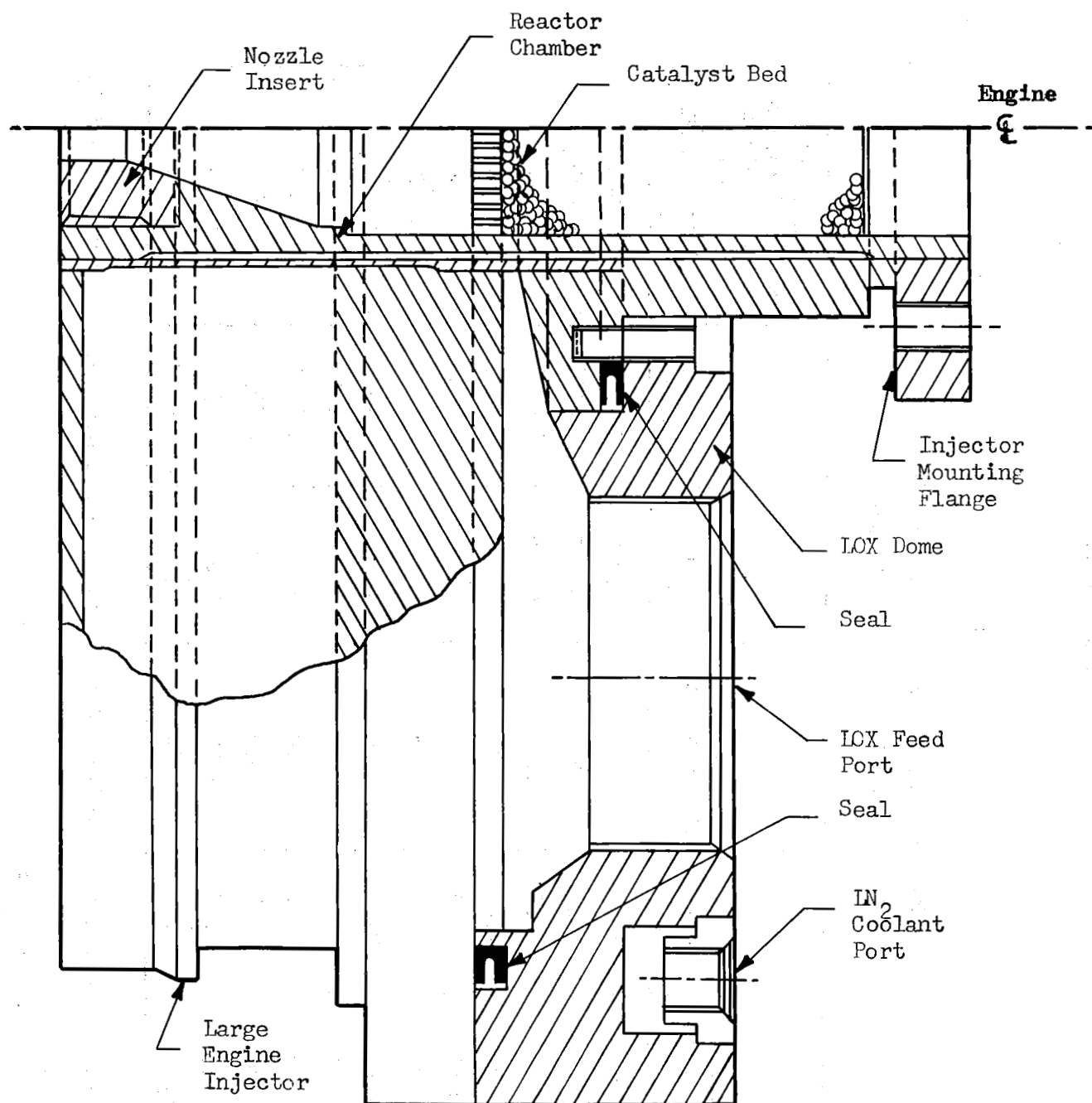


Figure 1. Cut-Away of Injector and LOX Dome for the Large Engine Used in the Parametric Engine Evaluation Task Illustrating Modifications to Adapt to the Catalytic Igniter

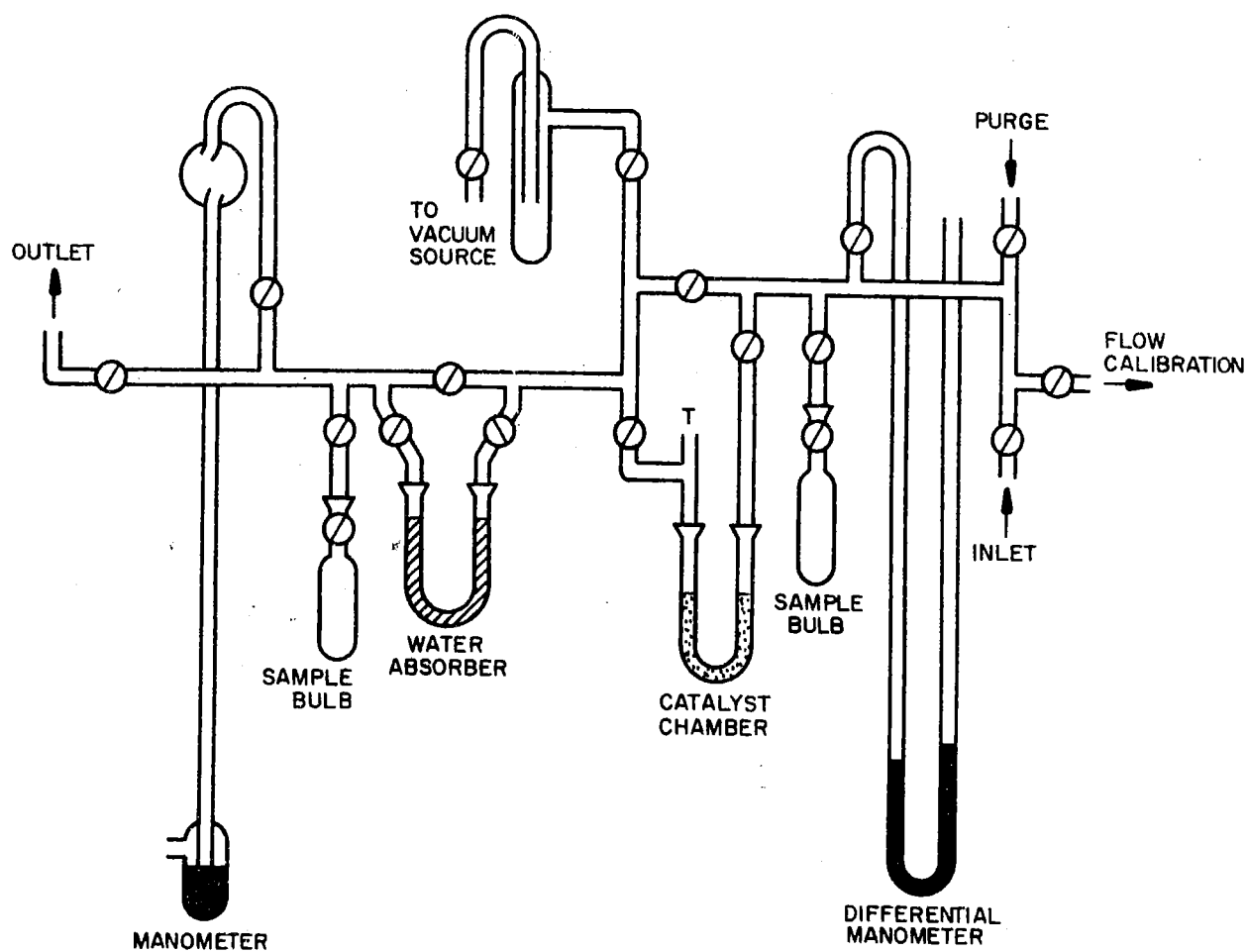


Figure 2. Small-Scale Laboratory Apparatus Used in the Preliminary Catalyst Evaluation Task with  $O_2/H_2$  Reactants

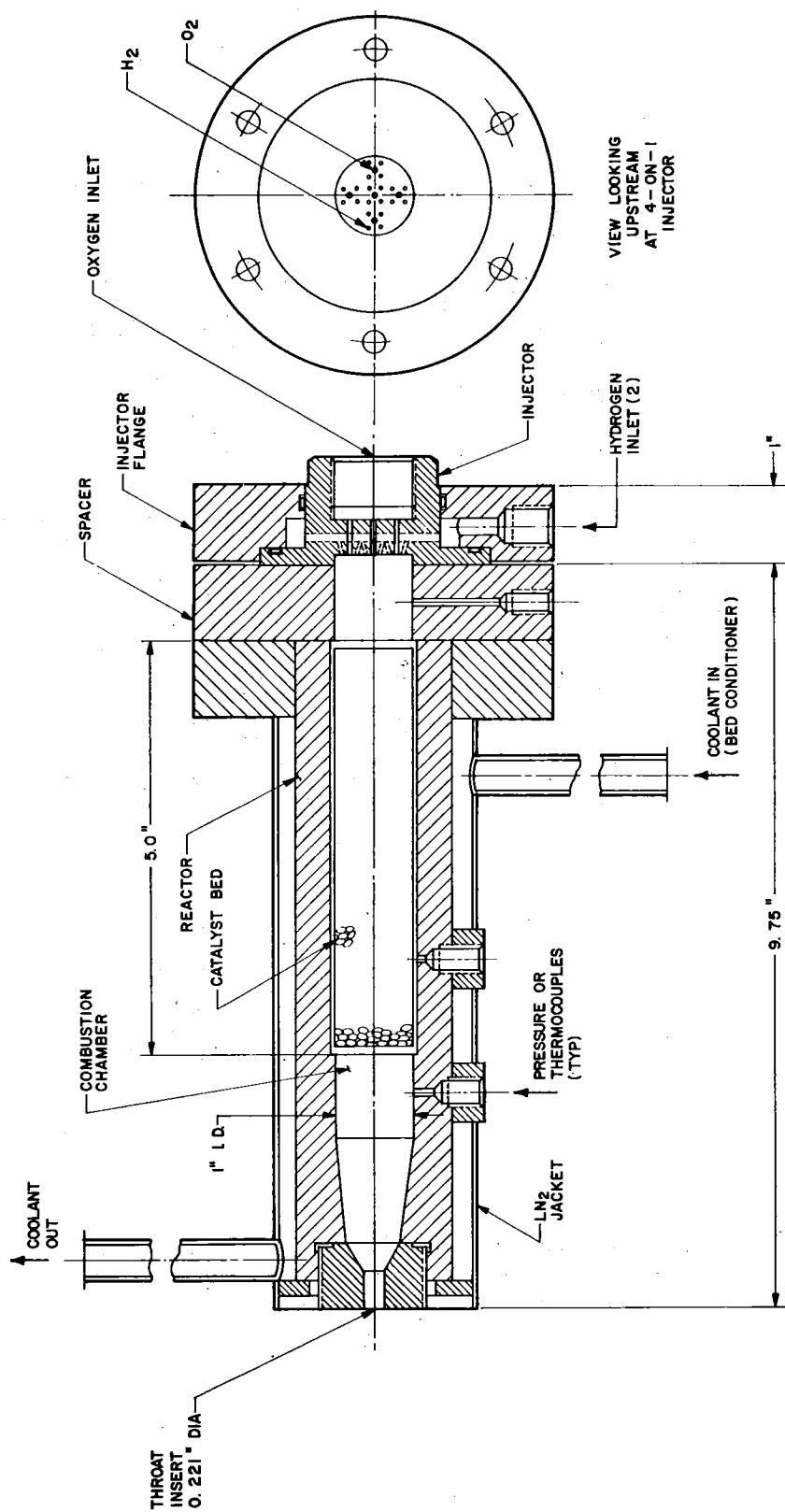


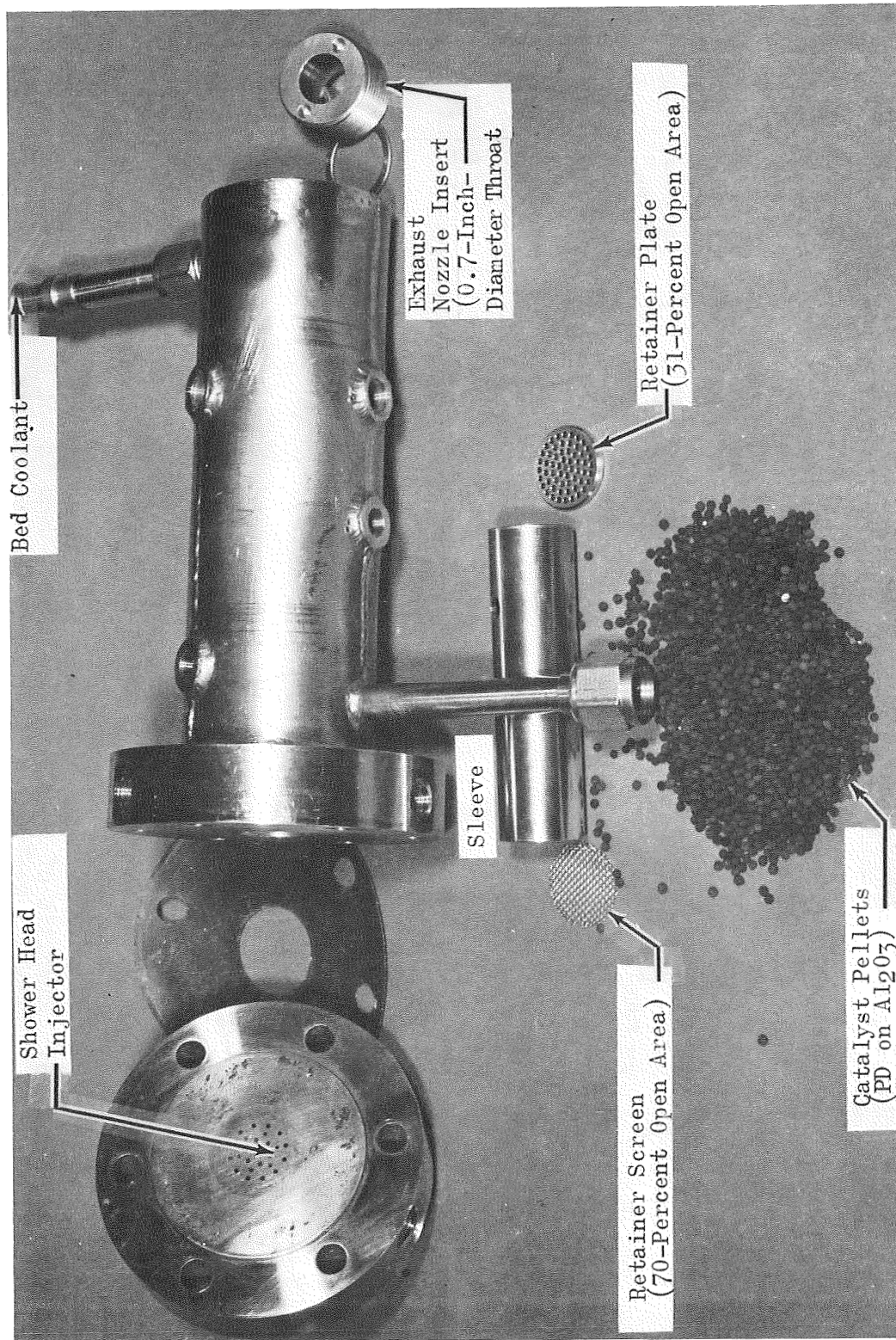
Figure 3. Schematic of 1-Inch-Diameter Catalytic Reactor Used in the Catalyst Selection Task Illustrating Location of Catalyst Bed and 4-on-1 Injector





ROCKETDYNE •

A DIVISION OF NORTH AMERICAN AVIATION, INC.



1247-8/16/62-SIF

Figure 4. Photograph of 1-Inch-Diameter Combustor Disassembled to Show Major Components (5-Inch Catalyst Bed Configuration)

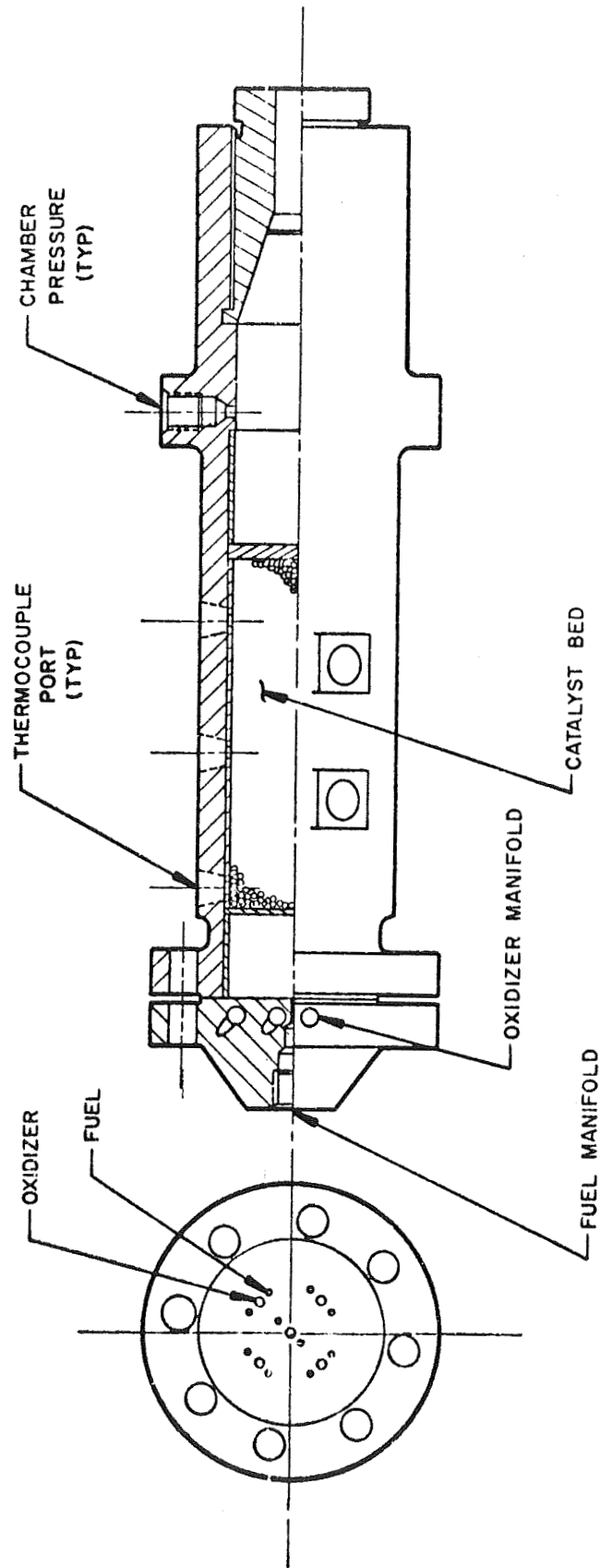


Figure 5. Schematic of the Catalytic Reactor Used in the Low-Temperature Catalyst Evaluation Experiments in the Catalyst Life Study Task

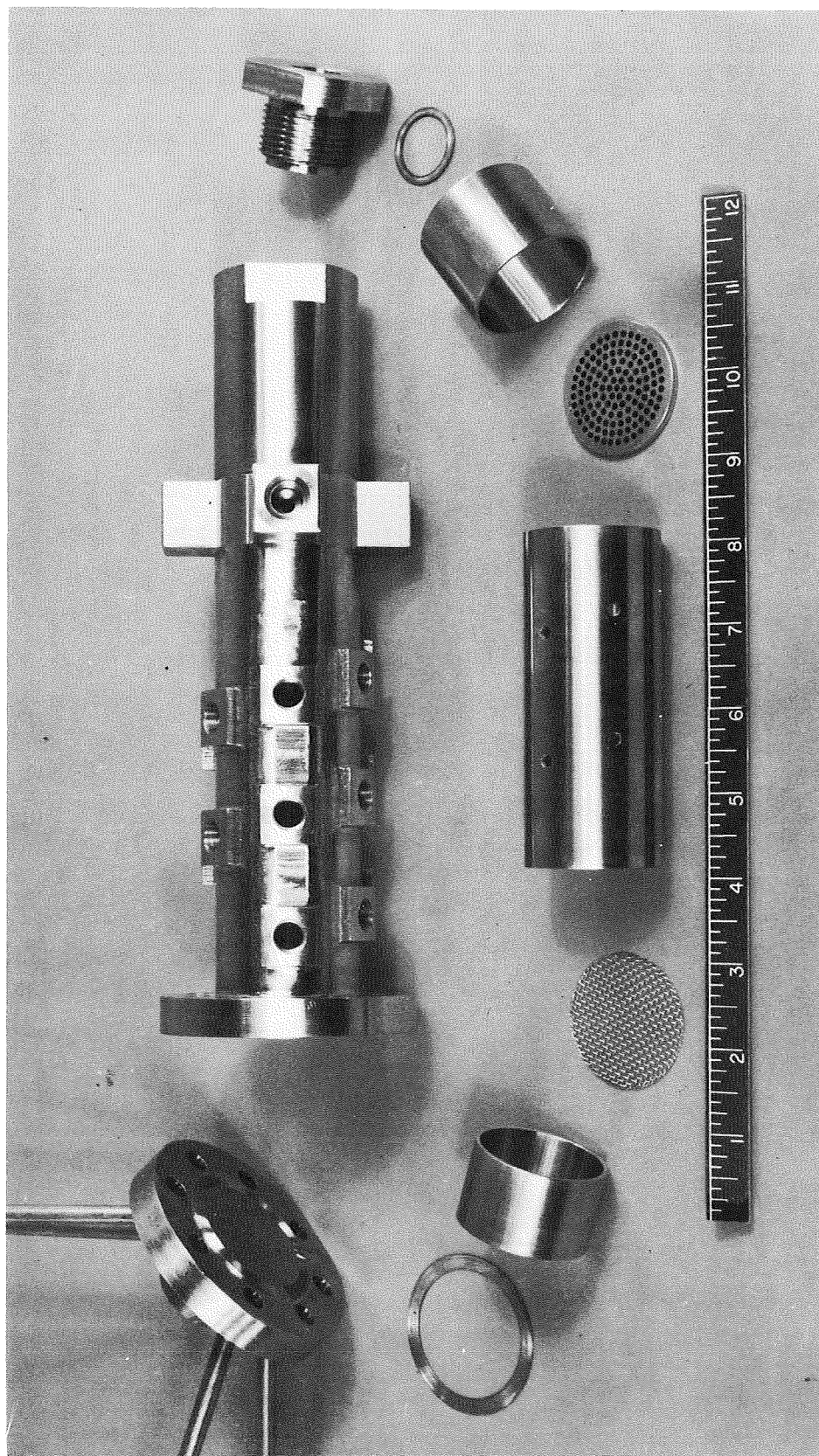


Figure 6. Photograph of 1-1/2-Inch-Diameter Reactor Used in the Catalyst Life Study Task Disassembled to Show Major Component Parts



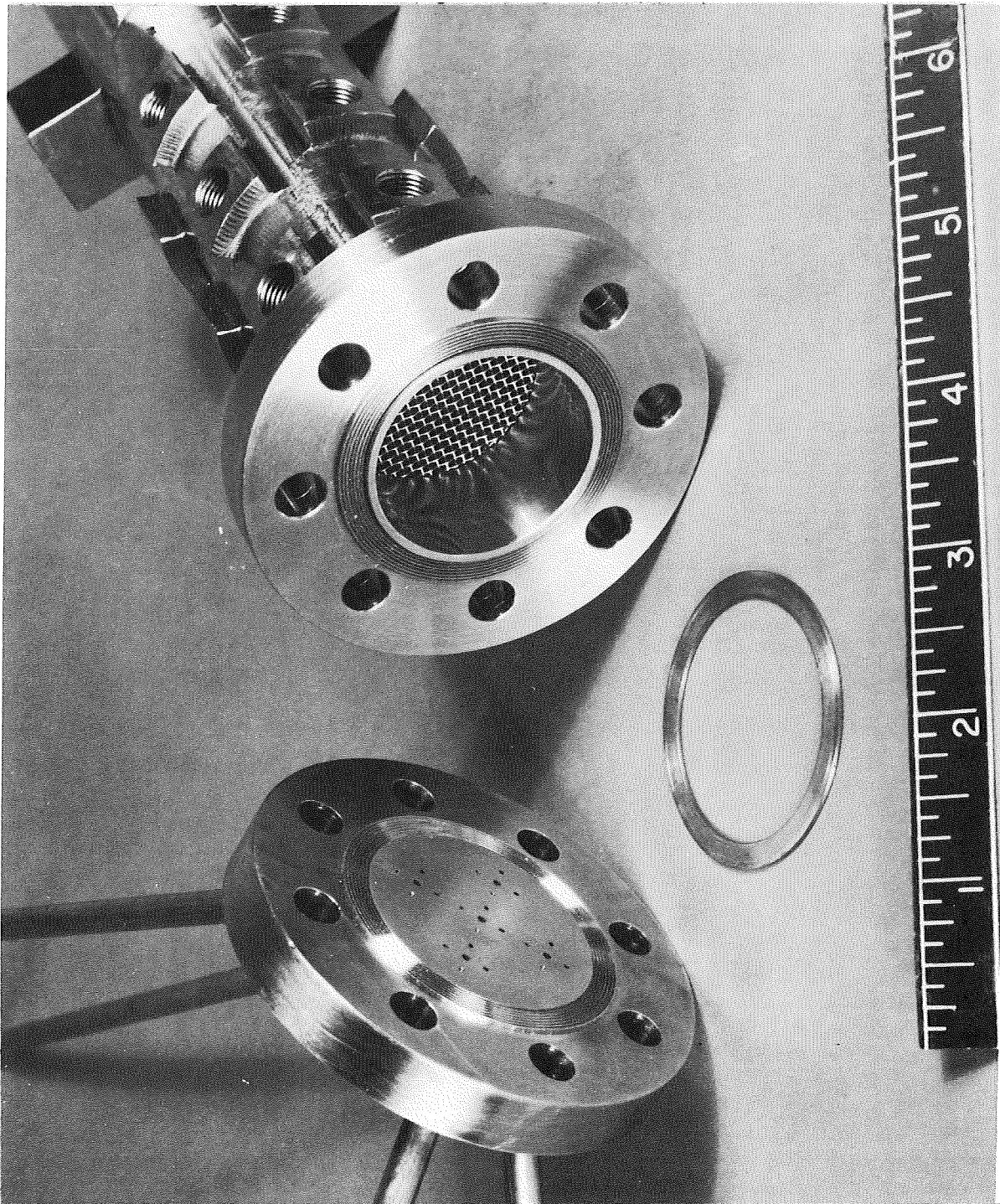
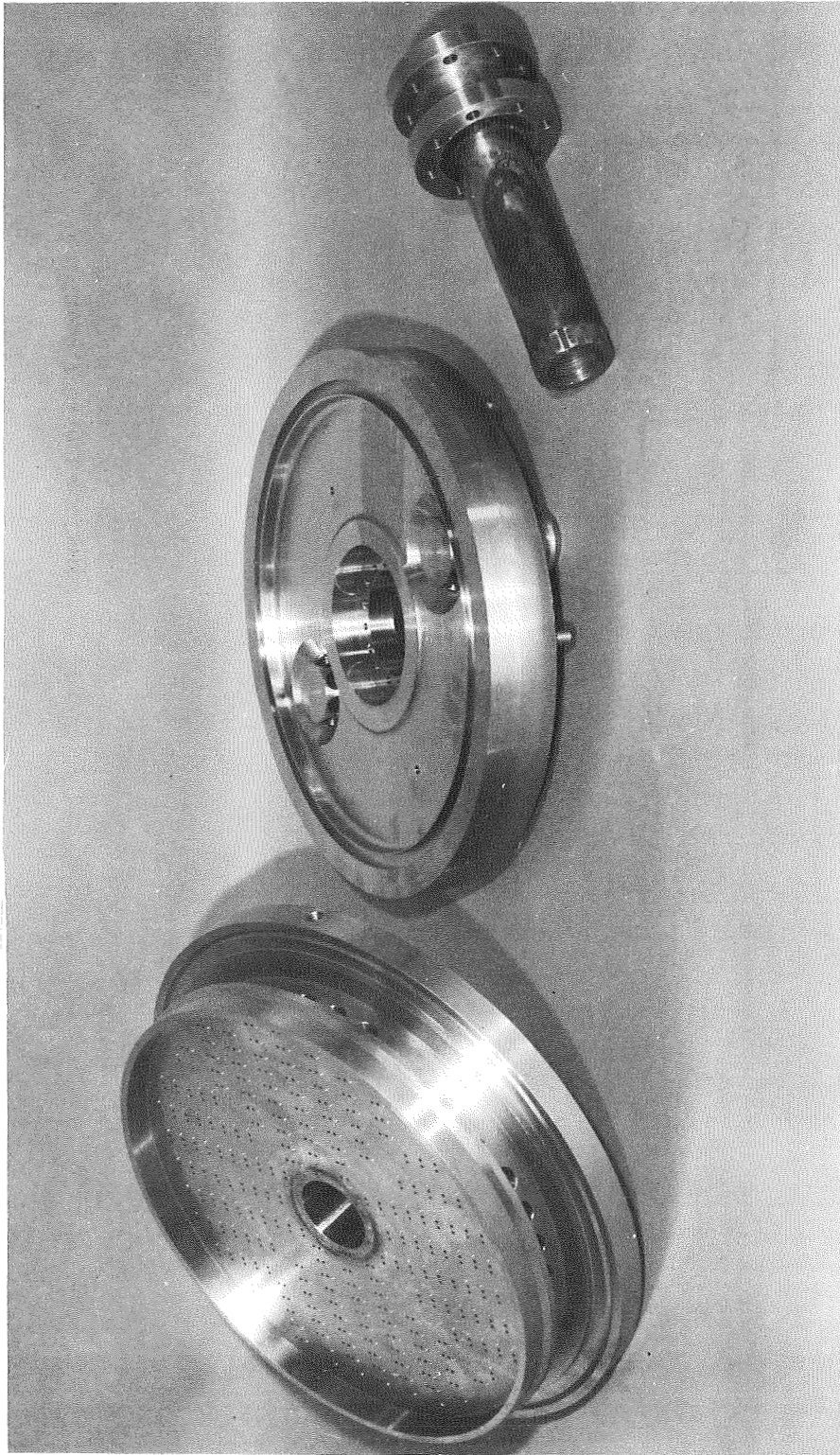


Figure 7. Assembled View of 1-1/2-Inch Catalytic Reactor Used in the Catalyst Life Study Task



5AA33-10/11/65-S1E

Figure 8. Illustration of the Injector, LOX Dome, and Catalytic Igniter Used in the Parametric Engine Evaluation Task

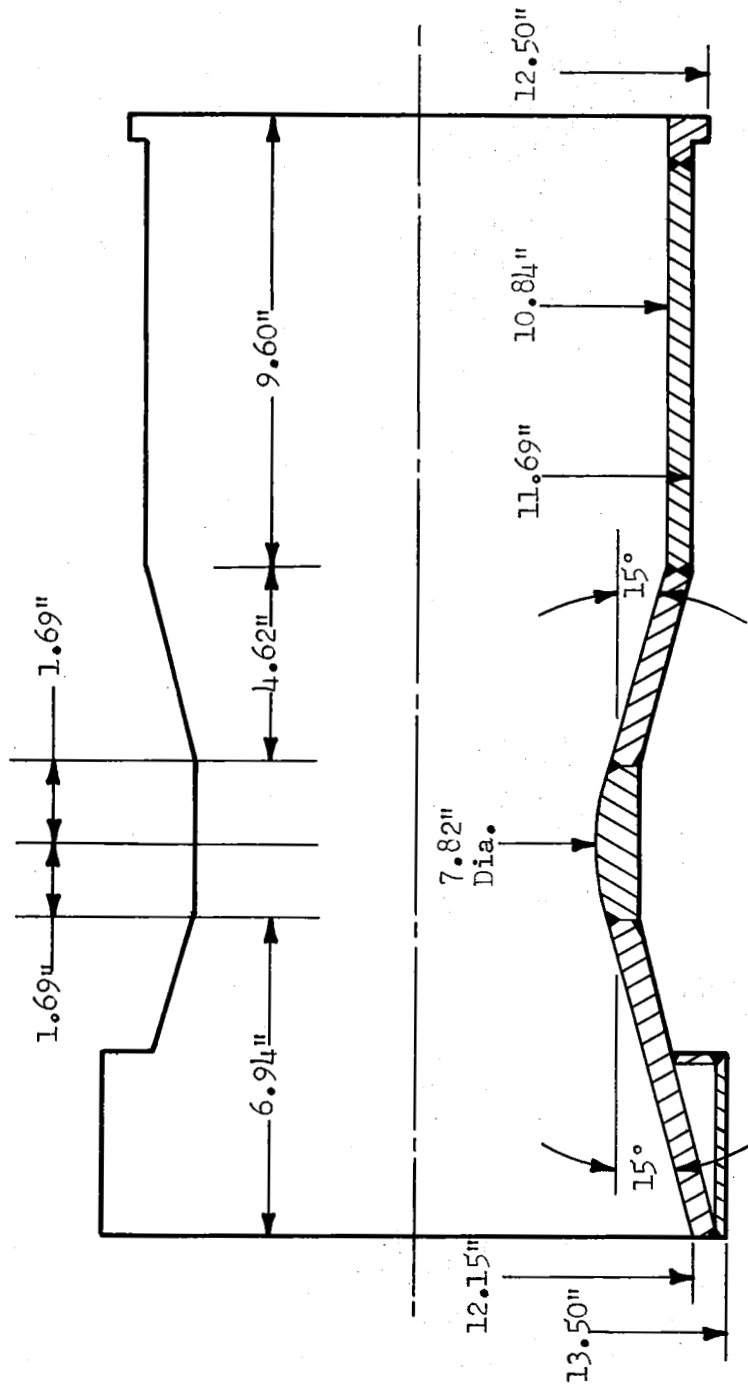
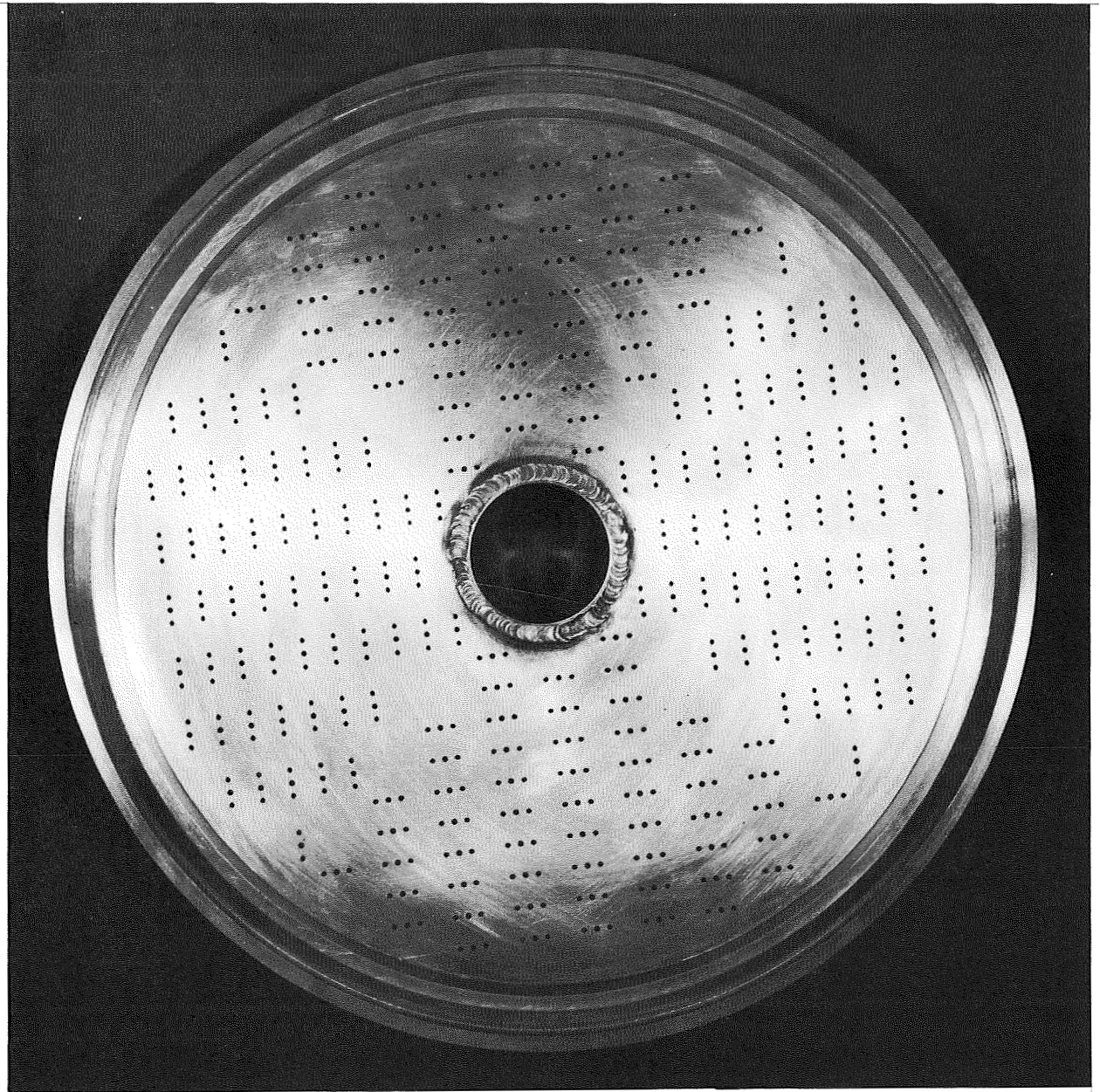


Figure 9. Schematic of Large-Engine Chamber Used in the Parametric Engine Evaluation Task Illustrating Size and Relative Dimensions





5AA33-10/11/65-S1A

Figure 10. Photographic Representation of the Injector Used in the Parametric Engine Evaluation Task Illustrating the Injection Pattern and Catalytic Igniter Adapter Port

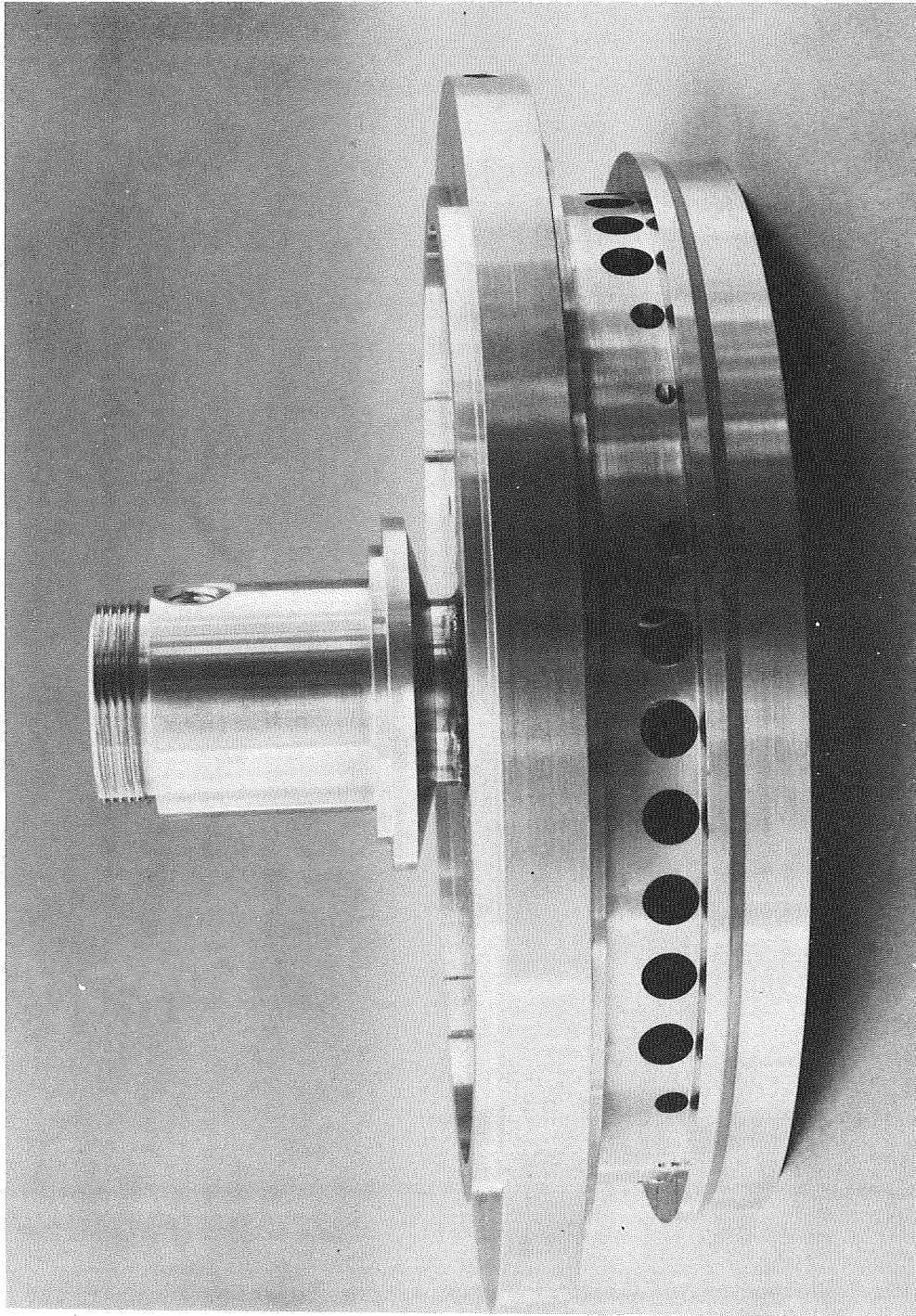
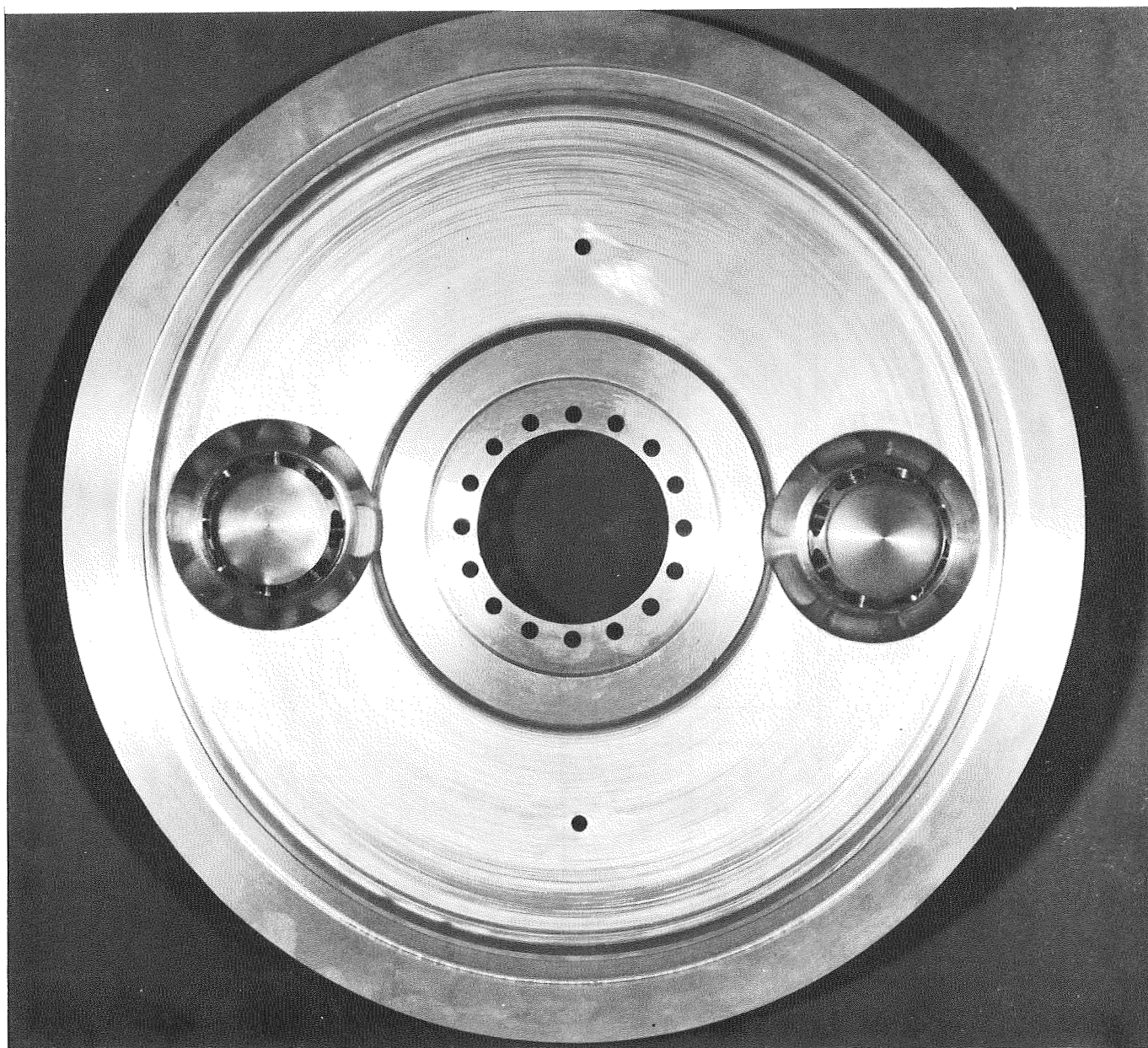


Figure 11. Side View of the Injector Used in the Parametric Engine Evaluation Task Illustrating the Fuel Manifold and Catalytic Igniter Adapter





5AA33-10/11/65-SID

Figure 12. Photographic Representation of the Liquid Oxygen Dome Used in the Parametric Engine Evaluation Task Illustrating the Catalytic Igniter Adapter Port and Oxygen Manifold

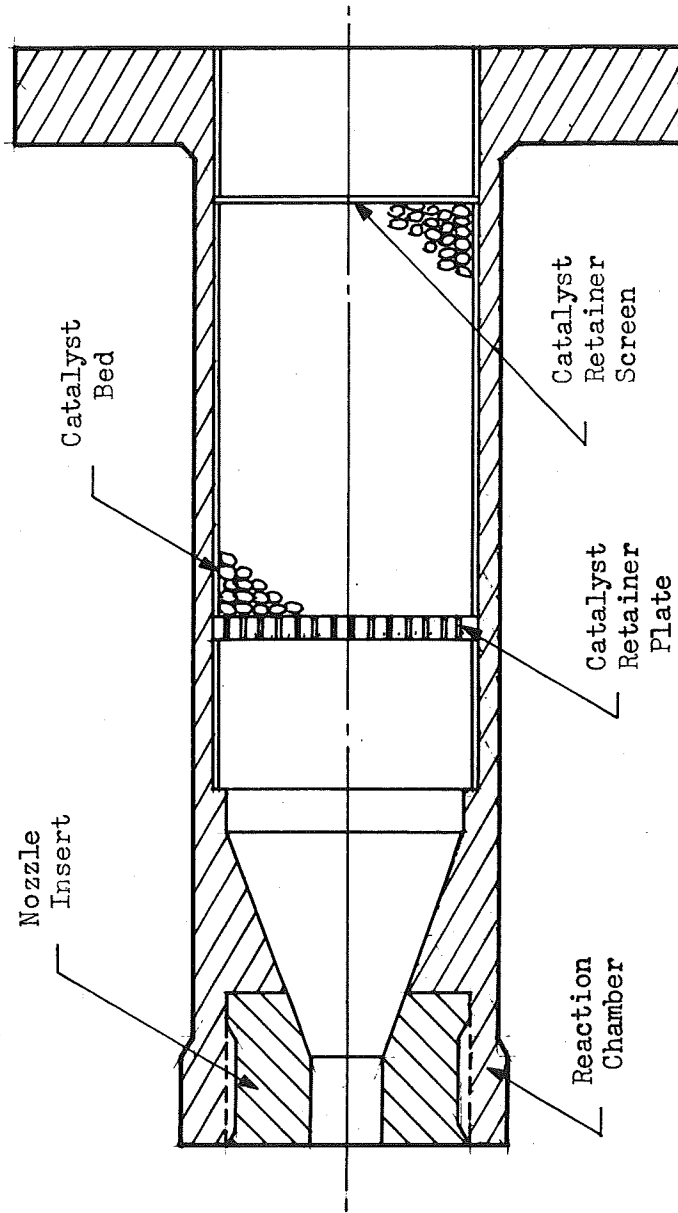


Figure 13. Schematic of the Catalytic Igniter Used for Large-Engine Ignition in the Parametric Engine Evaluation Task Illustrating Assembly and Component Parts



5AA33-10/11/65-SIC  
Figure 14. Photographic Representation of the Catalytic Igniter Used in the  
Parametric Engine Evaluation Task

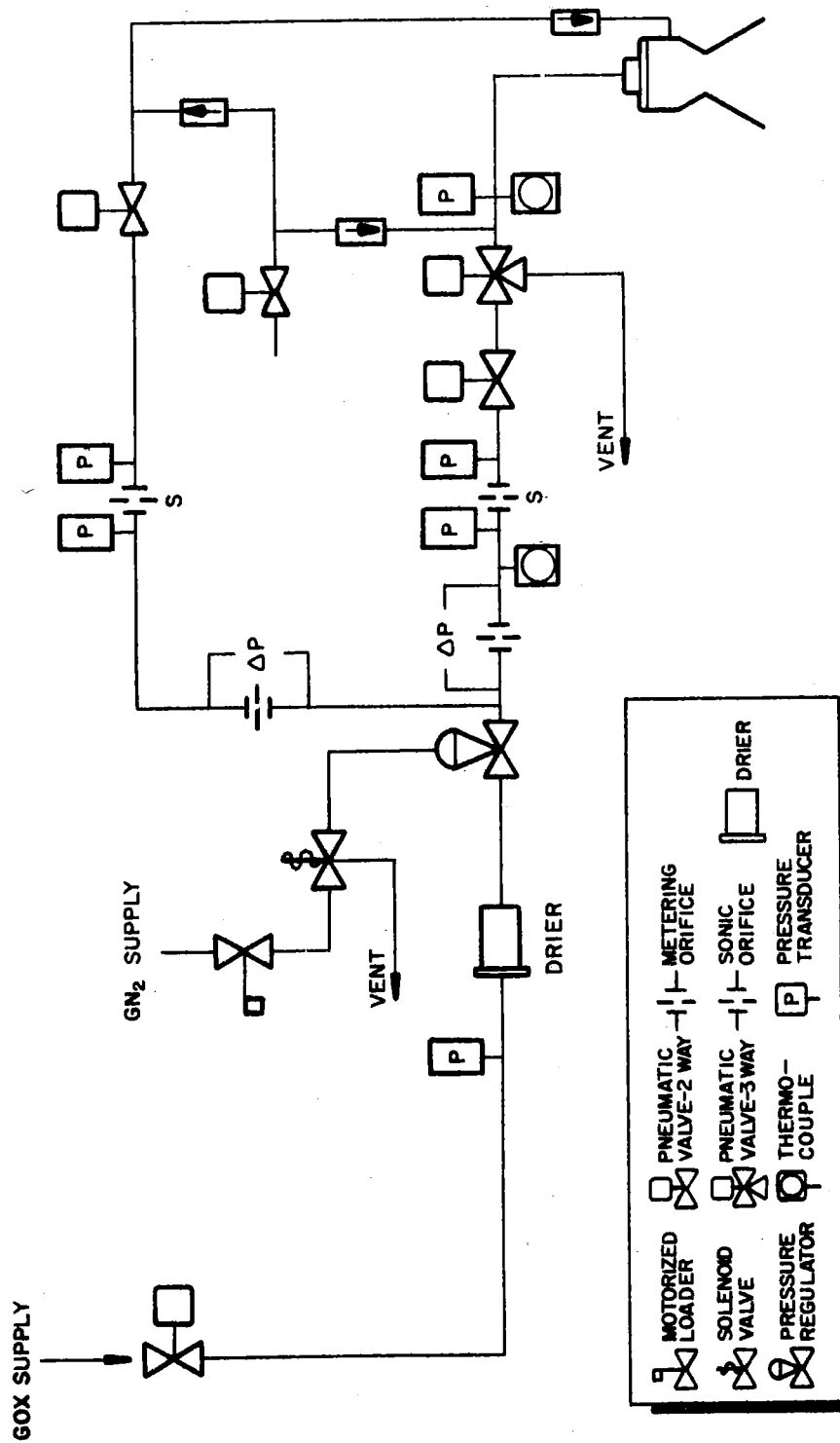
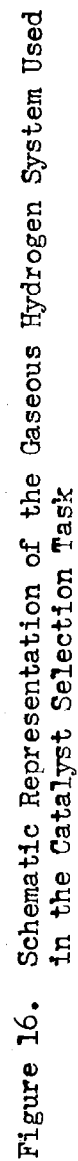


Figure 15. Schematic Illustration of the Gaseous Oxygen System Used in the Catalyst Selection Task



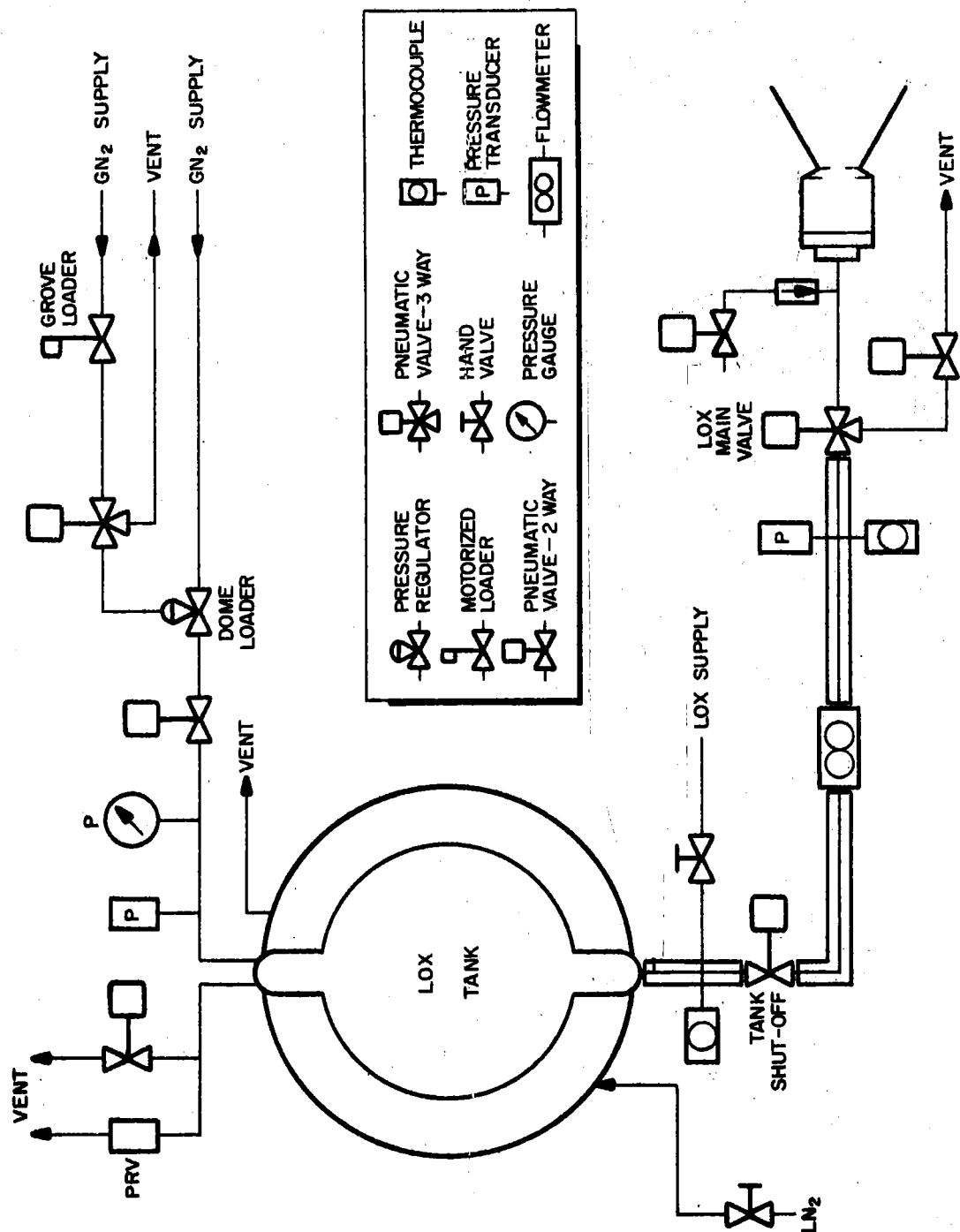


Figure 17. Schematic Representation of the Liquid Oxygen System Used in the Catalyst Life Study Task

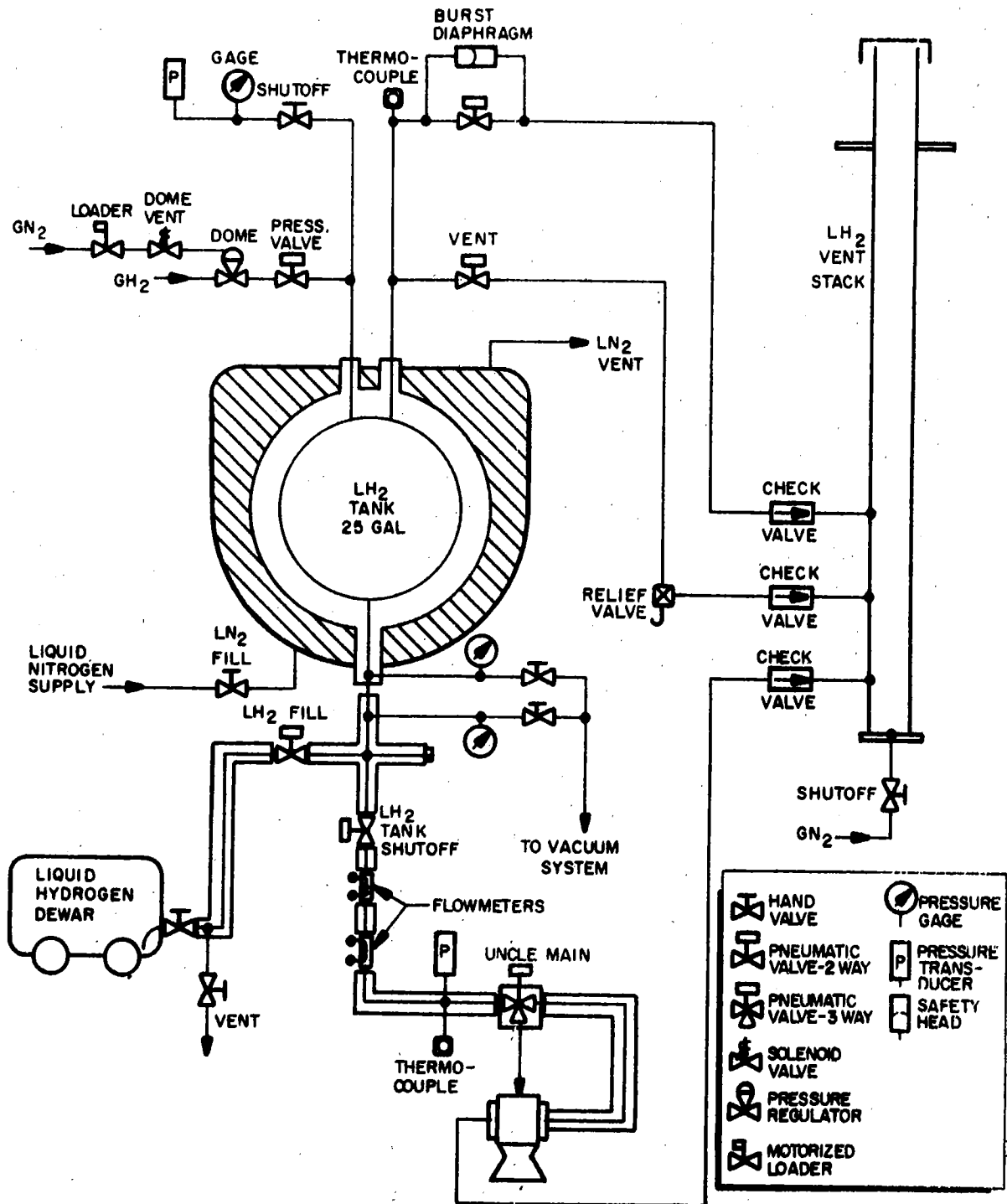


Figure 18. Schematic Representation of Liquid Hydrogen System Used in the Catalyst Life Study Task

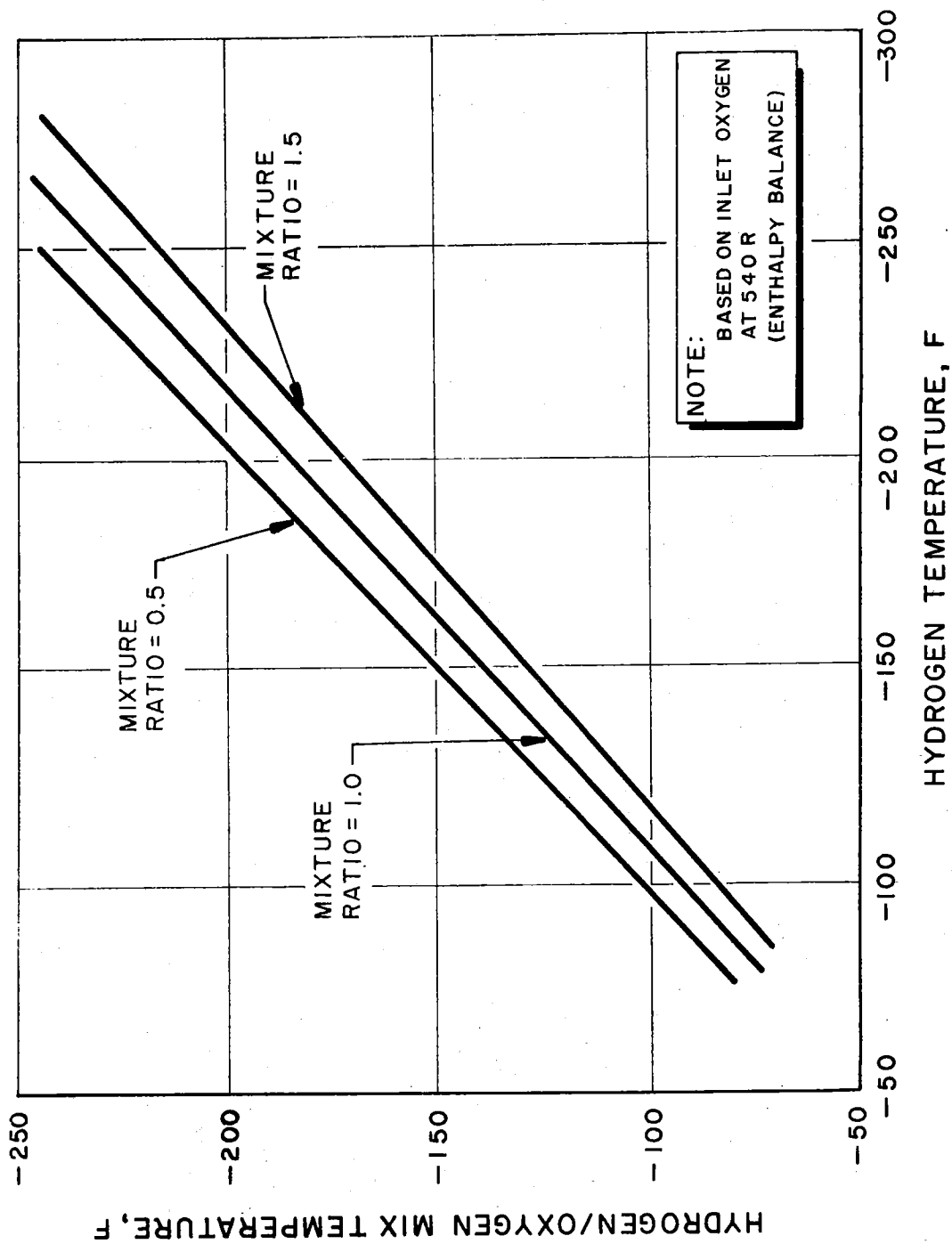


Figure 19. Theoretical Oxygen/Hydrogen Mixture Temperatures as a Function of Hydrogen Inlet Temperature and Mixture Ratio



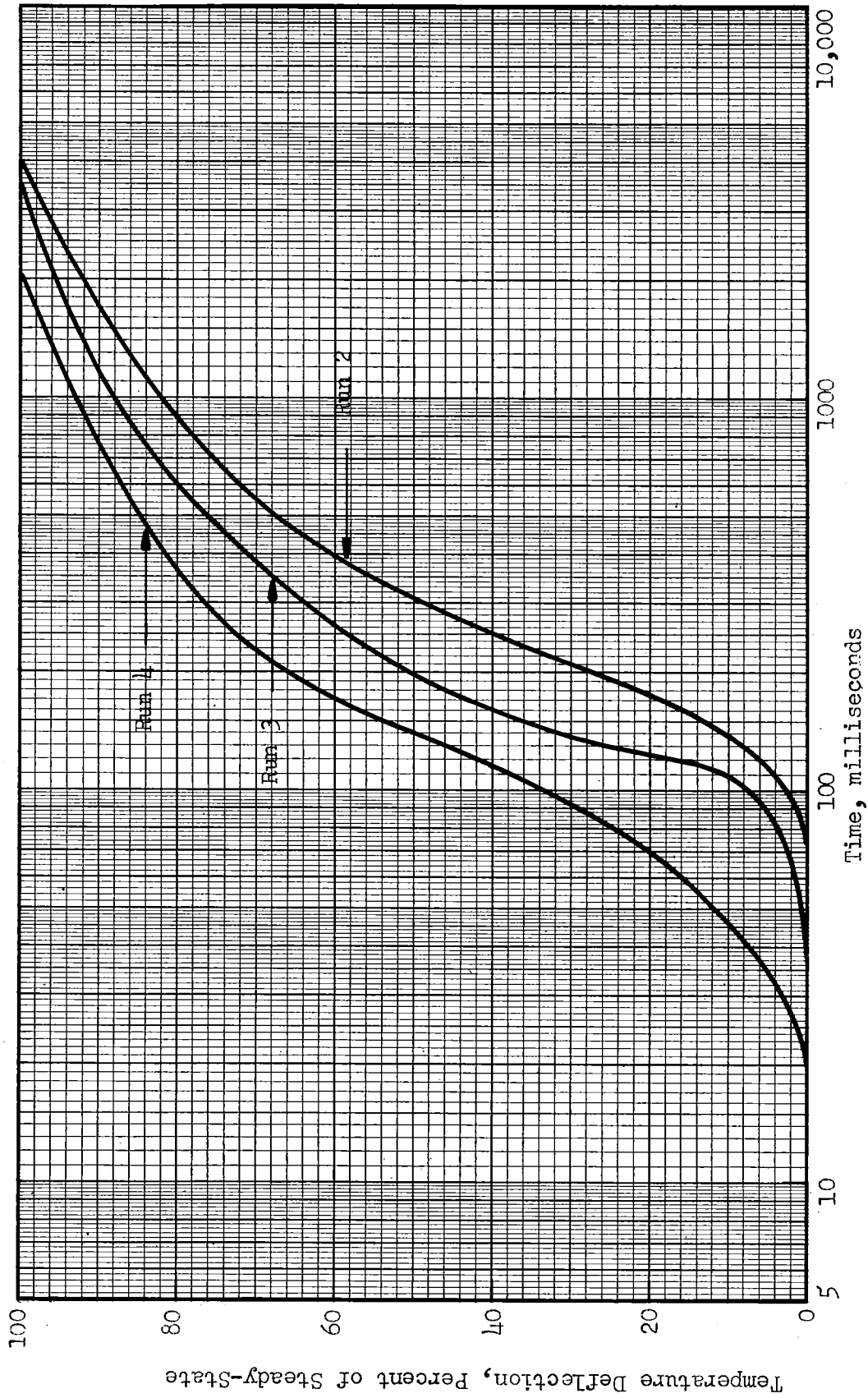


Figure 20. Comparison of Response Rates for the Engelhard MFSA Catalyst as a Function of the Rate of Approach to Steady-State Operating Temperature for Various Reactant Flowrates.

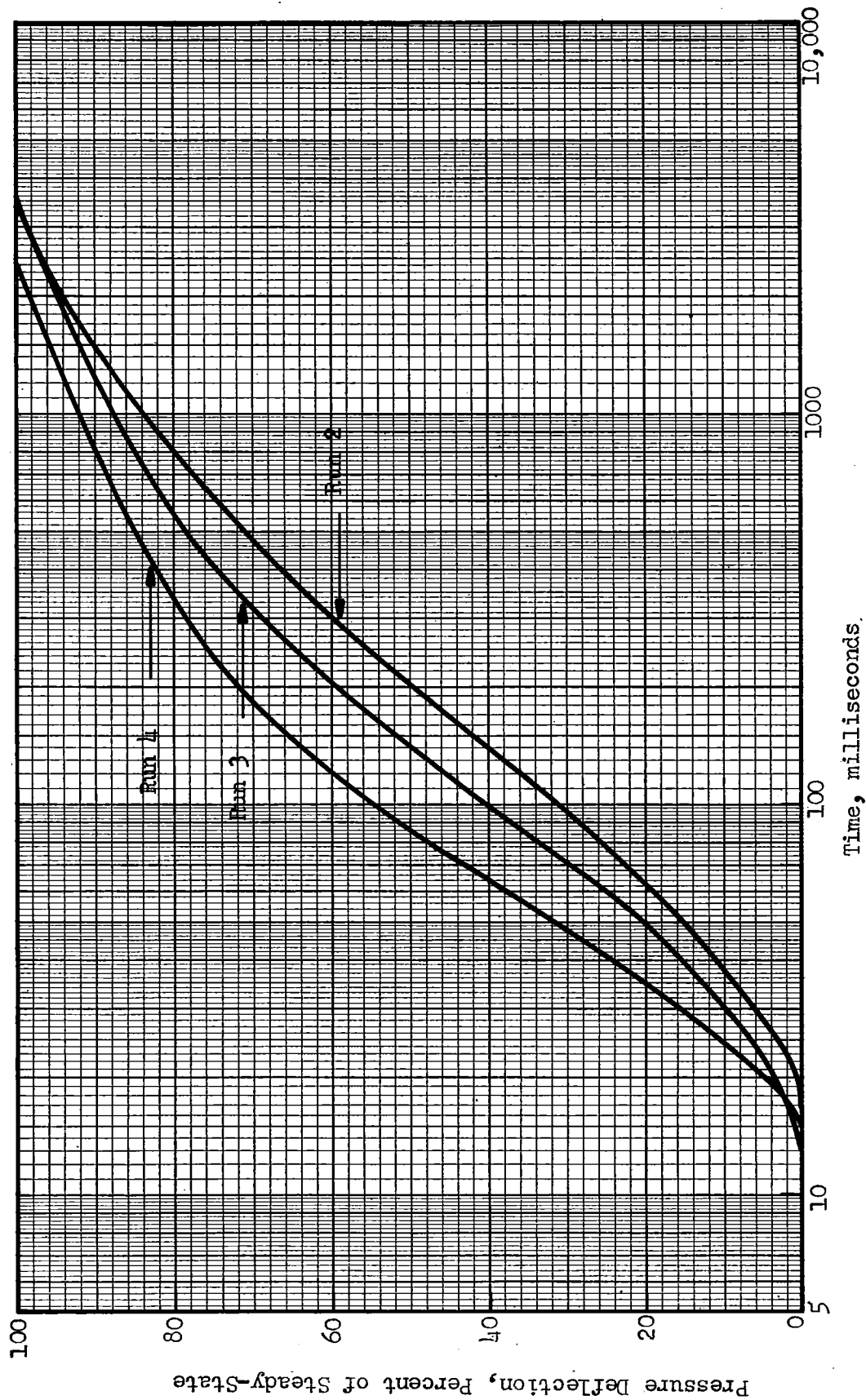


Figure 21. Comparison of Response Rates for the Engelhard MFSA Catalyst as a Function of the Rate of Approach to Steady-State Operating Pressure for Various Reactant Flowrates

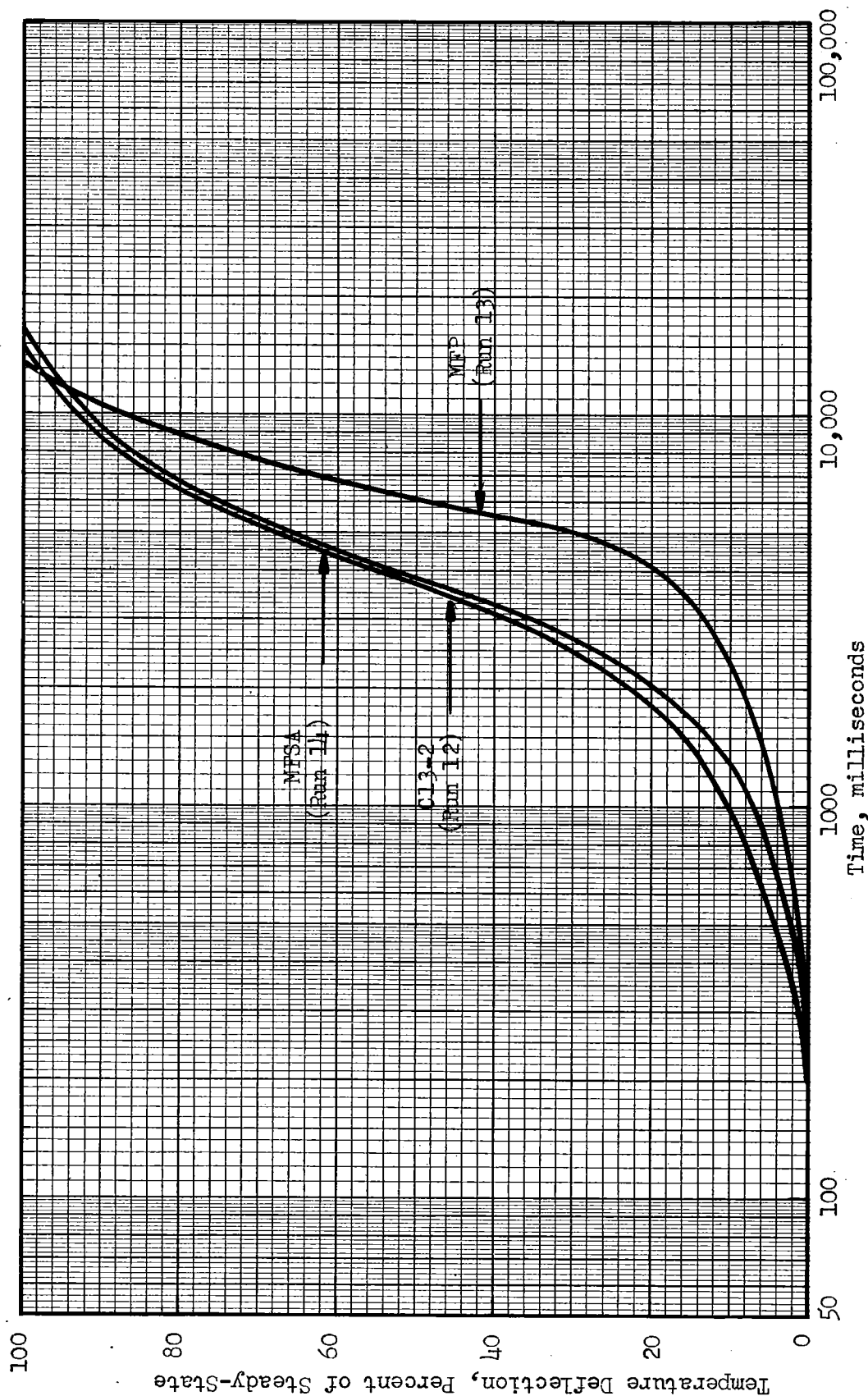


Figure 22. Comparison of Response Rates of Engelhard MFP and MFSA and Catalysts and Chemicals, Inc. Cl3-2 Catalysts in Oxidizer-Rich Reactants Under Comparable Conditions of Flowrate as a Function of the Rate of Approach to Steady State Operating Temperature.

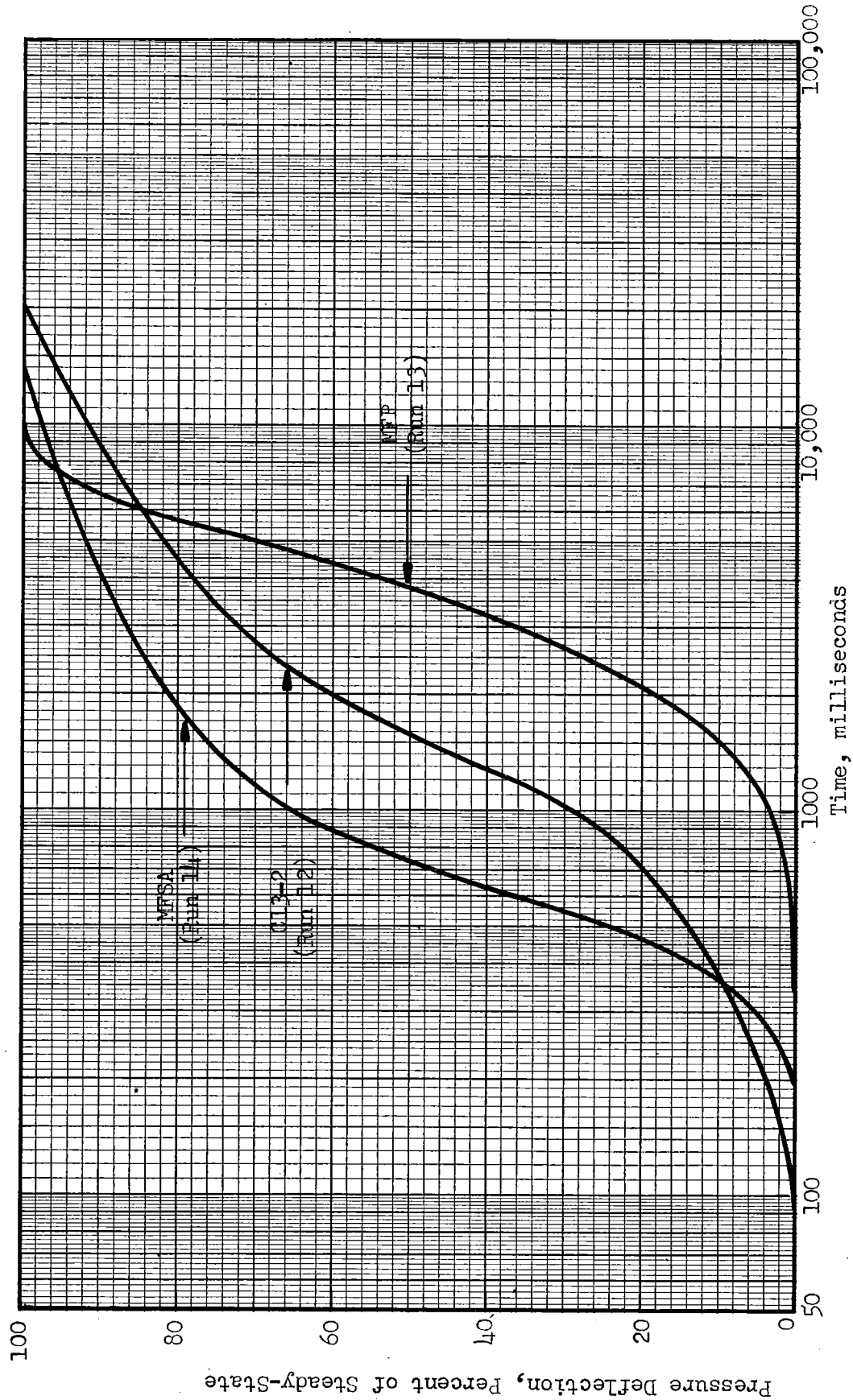


Figure 23. Comparison of Response Rates of Engelhard MFP and MFSA and Catalysts and Chemicals, Inc. Cl3-2 Catalysts in Oxidizer-Rich Reactants Under Comparable Conditions of Flowrate as a Function of the Rate of Approach to Steady-State Operating Pressure

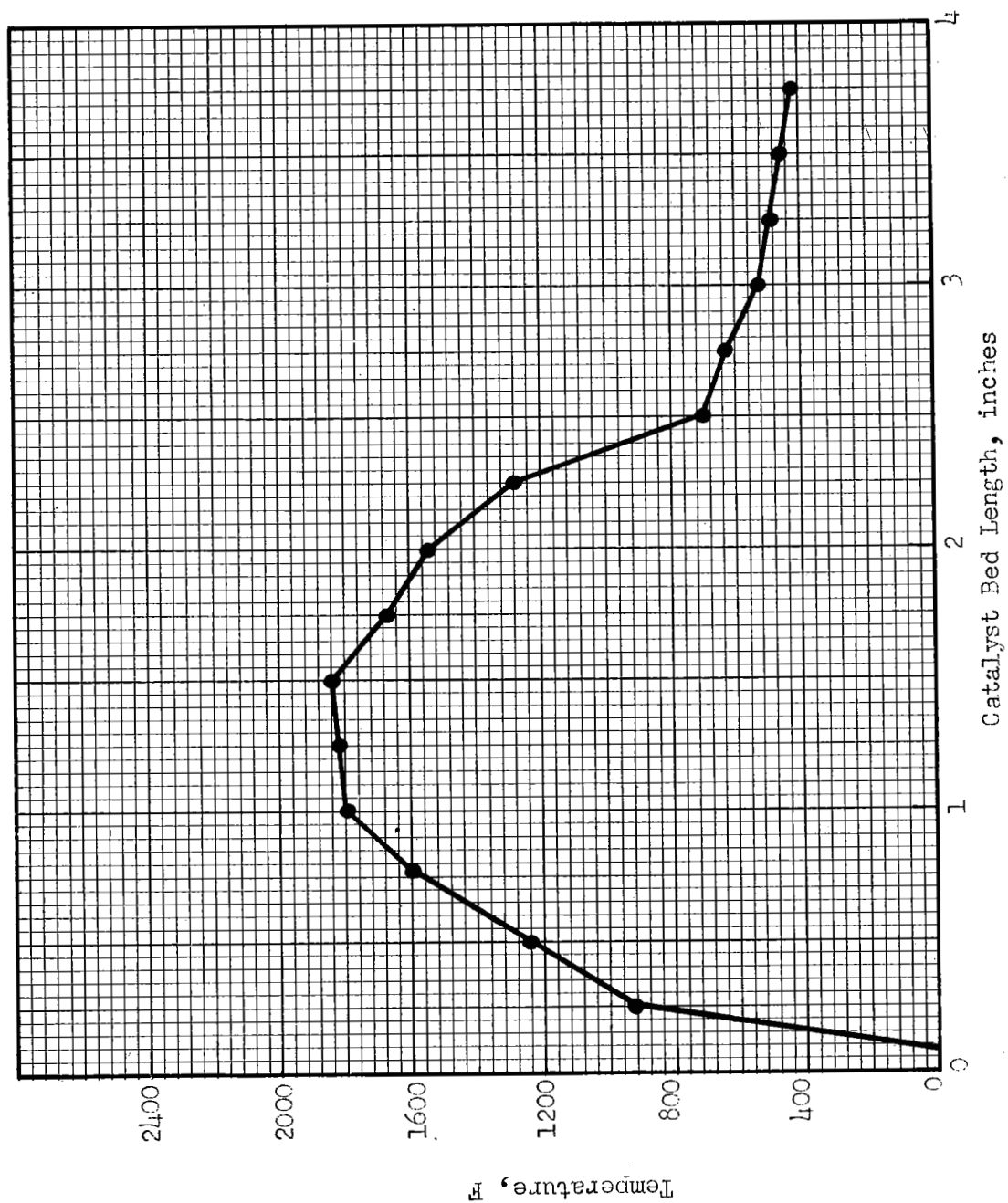


Figure 24. Temperature Gradation as a Function of Catalyst Bed Length Illustrating the Effects of Excess Catalyst Bed Length on Temperature for a 1.5-Inch-Diameter by 4-Inch-Long Catalyst Bed

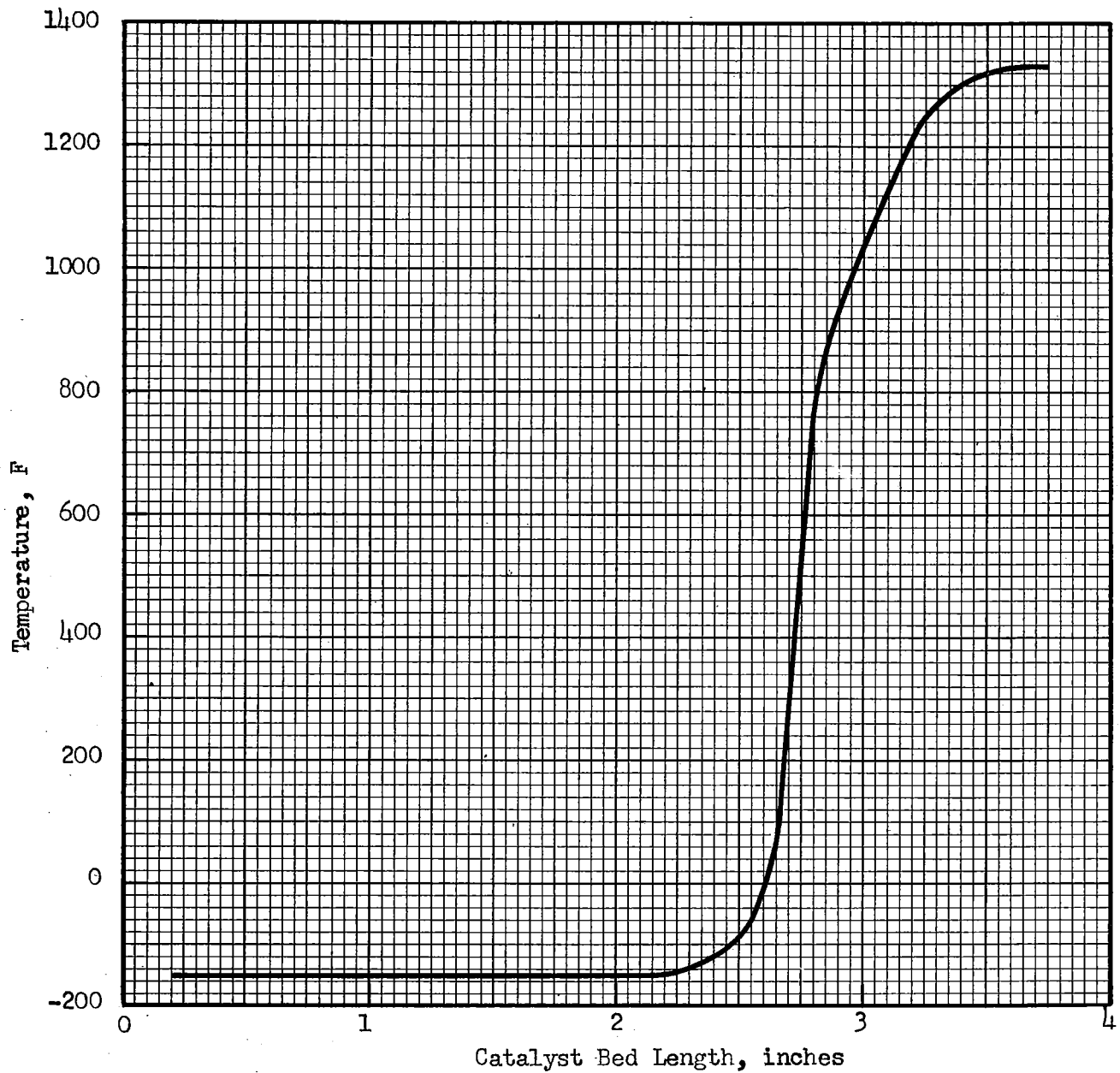


Figure 25. Temperature Gradation as a Function of Catalyst Bed Length for a Near-Optimum Catalyst Bed

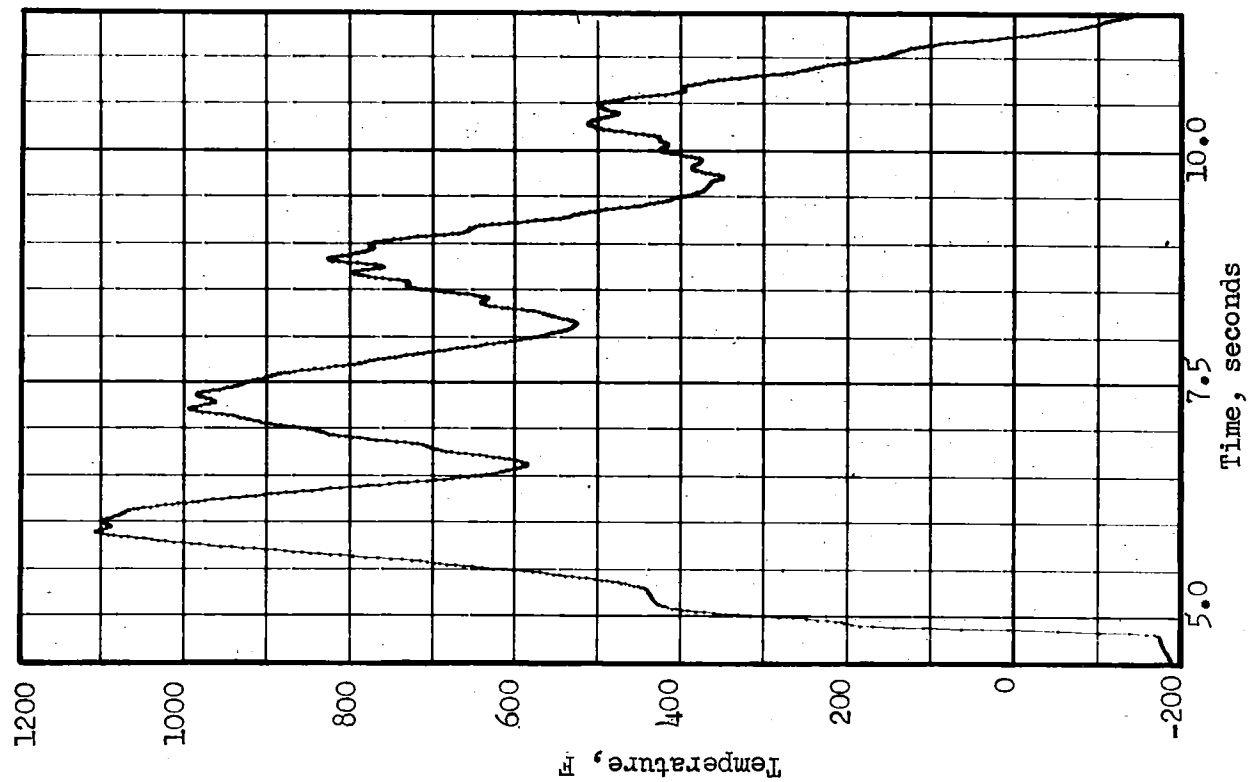
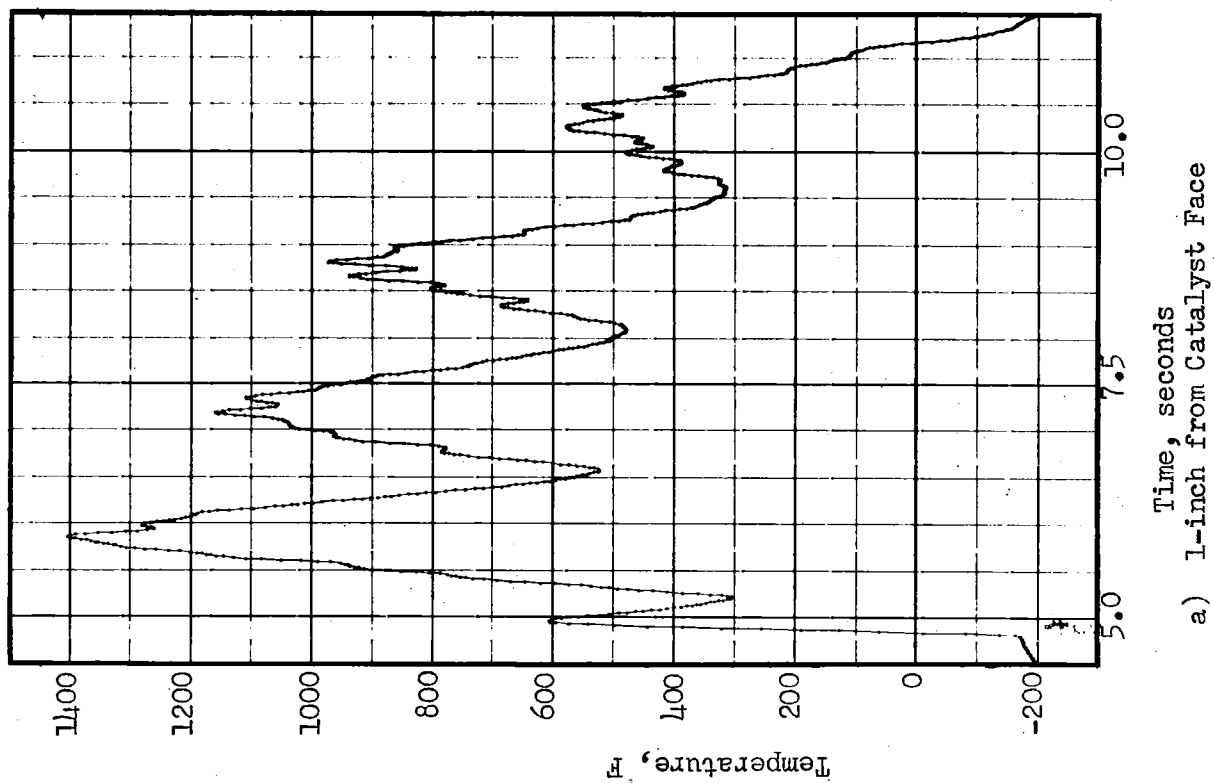


Figure 26. Illustration of the Effects of Reactant Flowrate Cycling on Temperature Within the Catalyst Bed for Two Bed Positions

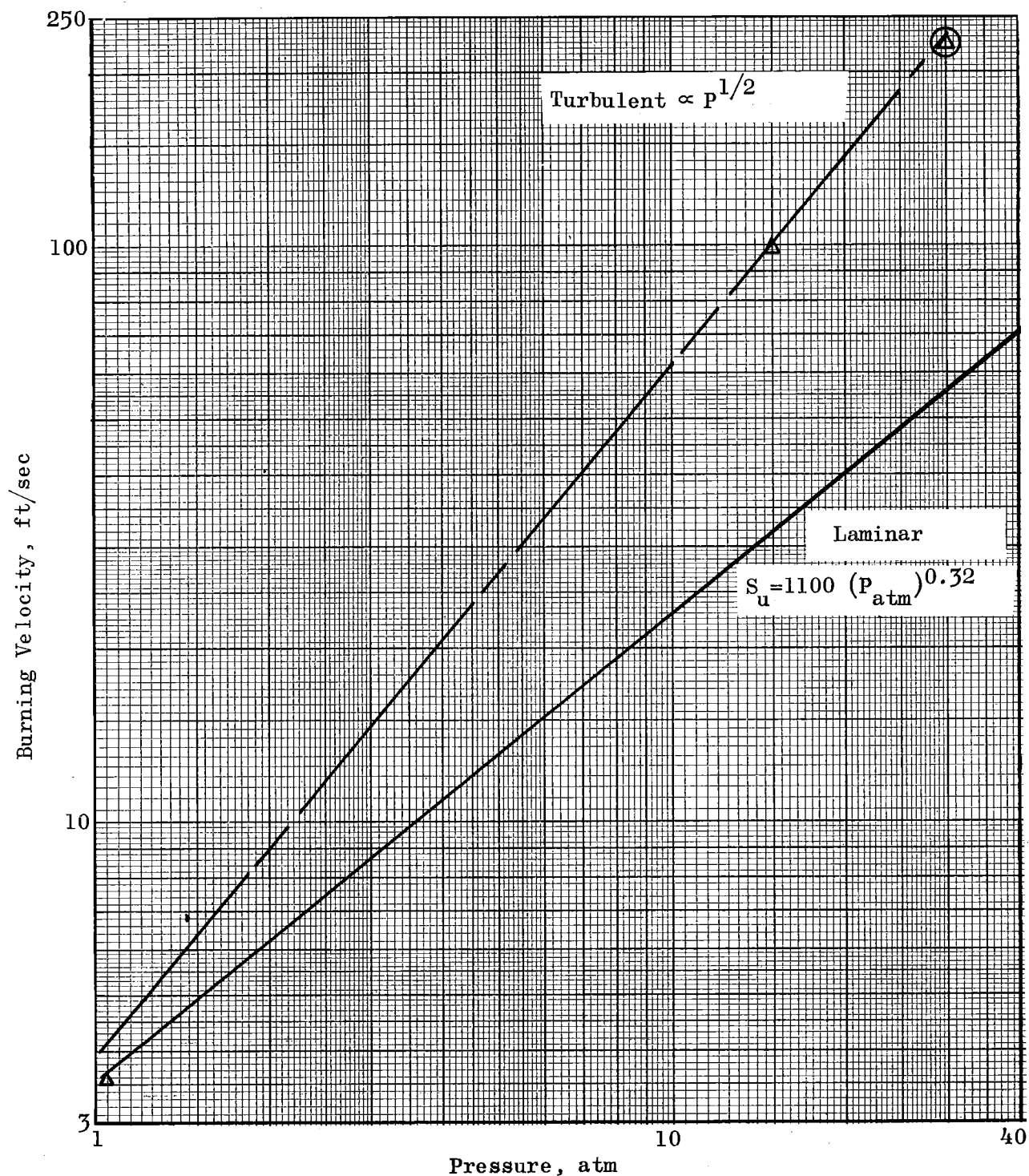


Figure 27. Flame Velocity Data Available From Literature (Ref. 20)  
⊠ Point is a Rocketdyne Point Taken From 2-Dimensional  
Transparent Chamber Studies (Ref. 21) for Stoichiometric  
 $O_2/H_2$  Blends



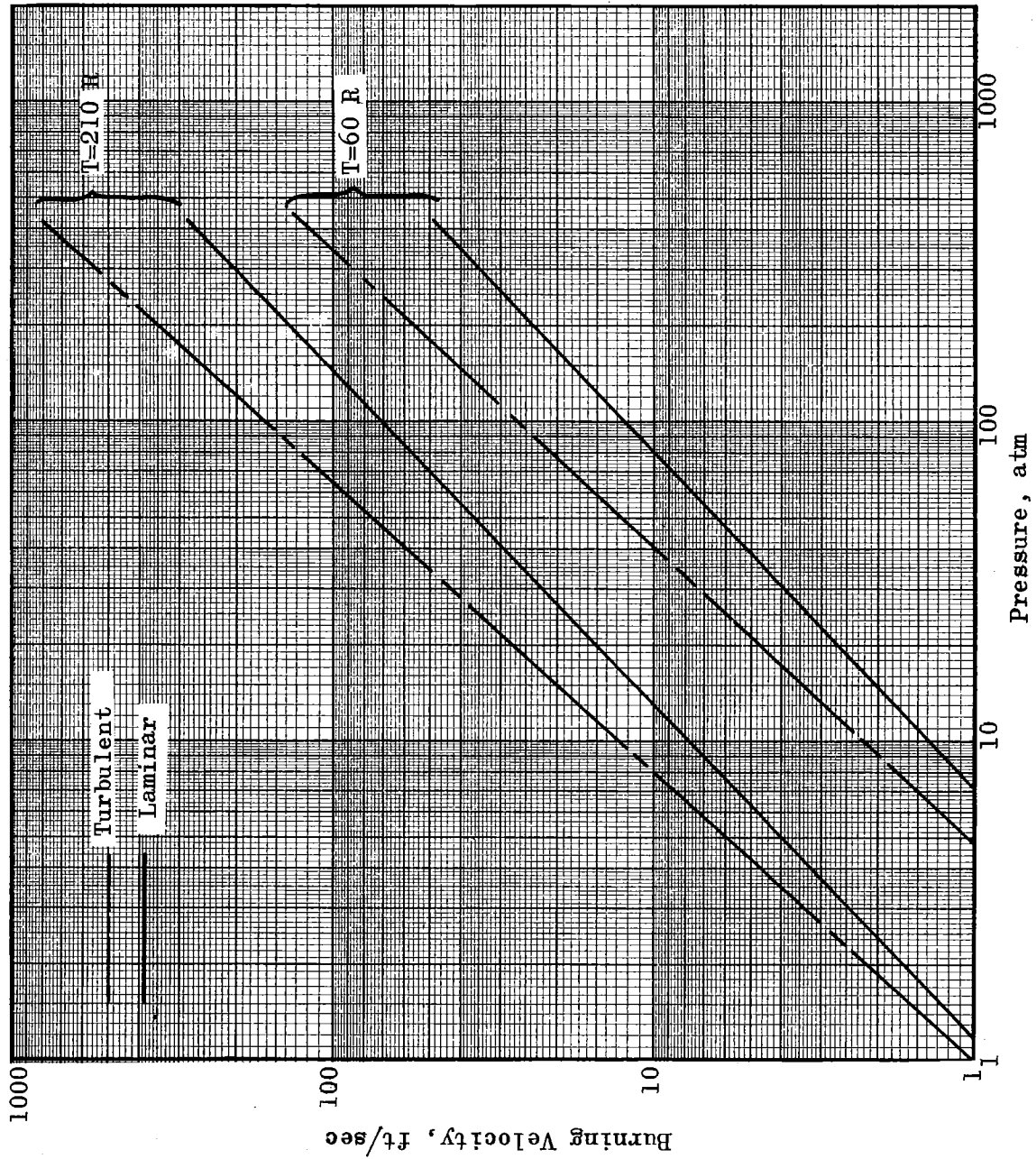


Figure 28: Flame Velocity Extrapolated Data to 60 and 210 R for Turbulent and Laminar Flames (Ref. 20)

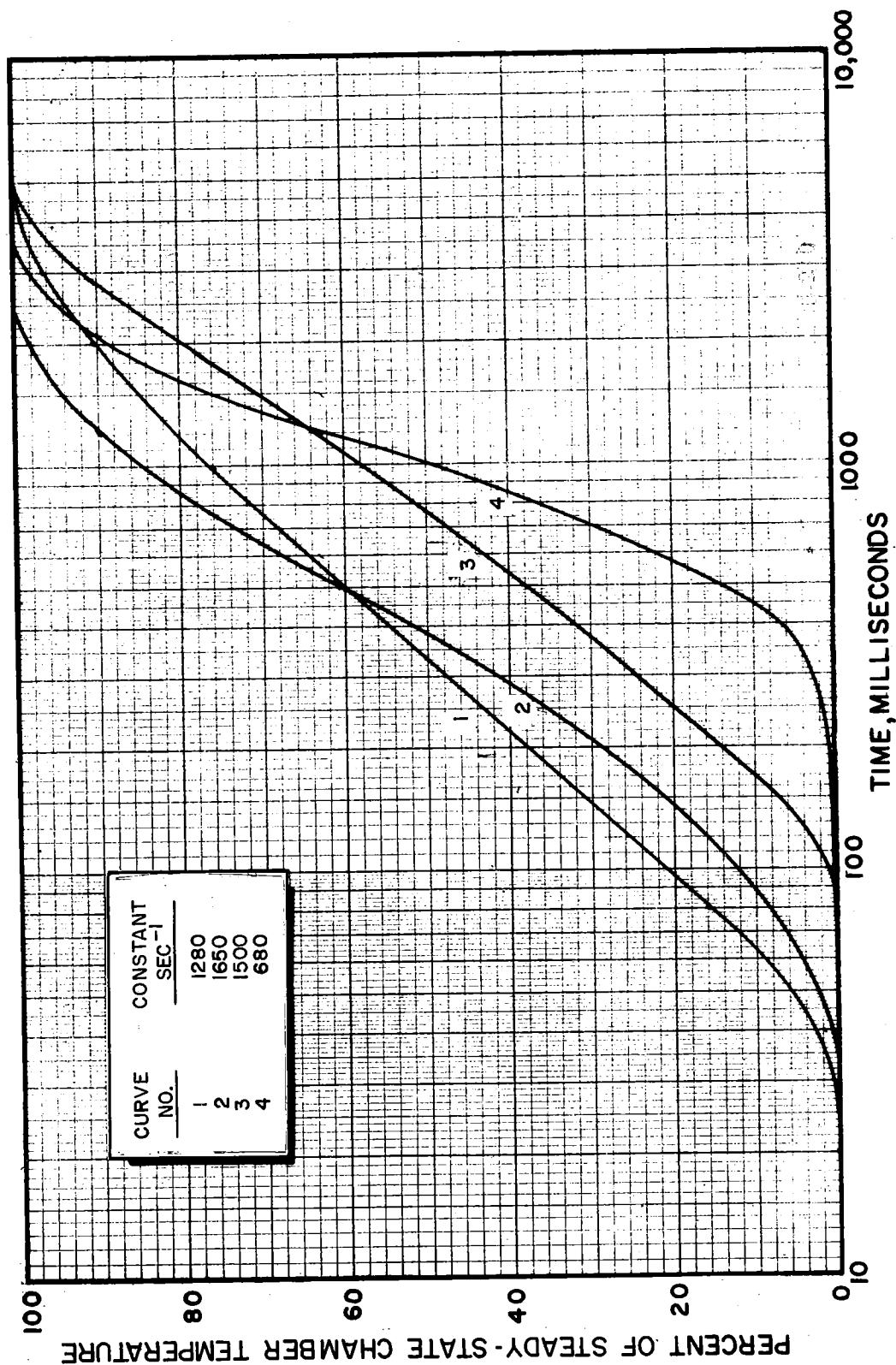


Figure 29. Typical Curves Presenting the Rate of Approach to Steady-State Chamber Temperature for the Engelhard MFSS Catalyst With the Gaseous  $O_2/H_2$  System Illustrating the Effects of Flowrate of Rate of Approach to Equilibrium

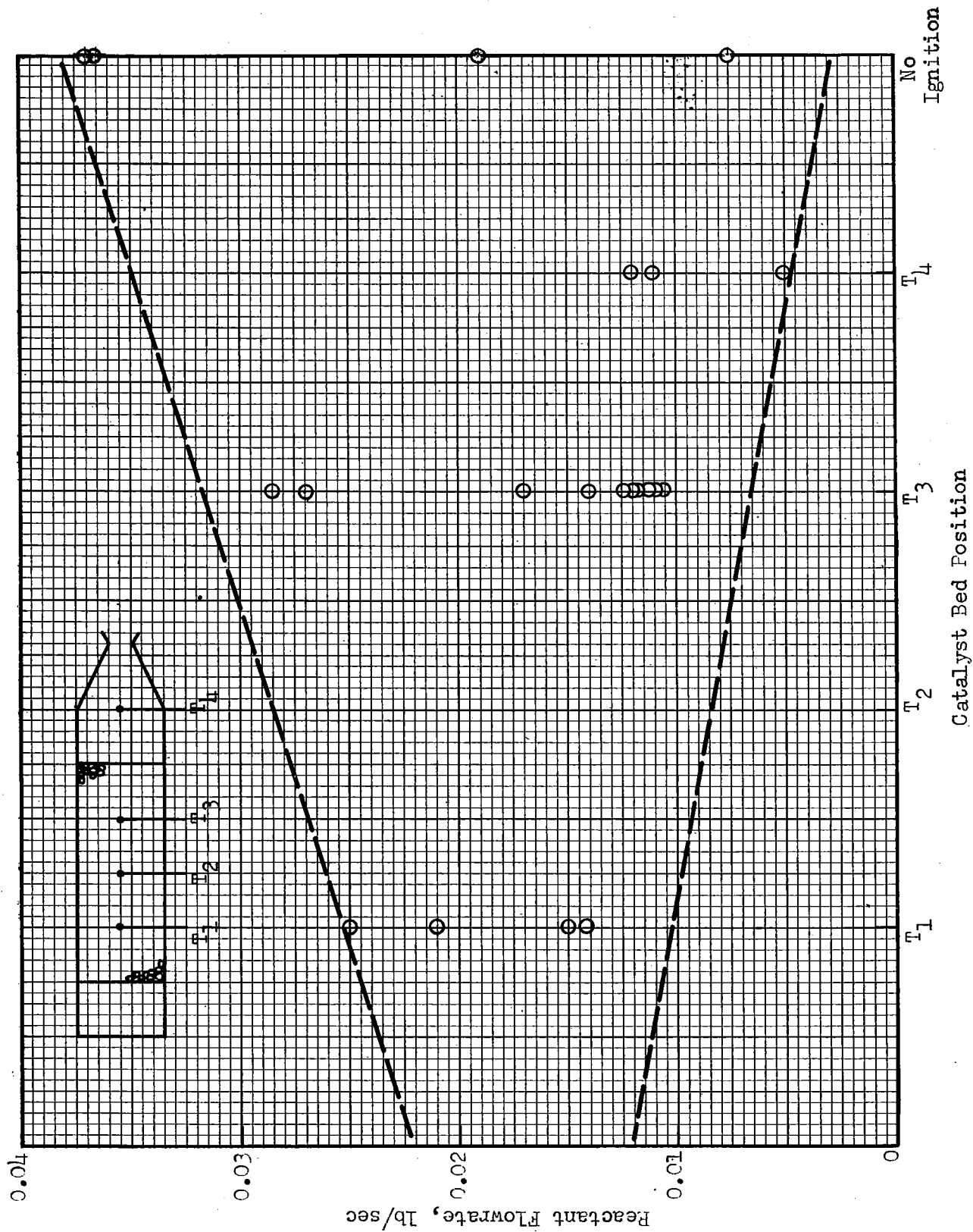


Figure 30. Minimum Catalyst Length Studies Showing Apparent Stability at Different Locations for Varying Total Flowrates for 21 Runs

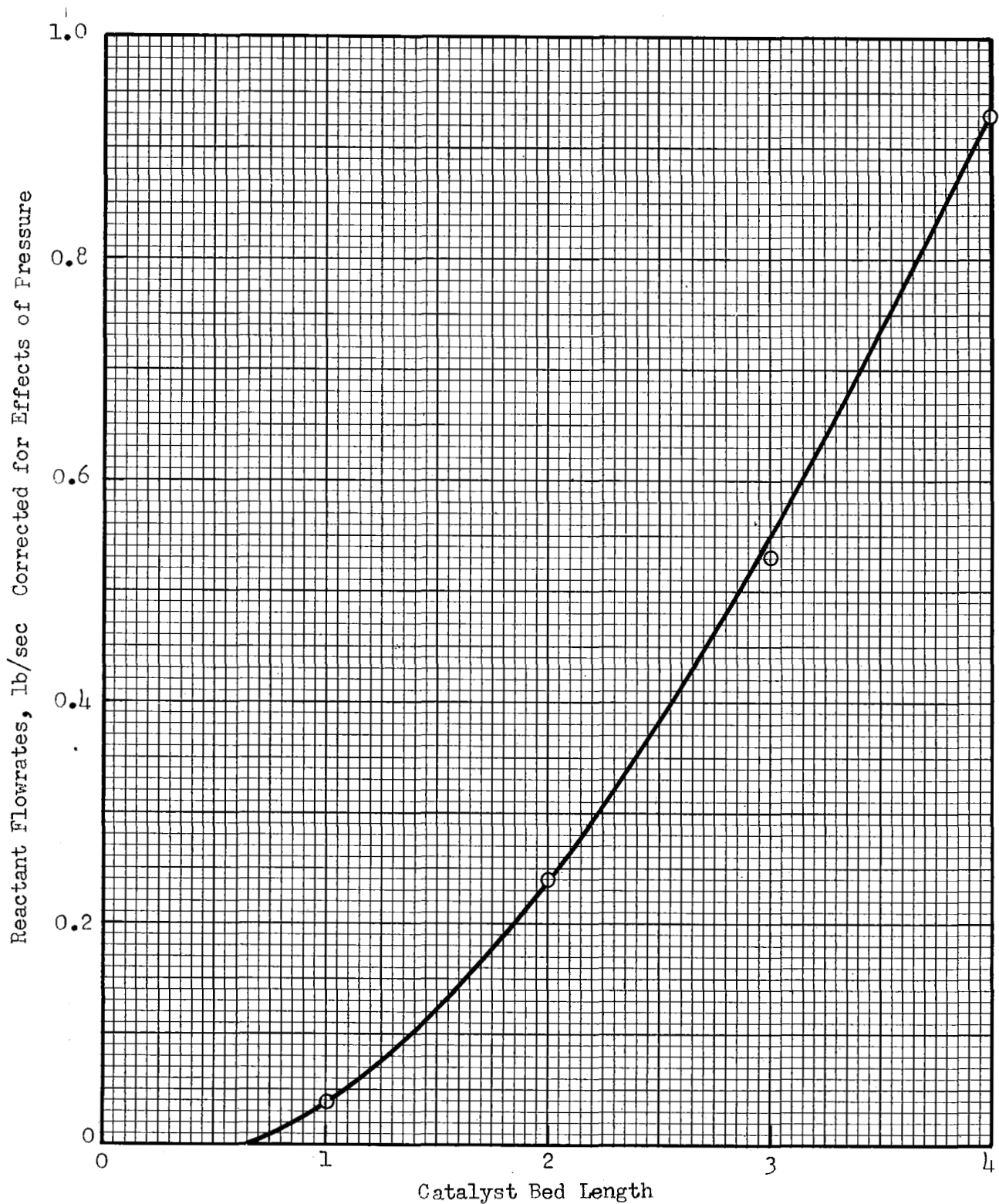


Figure 3L. Representation of Minimum Catalyst Bed Length Requirements as a Function of Reactant Flowrate Corrected to Comparable Mean Chamber Pressures.

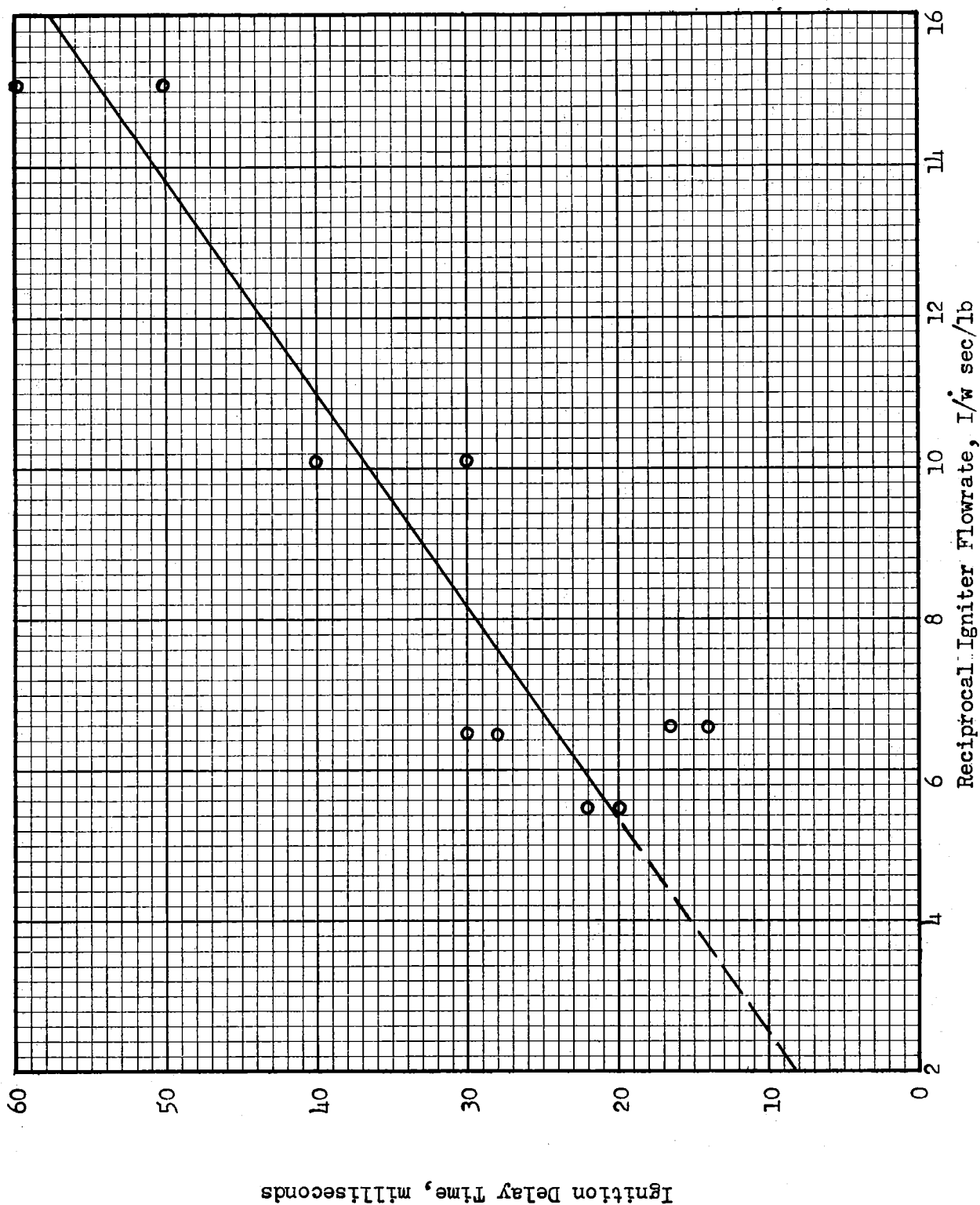


Figure 32. Representation of the Effects of Igniter Flowrate on Ignition Delay for the Nominally 20,000 lbf Thrust LOX/LH<sub>2</sub> Engine Operating at a Mixture Ratio of 5.5. The Igniter Chamber Temperature is Constant at 1500 F

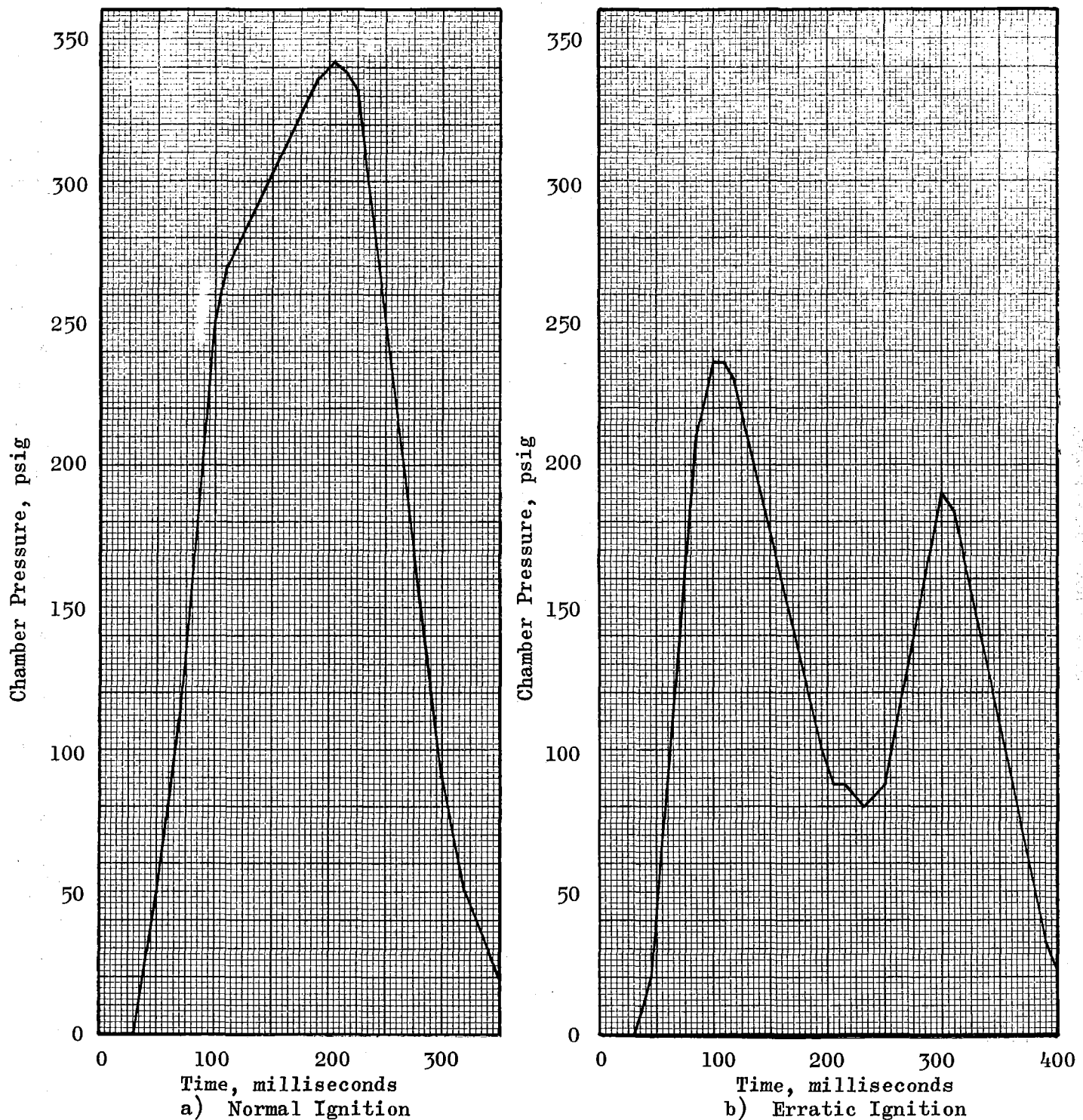


Figure 33. Illustration of Typical Large-Engine Ignition Transients, Comparing Normal Ignition in Which the Chamber Pressure Uniformly Approaches a Steady-State Value With Erratic Ignition Wherein a Tendency to Quench was Observed

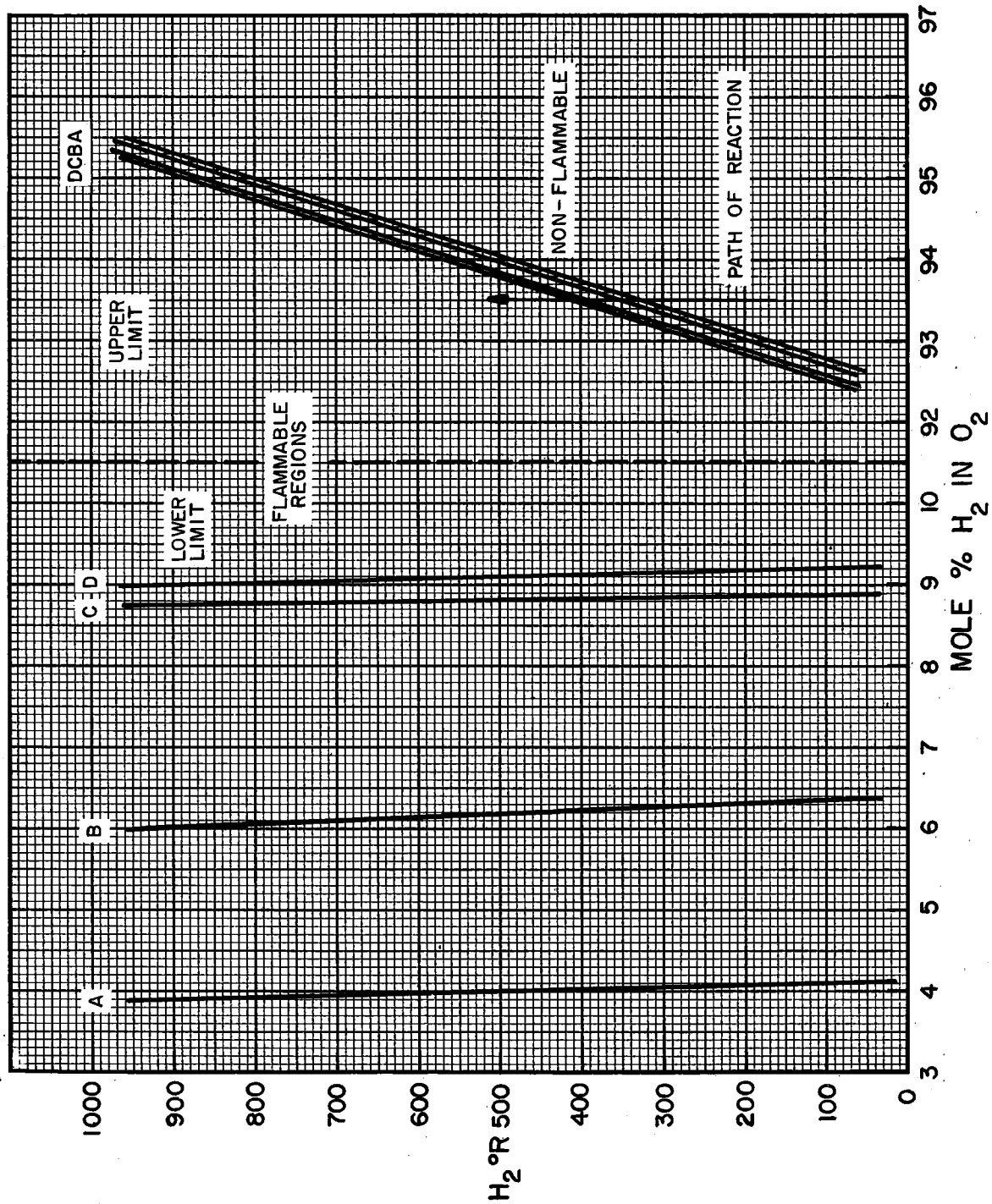


Figure 34. Flammability Limits of Hydrogen in Oxygen as Determined in Ref. 14. The Oxygen Inlet Temperatures for the A,B,C,D curves are:

- A -  $523^{\circ}R$
- B -  $162^{\circ}R$
- C -  $162^{\circ}R$ , liquid
- D -  $135^{\circ}R$ , liquid

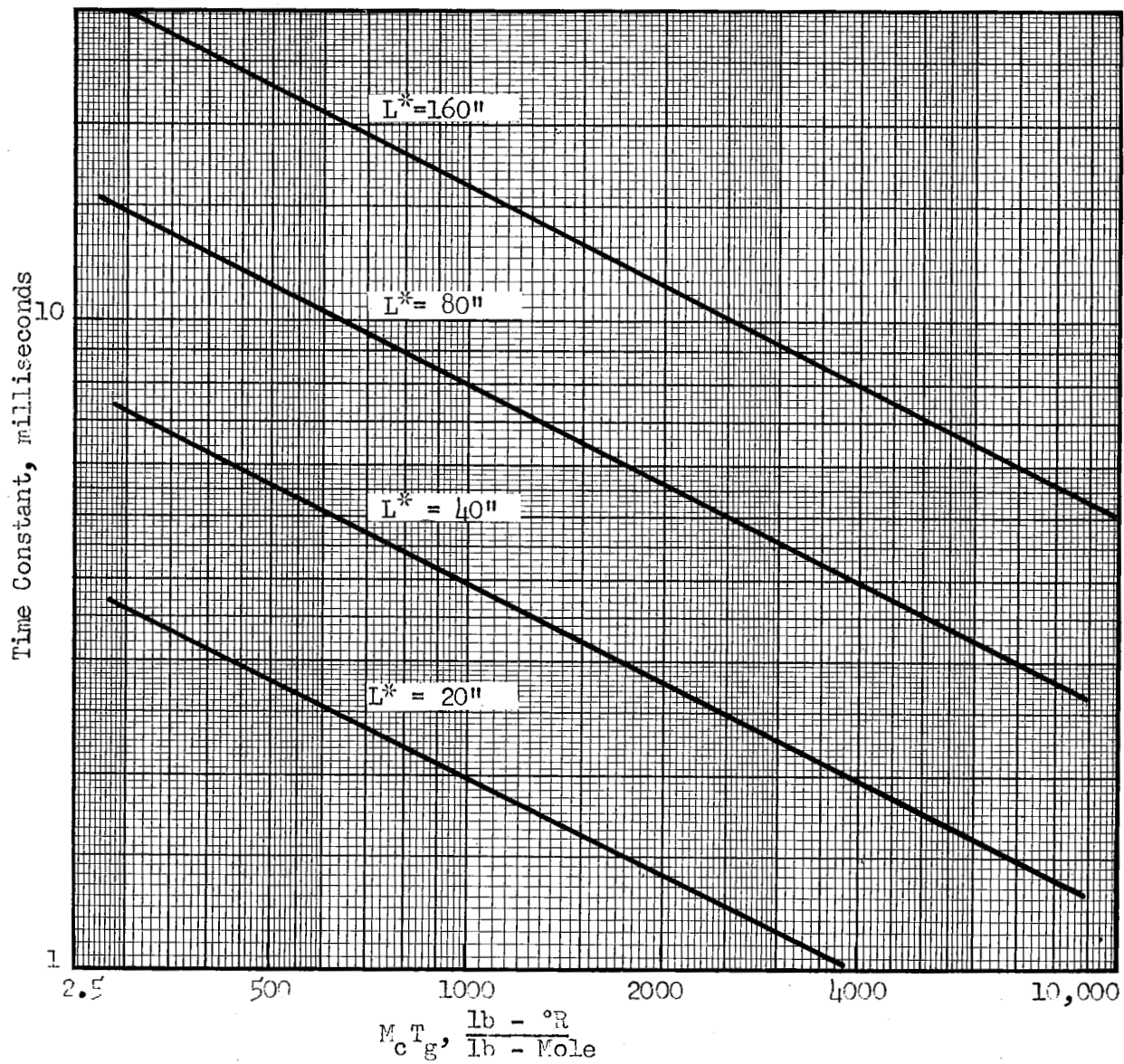


Figure 35. Pneumatic Filling Constant to 95-Percent Steady-State Pressure for Various Assumed Sizes of Reactor and Steady-State Temperatures



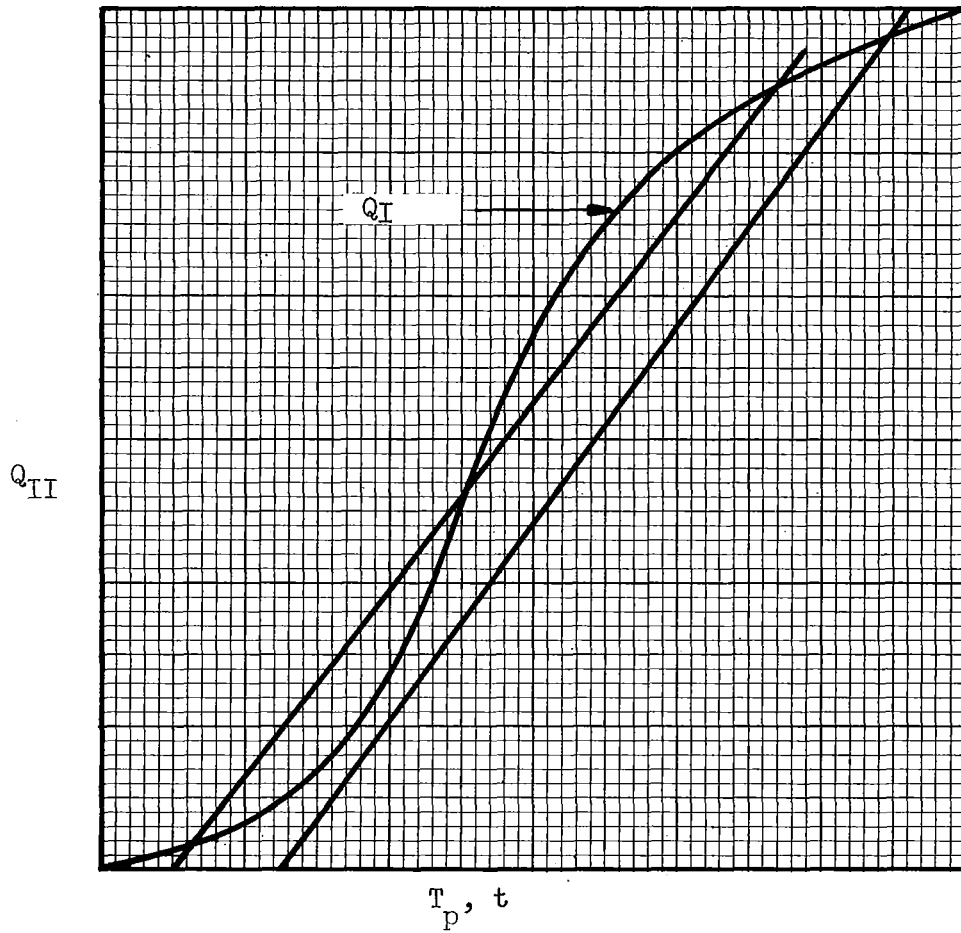


Figure 36. Stability Solution for Steady-State Operation in a Packed Catalyst Bed





CONTRACTUAL DISTRIBUTION

<u>Copies</u>	<u>Recipient</u>
12	NASA-Lewis Research Center 21000 Brookpark Road Cleveland, Ohio 44135 Attn: Contracting Officer Chemical Rocket Systems Procurement Section
4	NASA-Headquarters Washington, D. C. 20546 Attn: F. E. Compitello/RPL Chief, Liquid Propulsion Technology
20	Scientific & Technical Information Facility NASA Representative, Code CRT P. O. Box 5700 Bethesda, Maryland 20014
2	Ames Research Center Moffett Field, California 94035 Attn: Harold Hornby Mission Analysis Division
2	Goddard Space Flight Center Greenbelt, Maryland 20771 Attn: Merland L. Moseson Code 623
2	Jet Propulsion Laboratory California Institute of Technology 4800 Oak Grove Drive Pasadena, California 91103 Attn: R. F. Rose Propulsion Division 38
2	Langley Research Center Langley Station Hampton, Virginia 23365 Attn: F. L. Thompson Director
2	Lewis Research Center 21000 Brookpark Road Cleveland, Ohio 44135 Attn. Dr. A. Silverstein Director



<u>Copies</u>	<u>Recipient</u>
2	Marshall Space Flight Center Huntsville, Alabama 35812 Attn: H. K. Weidner Code R-P&VED
1	Marshall Space Flight Center Huntsville, Alabama 35812 Attn: R. Bailey Code R-P&VE-PAC
2	Manned Spacecraft Center Houston, Texas 77001 Attn: R. R. Gilruth Director
2	Western Operations Office 150 Pico Boulevard Santa Monica, California 90406 Attn: R. W. Kamm Director
1	Advanced Research Projects Agency Washington 25, D. C. Attn: D. E. Mock
1	Aeronautical Systems Division Air Force Systems Command Wright-Patterson Air Force Base Dayton, Ohio Attn: D. L. Schmidt Code ASRCNC-2
1	Air Force Missile Development Center Holloman Air Force Base, New Mexico Attn: Maj. R. E. Bracken Code MDGRT
1	Air Force Missile Test Center Patrick Air Force Base, Florida Attn: L. J. Ullian
1	Air Force Systems Command, Dyna-Soar Air Force Unit Post Office Los Angeles 45, California Attn: Col. Clark Technical Data Center



<u>Copies</u>	<u>Recipient</u>
1	Arnold Engineering Development Center Arnold Air Force Station Tullahoma, Tennessee Attn: Dr. H. K. Doetsch
1	Bureau of Naval Weapons Department of the Navy Washington 25, D. C. Attn: J. Kay Code RTMS-41
1	Defense Documentation Center Headquarters Cameron Station, Building 5 5010 Duke Street Alexandria, Virginia 22314 Attn: TISIA
1	Headquarters, U. S. Air Force Washington 25, D. C. Attn: Col. C. K. Stambaugh Code AFRST
1	Rocket Propulsion Laboratories Edwards Air Force Base Edwards, California 93523 Attn: Col. Silk
1	U. S. Atomic Energy Commission Technical Information Services Box 62 Oak Ridge, Tennessee
1	U. S. Army Missile Command Redstone Arsenal, Alabama 35809 Attn: Dr. W. Wharton
1	U. S. Naval Ordnance Test Station China Lake, California 93557 Attn: Chief, Missile Propulsion Division Code 451
3	Chemical Propulsion Information Agency John Hopkins University Applied Physics Laboratory 8621 Georgia Avenue Silver Spring, Maryland Attn: T. L. Reedy



Copies

Recipient

1	Aerojet-General Corporation P. O. Box 296 Azusa, California Attn: L. F. Kohrs
1	Aerojet-General Corporation P. O. Box 1947 Technical Library, Bldg. 2015, Dept. 2410 Sacramento, California 95809
1	Aeronutronic A Division of Ford Motor Company Ford Road Newport Beach, California Attn: D. A. Carrison
1	Aerospace Corporation 2400 East El Segundo Boulevard P. O. Box 95085 Los Angeles, California 90045 Attn: J. G. Wilder MS-2293 Propulsion Department
1	Arthur D. Little, Inc. Acorn Park Cambridge 40, Massachusetts Attn: A. C. Tobey
1	Astropower, Inc., Subsidiary of Douglas Aircraft Company 2968 Randolph Avenue Costa Mesa, California Attn: Dr. G. Moc Director, Research
1	Astrosystems, Inc. 1275 Bloomfield Avenue Caldwell Township, New Jersey Attn: A. Mendenhall
1	Atlantic Research Corporation Edsall Road and Shirley Highway Alexandria, Virginia Attn: A. Scurlock



<u>Copies</u>	<u>Recipient</u>
1	Beech Aircraft Corporation Boulder Facility Box 631 Boulder, Colorado Attn: J. H. Rodgers
1	Bell Aerosystems Company P. O. Box 1 Buffalo 5, New York Attn: W. M. Smith
1	Bendix Systems Division Bendix Corporation Ann Arbor, Michigan Attn: J. M. Brueger
1	Boeing Company P. O. Box 3707 Seattle 24, Washington Attn: J. D. Alexander
1	Chrysler Corporation Missile Division Warren, Michigan Attn: J. Gates
1	Curtiss-Wright Corporation Wright Aeronautical Division Wood-ridge, New Jersey Attn: G. Kelley
1	Douglas Aircraft Company, Inc. Missile and Space Systems Division 3000 Ocean Park Blvd. Santa Monica, California 90406 Attn: R. W. Hallet Chief Engineer, Advanced Space Technology
1	Fairchild Stratots Corporation Aircraft Missiles Division Hagerstown, Maryland Attn: J. S. Kerr
1	General Dynamics/Astronautics Library & Information Services (128-00) P. O. Box 1128 San Diego, California 92212 Attn: F. Dore



Copies

Recipient

2	General Electric Company Re-Entry Systems Department P. O. Box 8555 Philadelphia, Pennsylvania 19101 Attn: Library
1	General Electric Company Flight Propulsion Lab Department Cincinnati 15, Ohio Attn: D. Suichu
1	Grumman Aircraft Engineering Corp. Bethpage Long Island, New York Attn: J. Gavin
1	Kidde Aero-Space Division Walter Kidde and Company, Inc. 675 Main Street Belleville 9, New Jersey Attn: R. J. Hanville, Director Research Engineering
1	Lockheed California Company 10445 Glen Oaks Boulevard Pacoima, California Attn: G. D. Brewer
1	Lockheed Missiles and Space Company Attn: Technical Information Center P. O. Box 504 Sunnyvale, California Y. C. Lee Power Systems R&D
1	Lockheed Propulsion Company P. O. Box 111 Redlands, California Attn: H. L. Thackwell
2	The Marquardt Corporation 16555 Saticoy Street Box 2013 - South Annex Van Nuys, California 91409 Attn: W. P. Boardman, Jr.





<u>Copies</u>	<u>Recipient</u>
1	Martin Division Martin Marietta Corporation Baltimore 3, Maryland Attn: J. Calathes (3214)
1	Martin Denver Division Martin Marietta Corporation Denver, Colorado 80201 Attn: J. D. Goodlette Mail A-241
1	McDonnell Aircraft Corporation P. O. Box 6101 Lambert Field, Missouri Attn: R. A. Herzmark
1	North American Aviation, Inc. Space & Information Systems Division Downey, California Attn: H. Storms
1	Northrop Corporation 1001 East Broadway Hawthorne, California Attn: W. E. Gasich
1	Pratt & Whitney Aircraft Corp. Florida Research and Development Center P. O. Box 2691 West Palm Beach, Florida 33402 Attn: R. J. Coar
1	Radio Corporation of America Astro-Electronics Division Defense Electronic Products Princeton, New Jersey Attn: S. Fairweather
1	Reaction Motors Division Thiokol Chemical Corporation Denville, New Jersey 07832 Attn: A. Sherman
1	Republic Aviation Corporation Farmingdale Long Island, New York Attn: Dr. W. O'Donnell



Copies

Recipient

1	Rocketdyne (Library Dept. 586-306) Division of North American Aviation 6633 Canoga Avenue Canoga Park, California 91304 Attn: E. B. Monteath
1	Space General Corporation 9200 Flair Avenue El Monte, California Attn: C. E. Roth
1	Space Technology Laboratories Subsidiary of Thompson-Ramo-Wooldridge P. O. Box 95001 Los Angeles 45, California Attn: G. W. Elverum
1	Stanford Research Institute 333 Ravenswood Avenue Menlo Park, California 94025 Attn: T. Smith
1	TAPCO Division Thompson-Ramo-Wooldridge, Inc. 23555 Euclid Avenue Cleveland 17, Ohio Attn: P. T. Angell
1	Thiokol Chemical Corporation Redstone Division Huntsville, Alabama Attn: J. Goodloe
1	United Aircraft Corporation Research Laboratories 400 Main Street East Hartford 8, Connecticut 06108 Attn: E. Martin
1	United Technology Center 587 Methilda Avenue P. O. Box 358 Sunnyvale, California Attn: B. Abelman



<u>Copies</u>	<u>Recipient</u>
2	United Aircraft Corporation Pratt and Whitney FRDC P. O. Box 2691 West Palm Beach, Florida 33402 Library (1) Stan Mosier (1)
1	Vought Astronautics Box 5907 Dallas 22, Texas Attn: W. C. Trent
1	Sundstrand Aviation Division Sundstrand Corporation 2421 11th Street Rockford, Illinois Attn: R. N. Bailey
1	Picatinny Arsenal Dover, New Jersey 07801 Attn: I. Forsten, Chief, Liquid Propulsion Laboratory

UNCLASSIFIED  
Security Classification

<b>DOCUMENT CONTROL DATA - R&amp;D</b> <small>(Security classification of title, body of abstract and indexing annotation must be entered when the overall report is classified)</small>		
<b>1. ORIGINATING ACTIVITY</b> <small>(Corporate author)</small> Rocketdyne, a Division of North American Aviation, Inc., 6633 Canoga Avenue, Canoga Park, California		<b>2a. REPORT SECURITY CLASSIFICATION</b> UNCLASSIFIED
		<b>2b. GROUP</b>
<b>3. REPORT TITLE</b>  INVESTIGATION OF CATALYTIC IGNITION OF OXYGEN/HYDROGEN SYSTEMS		
<b>4. DESCRIPTIVE NOTES</b> <small>(Type of report and inclusive dates)</small> Final (15 June 1964 through 15 October 1965)		
<b>5. AUTHOR(S)</b> <small>(Last name, first name, initial)</small>  Roberts, R. W., Burge, H. L., Ladacki, M.		
<b>6. REPORT DATE</b> 30 December 1965	<b>7a. TOTAL NO. OF PAGES</b> 219	<b>7b. NO. OF REFS</b> 39
<b>8a. CONTRACT OR GRANT NO.</b> NAS 3-4185	<b>9a. ORIGINATOR'S REPORT NUMBER(S)</b> R-6303	
<b>b. PROJECT NO.</b>  <b>c.</b>  <b>d.</b>	<b>9b. OTHER REPORT NO(S)</b> <small>(Any other numbers that may be assigned this report)</small> NASA CR-54657	
<b>10. AVAILABILITY/LIMITATION NOTICES</b>		
<b>11. SUPPLEMENTARY NOTES</b>	<b>12. SPONSORING MILITARY ACTIVITY</b> Advanced Rocket Technology Branch NASA Lewis Research Center Cleveland, Ohio	
<b>13. ABSTRACT</b>  The results and interpretations of an investigation of catalytic ignition of the oxygen/hydrogen system are presented. The experimental phase of the program is divided into three fundamental tasks: (1) Catalyst Selection and Evaluation, (2) Catalyst Life Studies, and (3) Parametric Engine Evaluation. During the first task, selected noble metal and metal oxide catalysts having potential for promoting the liquid phase oxygen/hydrogen reaction were evaluated. On the basis of these evaluations, four noble metal catalysts were compared in liquid phase reactants at an environmental temperature of approximately -400 F. The best of these four was used during a catalytic reactor configuration optimization study, and later during a catalyst life study to evaluate the reignition characteristics of the catalyst. During the final task, the catalytic igniter was used as an ignition source in a large engine (~14,000-pound thrust) to evaluate the effects of variations in engine and igniter parameters on liquid oxygen/liquid hydrogen engine ignition and ignition delay characteristics.		

14.	KEY WORDS	LINK A		LINK B		LINK C	
		ROLE	WT	ROLE	WT	ROLE	WT
	Catalytic ignition Oxygen Hydrogen Noble metal Metal oxides						

#### INSTRUCTIONS

1. **ORIGINATING ACTIVITY:** Enter the name and address of the contractor, subcontractor, grantee, Department of Defense activity or other organization (*corporate author*) issuing the report.

2a. **REPORT SECURITY CLASSIFICATION:** Enter the overall security classification of the report. Indicate whether "Restricted Data" is included. Marking is to be in accordance with appropriate security regulations.

2b. **GROUP:** Automatic downgrading is specified in DoD Directive 5200.10 and Armed Forces Industrial Manual. Enter the group number. Also, when applicable, show that optional markings have been used for Group 3 and Group 4 as authorized.

3. **REPORT TITLE:** Enter the complete report title in all capital letters. Titles in all cases should be unclassified. If a meaningful title cannot be selected without classification, show title classification in all capitals in parenthesis immediately following the title.

4. **DESCRIPTIVE NOTES:** If appropriate, enter the type of report, e.g., interim, progress, summary, annual, or final. Give the inclusive dates when a specific reporting period is covered.

5. **AUTHOR(S):** Enter the name(s) of author(s) as shown on or in the report. Enter last name, first name, middle initial. If military, show rank and branch of service. The name of the principal author is an absolute minimum requirement.

6. **REPORT DATE:** Enter the date of the report as day, month, year, or month, year. If more than one date appears on the report, use date of publication.

7a. **TOTAL NUMBER OF PAGES:** The total page count should follow normal pagination procedures, i.e., enter the number of pages containing information.

7b. **NUMBER OF REFERENCES:** Enter the total number of references cited in the report.

8a. **CONTRACT OR GRANT NUMBER:** If appropriate, enter the applicable number of the contract or grant under which the report was written.

8b, 8c, & 8d. **PROJECT NUMBER:** Enter the appropriate military department identification, such as project number, subproject number, system numbers, task number, etc.

9a. **ORIGINATOR'S REPORT NUMBER(S):** Enter the official report number by which the document will be identified and controlled by the originating activity. This number must be unique to this report.

9b. **OTHER REPORT NUMBER(S):** If the report has been assigned any other report numbers (*either by the originator or by the sponsor*), also enter this number(s).

10. **AVAILABILITY/LIMITATION NOTICES:** Enter any limitations on further dissemination of the report, other than those

imposed by security classification, using standard statements such as:

- (1) "Qualified requesters may obtain copies of this report from DDC."
- (2) "Foreign announcement and dissemination of this report by DDC is not authorized."
- (3) "U. S. Government agencies may obtain copies of this report directly from DDC. Other qualified DDC users shall request through \_\_\_\_\_."
- (4) "U. S. military agencies may obtain copies of this report directly from DDC. Other qualified users shall request through \_\_\_\_\_."
- (5) "All distribution of this report is controlled. Qualified DDC users shall request through \_\_\_\_\_."

If the report has been furnished to the Office of Technical Services, Department of Commerce, for sale to the public, indicate this fact and enter the price, if known.

11. **SUPPLEMENTARY NOTES:** Use for additional explanatory notes.

12. **SPONSORING MILITARY ACTIVITY:** Enter the name of the departmental project office or laboratory sponsoring (*paying for*) the research and development. Include address.

13. **ABSTRACT:** Enter an abstract giving a brief and factual summary of the document indicative of the report, even though it may also appear elsewhere in the body of the technical report. If additional space is required, a continuation sheet shall be attached.

It is highly desirable that the abstract of classified reports be unclassified. Each paragraph of the abstract shall end with an indication of the military security classification of the information in the paragraph, represented as (TS), (S), (C), or (U).

There is no limitation on the length of the abstract. However, the suggested length is from 150 to 225 words.

14. **KEY WORDS:** Key words are technically meaningful terms or short phrases that characterize a report and may be used as index entries for cataloging the report. Key words must be selected so that no security classification is required. Identifiers, such as equipment model designation, trade name, military project code name, geographic location, may be used as key words but will be followed by an indication of technical context. The assignment of links, rules, and weights is optional.